O_2 Oxidation and Sublimation Kinetics of Single Silicon Nanoparticles at 1200 to 2050 K: Variation of Reaction Rates, Evolution of Structural and Optical Properties, and the Active-to-Passive Transition

*Daniel J. Rodriguez[1], Chris Y. Lau[1], Abigail M. Friese[1], Bryan A. Long[1], and Scott L. Anderson[1]**

[1]Department of Chemistry, University of Utah, 315 S. 1400 E., Salt Lake City, UT 84112

ABSTRACT: Sublimation and O_2 etching kinetics for a series of individual silicon (Si) nanoparticles (NPs) were studied for NP temperatures (T_{NP}) from 1200 to 2050 K, using a single NP mass spectrometry technique. Sublimation was significant for T_{NP} > 1700 K, with rates reasonably well fit to Arrhenius kinetics, but evolving, particularly during initial heating. O_2 etching efficiencies varied from NP-to-NP and with changing T_{NP}, but also evolved dramatically over time. For $T_{NP} \leq 1500$ K, NPs were observed to passivate after losing 30 to 50% of the initial NP mass. At higher T_{NP}, etching efficiency decreased over time, but never passivated. Interestingly, bulk Si passivation has not been observed for the range of T_{NP} and O_2 pressures used here, and a model was developed to test the effects of several NP-specific mechanistic parameters on both the initial and time-dependent etching behavior. The optical properties of the hot NPs were also found to evolve as the NPs etched, particularly during the initial fast mass loss, and correlations between emission intensities and etching kinetics were examined.

I. Introduction

In surface reactions, atomic scale surface structure strongly influences the kinetics, with low-coordination/defective sites typically having higher reactant binding energies, which often translates to higher reactivity compared to fully-coordinated terrace sites. For reactions of nanoparticles (NPs) and nano-crystalline surfaces, the numbers of accessible low-coordination sites can vary substantially from NP-to-NP, resulting in large variations in reactivity. Furthermore, because surface reactions can alter the surface site distributions, the reactivity for individual NPs tends to evolve over time under reaction conditions. For example, in experiments using single NP mass spectrometry to study kinetics for individual carbon NPs in the 1200 to 2100 K range, we found that both sublimation[1] and O_2 oxidative etching[2-3] kinetics varied substantially for NPs from different feedstocks (graphitic, graphene oxide, carbon black, diamond, nano-onion), but that even for NPs from the same feedstock, the initial rates varied by up to an order of magnitude. More surprisingly, the etching rates varied over time, with rates oscillating by orders of magnitude. All types of carbon NPs were found to evolve to become essentially inert to O_2 etching, but the time required for this evolution varied strongly for different carbon materials and for different NPs. The initial NP-to-NP variations were attributed to variations in the number of under-coordinated reactive sites present on each NP surface, and the evolution over time to evolution of the NP surface under reaction conditions. The eventual transition to near-complete O_2 inertness implies that the NPs evolved to have almost no under-coordinated surface sites, which was attributed to O_2-catalyzed isomerization to form fully-coordinated, fullerene-like surface layers. The ability to monitor structural evolution for individual NPs over time under reaction conditions is one of the strengths of the single NP mass spectrometry method. Here we apply this approach to Si NP oxidative etching.

The single NP mass spectrometry method works by simply measuring the NP mass repeatedly, allowing the absolute kinetics for mass-changing reactions to be monitored over time. For carbon NPs, interpreting the mass changes is simple because surface-oxygen groups are unstable at high temperatures, such that O_2 chemisorption leads to rapid desorption of CO or CO_2, etching the NP, or of O or O_2, resulting in no net mass change. As a result, the surface composition does not change with time, and the evolution of etching rates clearly must result from changes in the NP surface structure.

For metal and semi-metal NPs, sublimation is still straightforward to interpret, but oxidation is more complex because etching reactions that remove mass compete with reactions (e.g. oxide formation) that add mass and change the NP composition as it reacts. Materials of interest as high or ultra-high temperature protective layers are often refractory compounds (e.g. SiC, HfC, ZrB_2, …), and these also have oxidative etching reactions that remove mass (e.g. CO or B_xO_y desorption) competing with reactions that add mass (e.g. SiO_2, HfO_2, ZrO_2 formation) and change the surface composition. Furthermore, at high enough temperatures, the oxidized surface layer can decompose or desorb, leading to additional losses. Silicon exhibits all these effects over the wide temperature range studied, and the principle goal of this study is to understand this interplay of competing processes, and how it changes with temperature and time under reaction conditions for a material of great fundamental and practical importance. In the process, we developed methods to analyze the results that should allow kinetics studies at the much higher temperatures of interest for ultrahigh temperature materials.

In one respect, studying metal or semi-metal NPs is simpler than carbon NPs, because carbon cannot be melted except at high pressures, and the NPs retain the large variations of shape and surface structure present in the NP feedstocks. For silicon and some metals, however, it is

possible to heat the NPs well above the bulk T_{melt}, which should result in spherical NPs that are essentially clean of oxides or other contaminants, as discussed below. This capability also allows us to study reactions and sublimation at NP temperatures (T_{NP}) ranging from well below to well above the bulk T_{melt}. Here, we report a study of the O_2 etching chemistry for silicon (Si) NPs, chosen because O_2 etching and oxide layer formation have been well studied for bulk Si, [4-36] including a few studies that overlapped the lower end of our T_{NP} range.

Because of the importance of Si and its oxides in semiconductors, there is extensive literature for Si oxidation, and papers with particular relevance to the present experiments are reviewed in the **Supporting Information** (SI) and compared to our results below. Furthermore, several technological applications involve the passivation of Si NPs, and these include single monolayer SiO_2 growth for thermo-electrics[37] and tuning of the oxygen concentration in SiO_x NPs for batteries and optoelectronics. [38] Therefore, it is useful to have the essentials of the bulk Si oxidation behavior in mind when viewing the results for NPs. O_2 etching of Si surfaces can be thought of as involving the following major steps: O_2 dissociative adsorption with sticking coefficient = S, [8, 13, 16-18, 23] isomerization processes that convert between various geometries of adsorbed oxygen (O_{ads}), [8, 12, 39] diffusion to sub-surface absorption sites especially at higher temperatures, [40-41] etching primarily due to desorption of $SiO_{(g)}$, [8, 10, 12, 14, 16-17, 26-27] and passivation by nucleation and growth of a silica layer that is more thermally stable than O_{ads}. [7-8, 12-13, 17, 19-20] Another important observation is that thin SiO_2 surface layers can decompose by reaction with underlying bulk Si to form SiO, that desorbs at temperatures above 1000 K. [32, 42-49] Finally, even bulk silica decomposes at temperatures above 1800 K, with Si, SiO, Si_2O_2, O, and O_2 reported to be present in the vapor phase. [50-53]

Previous studies of bulk Si oxidation have identified ranges of P_{O2} and temperature with distinct oxidation mechanisms. At low T and high P_{O2}, oxidation is inhibited by formation of a passivating silica surface layer ("passive oxidation"), whereas at high T and low P_{O2}, silica layers do not form, and the surface etches continuously ("active oxidation"). [4, 7, 17] Under "transitional" conditions, the surface may etch initially, but passivate over time. Our experimental conditions are in range where passivation of bulk Si has not been observed. Because similar transitions between active and passive oxidation are also observed or expected for many high temperature materials, understanding oxidation of Si NPs is important in understanding the active ↔ passive transition of SiC and other Si-containing materials, and more generally relevant to many other materials that can form passivating oxides under similar conditions.

II. Experimental

A. Single NP Mass Spectrometry

The instrument used has been described previously, [54] along with the methods for single NP injection, detection, mass analysis, spectroscopic T_{NP} determination, [55-56] and measurement of surface reaction kinetics. [1-3] Briefly, NPs are injected into the gas phase using an electrospray ionization source, pass through several stages of differential pumping, are pre-filtered by a quadrupole ion guide, and then are injected into a split-ring-electrode quadrupole trap, [57-58] where they are detected optically. In addition to NP injection, the trap allows high solid angle optical collection along two axes and allows lasers to be focused through the trap along two other axes to excite emission from the NP. In typical experiments, NPs are heated by either a duty-factor-modulated, 10 W, quasi-cw CO_2 laser (10.6 μm), a cw diode-pumped solid-state laser (2 W at 532 nm), or occasionally by both. The lasers are focused loosely so that the beam radius at the trap center is larger than the amplitude of NP motion in the trap, i.e., the NP remains within the laser beam.

To trap a single NP, a low intensity NP beam is injected continuously into the trap while the trap center is irradiated by the CO_2 laser, which is absorbed by Si. Light emitted from a ~50 μm volume at the trap center is collected, passed through a 550 nm long-pass filter to block scattered 532 nm light, and focused onto an avalanche photodiode (APD) for NP detection and mass determination. The APD detects light in the 550 to 1000 nm range and is blind to the CO_2 laser. When an NP becomes trapped, it is heated to high enough temperature (T_{NP}) to allow its thermal emission to be detected by the APD, at which point both the NP beam and CO_2 laser are automatically shut off. For subsequent spectral and kinetics measurements, the 532 nm laser was used for heating because, unlike the CO_2 laser, it is truly continuous and is also more easily controlled (via a variable attenuator) to allow T_{NP} to be set and stabilized. We have not seen any differences in emission spectra or chemistry for NPs heated at 532 nm vs. 10.6 μm. As shown below, the Si NP emission spectra are blackbody-like, implying that energy is thermalized on a fast time scale compared to emission.

A trapped NP with mass, M, and charge, Q, oscillates in the trap with well-defined frequencies for axial and radial motion. [57-58] The axial frequency, F_z, is described by **Eqn. 1**, where z_0 is a trap geometric parameter, and F_{RF} and V_0 are the frequency (Hz) and amplitude of the AC potential applied to the trap.

$$F_z = \left(\frac{Q}{M}\right)\left(\frac{\sqrt{2}V_0}{4\pi^2 F_{RF} z_0^2}\right) \qquad (1)$$

For the small NPs of interest here, F_z is measured by a resonance excitation method, [59] and to obtain M from F_z, it is necessary to know Q, which is determined by fitting the series of F_z steps observed as Q is changed by ±e using a vacuum ultraviolet (VUV) lamp (**Fig. S1**). Occasionally, spontaneous Q steps occur (e.g. from thermionic emission) during the kinetics experiments, but the resulting F_z steps are easily recognized and accounted for in calculating M. Because the measurement is non-destructive, M and Q can be monitored continuously over time to extract kinetics for reactions, as long as they result in a net mass change. The dominant contributor to the *absolute* mass uncertainty (~±1.3%) is the construction accuracy of the trap, [1, 3] which, however, cancels for mass ratios (M_1/M_2), and partly cancels when calculating rates

per unit surface area ($\propto \frac{M_1-M_2}{M^{2/3}}$). The *relative* uncertainty in comparing M values is primarily determined by the APD signal/noise and the resulting error in F_z, and is typically <±0.2%.

B. Emission Spectroscopy and NP Temperature (T_{NP}) Determination

The approach to extracting T_{NP} by fitting emission spectra has been described previously.[55-56] Briefly, light emitted into a ~1 steradian solid angle about the trap axis is collected and sent to a pair of spectrographs that simultaneous measure the "nIR" ($980 < \lambda < 1600$ nm) and "visible" ($550 < \lambda < 980$ nm) spectral regions. The detection sensitivity, $S(\lambda)$, is calibrated using a CO_2 laser-heated micro-thermocouple inserted into the trap center as a miniature vacuum-compatible calibration emitter. The sensitivity-corrected NP spectra are fit by a thermal emission model to extract T_{NP}, which is used as feedback for temperature (T_{NP}) control. The thermal emission model function is simply Planck's law for ideal blackbody emission times an emissivity function, $\epsilon(\lambda, T_{NP})$. From scattering theory[60] for NPs much smaller than λ:

$$\epsilon(\lambda, T_{NP}) = \frac{8\pi r}{\lambda} \cdot Im\left(\frac{m^2-1}{m^2+2}\right), \qquad (2)$$

where r is the NP radius, and m is the complex refractive index. For bulk Si, $\epsilon(\lambda, T)$ data is available up to 1800 K,[61] however, surface and defect states modify NP emissivities significantly, and ϵ also will evolve as the NPs react under oxidizing conditions. Because the correct $\epsilon(\lambda, T_{NP})$ is unknown, we approximate it by a power law previously shown[55-56] to give reasonable spectral fits: $\epsilon(\lambda, T_{NP}) \propto \lambda^{-n}$, where n is a fitting parameter. With this approximation to ϵ, the thermal emission model function is:

$$I(\lambda, T_{NP}) = \frac{K \cdot \lambda^{-(4+n)}}{\exp\left(\frac{hc}{\lambda k T_{NP}}\right) - 1} \qquad (3)$$

This has just two adjustable parameters, T_{NP} and n, that affect the spectral shape (K is determined by normalization). The uncertainty in the extracted T_{NP} values has been analyzed in detail, [56] and for spectra with reasonable signal-to-noise, as here, T_{NP} was estimated to have absolute uncertainty of ±6.2%, with ~±2% uncertainty for comparing T_{NP} values extracted from spectra with similar shapes (also true here).

In addition to extracting T_{NP}, we are also interested in the intensity of the NP spectra and how that changes with T_{NP} and time under reactive conditions. We will mostly present and discussed "integrated emission intensities", I_{NP}, determined by simply integrated the emission spectra over 600 to 1580 nm. Emission intensity scales like the emitting surface area for a macroscopic black body, and **Eqn. 2** shows that there is an additional factor of r in the emissivity for small NPs, thus NP emission intensities should scale roughly like the NP volume, i.e., roughly as the NP mass. Thus, mass scaling provides a simple way to compare emission intensities for different size NPs, or for a single NP at different stages of etching. Because emissivity and absorptivity (for laser heating) are related, both should scale similarly with NP size.

C. NP Sample Preparation and Reactant Gases

The Si NP feedstock is reported to consist of roughly spherical NPs with a nominal diameter of ~30 nm, and purity of ≥ 98.5% (*Skyspring Nanomaterials #9717HK*). A 30 nm sphere with the bulk Si density (2.329 g/cm^3) [62] would have a mass of ~20 MDa. Listed impurities are: O < 1%, Mg = 0.1%, Ca = 0.1%, Al = 0.05%, Ni = 0.07%, Fe = 0.03%, and Cu = 0.001%. Samples are prepared for electrospray ionization (ESI) by adding the Si nanopowder to a ~2.0 mM ammonium acetate solution in HPLC-grade methanol and sonicating for five minutes to form a dilute suspension. As introduced into vacuum, the NPs probably have excess ammonium acetate and methanol on their surfaces, however, these should desorb or decompose to gaseous products

well below the T_{NP} range of interest here. Typical NPs have a few dozen charges, with $Q/M < 10^{-5}$ e/Da. For this low level of NP charging, neither the emission spectra nor the kinetics show measurable effects of the charge state, as shown by experiments in which Q changed spontaneously during reaction under constant T_{NP} conditions.

The reactant gases used in the experiments are ultra-high purity (UHP) grade Ar and O_2, handled in metal-gasketed stainless steel lines. The total pressure in the trap vacuum chamber is typically in the 10^{-3} Torr range (mostly Ar), monitored using a capacitance manometer with resolution of ~10^{-6} Torr, and the chamber base pressure is ~10^{-7} Torr, monitored by a cold cathode ionization gauge (turned off during experiments).

III: Results

Experiments were done to probe the effects on reactivity of varying T_{NP}, melting the NP, and varying the oxygen partial pressure (P_{O2}), as well as studying the evolution of reactivity over time. In some experiments, NPs were heated in inert atmosphere prior to oxidation to probe sublimation kinetics and examine the effects of pre-heating and pre-melting on subsequent etching. Each experimental protocol is demonstrated for a single NP below. Additional examples are presented in the SI, and the results from all experiments are aggregated and discussed at the end of the **Results** section.

A. Silicon NP Emission Spectroscopy and Sublimation Kinetics

Before discussing O_2 etching, it is important to understand Si NP behavior when heated in inert atmosphere, including sublimation, changes in optical properties, and reactions with background gases. **Fig. 1A** shows an experiment in which a Si NP with $M_{initial} \approx 88.3$ MDa was trapped in ~2.0 mTorr of UHP argon, added to damp NP motion to allow more rapid mass measurements. Both M and the integrated emission intensity, I_{NP}, were measured every 30 seconds

as T_{NP} was ramped up and down in 100 K steps, passing through the bulk Si melting point (1687 K). [63] Prior to the start of the record shown, the NP had been held at ~1200 K and Q-stepped (**Fig. S1**) but never heated above 1200 K. Mass loss rates were determined by linear fits (blue lines) to the M vs. time data (open circles) for each constant T_{NP} period. For time periods when M vs. time showed significant curvature (e.g. III, IV, and V), the linear fits provide the average rate for each period. In **Fig. 1B**, we plot the rates, R, extracted from the fits, as ln(R) vs. $1000/T_{NP}$, with a T_{NP} scale at the top. Colors denote the heating/cooling ramps, and points shared between heating/cooling ramps are indicated by bi-colored symbols. R is given in terms of Daltons lost *per* second *per* nm^2 of NP surface area, using surface areas estimated from the average mass in each time period, assuming spherical shape with the bulk Si density (2.329 g/cm^3). [62]

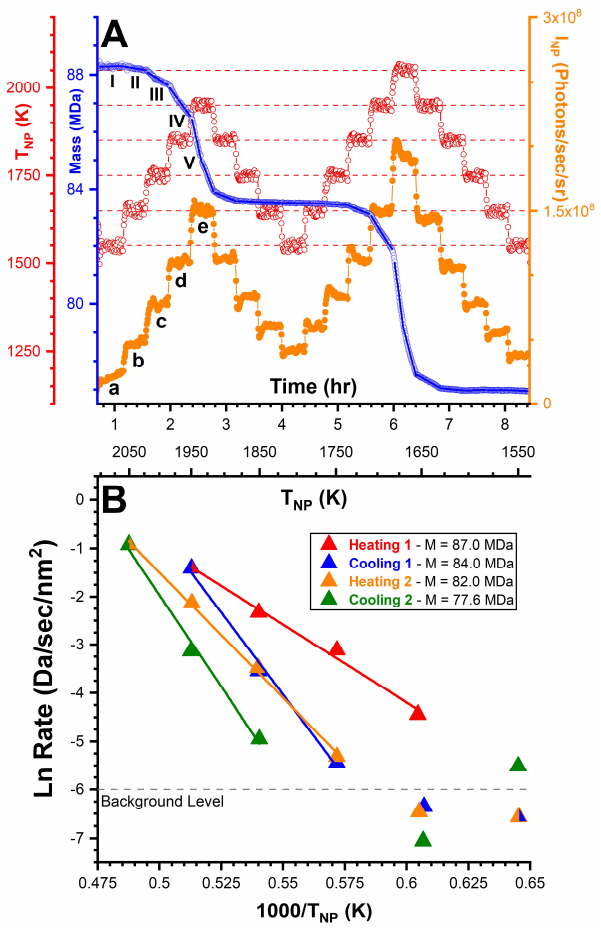

Figure 1: A). A Si NP was T_{NP} ramped in argon causing the NP to sublime at high T_{NP} values. I_{NP} is also plotted with time. B). Mass loss rates vs. T_{NP} for heating/cooling ramps.

$M_{initial}$ would correspond to a single spherical NP of ~49 nm diameter, however, the reported average diameter of the feedstock was 30 nm, (~20 MDa), thus it is likely that the NP was initially an aggregate of a few primary particles. Given that T_{NP} was ramped through the bulk T_{melt} (1687 K), the NP would have melted and coalesced early in the first heating ramp. Thus, the

assumption of spherical shape in calculating R should be a good approximation once the NP melted.

For all ramps, the mass loss rates for $T_{NP} \leq$ ~1650 K were small, with no obvious dependence on T_{NP}, and we attribute this mass loss primarily to etching reactions with species such as H_2O and O_2 present in the chamber background, and we will refer to this mass loss rate as $R_{background}$. At higher T_{NP}, the mass loss rates increased sharply with T_{NP}, with the rates in each of the four ramps well fit by the Arrhenius form: $R=A\cdot\exp^{\frac{-Ea}{kT}}$, i.e., they result from endothermic desorption processes. The mass loss rates during the "Heating 1" ramp were much higher than at the same temperatures during subsequent ramps, suggesting that in addition to Si sublimation, there was significant desorption of surface contaminants as the NP was heated for the first time. Volatile contaminants like methanol or ammonium acetate from the ESI process would have desorbed at even lower temperatures, but oxides/hydroxides present on the as-introduced NP surface would be expected to desorb in this T_{NP} range. [32, 42-43, 47-48] Studies of decomposition and desorption of silica films on bulk Si suggest that there should have been little or no oxygen remaining on the surface after ~20 minutes at 1900 K, [36, 42] i.e., after the Heating 1 ramp the main mass loss process would have been Si sublimation, with some contribution from background reactions, significant only at the lower temperatures. The kinetics continued to slow during the experiment, as the NP lost ~11.4 MDa (~12.9% of $M_{initial}$) corresponding to ~4 monolayer's worth of material for a spherical NP of this mass. Most of this mass loss occurred at $T_{NP} > 1750$ K, i.e., well above the bulk T_{melt}.

As expected for thermal emission, the emission intensities (**Figs. 1A, S2,** and **S3**) increased and decreased with T_{NP}, however, the changes were only partly reversible. Particularly at the lower T_{NP} values, the integrated intensities (I_{NP}) were substantially lower during the Heating 1

ramp (**Fig. 1A**, a – d), compared to later ramps, even though the NP lost mass and its surface area had presumably decreased due to melting/coalescence during the first ramp. The emission brightening is also obvious as increases in I_{NP} at constant T_{NP} during the first few steps in the Heating 1 ramp. The effects on emission brightening on the spectra during all four ramps are shown in **Fig. S2**, and the changes in the "n" fitting parameter and in the heating laser power required to reach each T_{NP} value are shown in **Fig. S3**. The initial heating of the NP resulted in a substantial increase in its emissivity (~2x at low T_{NP}), but the spectral shape showed only modest effects.

Fig. S4 shows the sublimation kinetics for another, larger Si NP (a larger aggregate NP) studied with the same protocol as in **Fig. 1**. Because the mass loss rates are normalized to the nominal (spherical) NP surface area, they should be roughly comparable. In fact, the sublimation rates were similar for the two NPs at all T_{NP} values during the "Heating 1" ramp (red) but decreased less in subsequent ramps for the larger NP from **Fig. S4**. As in **Fig. 1**, I_{NP} at the lower T_{NP} values increased after the Heating 1 ramp but remained roughly constant thereafter.

There are several factors that probably contributed to the slowing of the sublimation rates and the irreversible emission brightening, which occurred primarily as the NPs were first heated. Both NPs were probably aggregates with substantially higher surface areas than spherical NPs of the same mass. Because the area-normalized rates in the lower frames of the figures are based on surface areas of spherical NPs, the initial rates for aggregates would have been artificially enhanced, with the enhancement disappearing as T_{NP} increased through the bulk T_{melt} (1687 K) as the aggregates melted and coalesced. Another factor is, as discussed above, the native oxide layers present on the air-exposed NPs would have desorbed during the first heat ramp[42] as ~5% of $M_{initial}$ sublimed away (~1 ML's worth of SiO_2). This change in surface composition may also have

affected the NP emissivity. There may also have been a contribution from changes in the NP bulk structure or development of a strained surface layer as the NPs were heated above T_{melt}.

In the T_{NP} ramp experiments, the largest changes in both sublimation behavior and emissivity occurred as the NPs were first heated above T_{melt}, but both experiments had low total mass losses (12.9% in **Fig. 1**, 5.2% in **Fig. S4**). An obvious question is whether further changes in sublimation rates or optical properties might occur if sublimation were continued, removing a larger fraction of $M_{initial}$. **Fig. S5** shows an experiment in which a ~48 MDa Si NP was first pre-heated to 2000 K to clean and melt it, charge stepped at $T_{NP} \approx 1300$ K then held in argon at 1900 K for ~7.5 hours, subliming away ~36% of $M_{initial}$. The initial 1900 K $R_{sublimation}$ was ~0.2 Da/sec/nm^2, which is in the same range as the NPs in **Figs. 1** and **S4** *after* the 1st ramps, indicating that 2000 K pre-heating had similar effects to a T_{NP} ramp (melting, desorbing contaminants). $R_{sublimation}$ remained nearly constant over the ~7.5 hour 1900 K period, indicating that the surface structure and its sublimation energy were stable as ~9 ML's worth of material sublimed, which is unsurprising for a molten nano-droplet. Interestingly, however, the NP optical properties evolved noticeably even though the rates were constant. I_{NP} gradually dropped by ~20%, however, the NP lost 36% of its initial mass, thus the NP emissivity dropped less than would be expected from volume/mass scaling. The laser power required to hold the NP at 1900 K increased by ~19%.

B. O_2 Oxidation of Silicon NPs: T_{NP} and P_{O2} Dependence

Our main interest is understanding the oxidative etching of Si NPs, how it evolves under different conditions, and what effect this has on NP optical properties. Raw mass loss rates measured with O_2 present were corrected for the much smaller baseline mass loss rates ($R_{base} = R_{sublimation} + R_{background}$), obtained by measured mass loss rates with no added O_2 before and after each oxidative etching period. The R_{base}-corrected oxidative mass loss rates, R_{oxid}, are reported in

terms of Da/sec/nm^2 of nominal (spherical) NP surface area, the process is illustrated in **Fig. S6**. One question is whether the NP emissivity changes significantly under inert vs. oxidizing conditions, and **Fig. S7** demonstrates that neither the intensities nor shapes of NP emission spectra change significantly when comparing spectra measured just before and after starting and stopping O_2 flows into the trap.

Stepped T_{NP} ramp oxidation experiments were done to examine the T_{NP} dependence of R_{oxid}. Prior to the start of the time record shown in **Fig. 2A**, a Si NP was trapped, pre-heated above 1650 K (just below the bulk T_{melt}) for ~2 minutes to desorb contaminants, then held at 1500 K for Q stepping, which found $M_{initial}$ to be 94.8 MDa. T_{NP} was then ramped from 1200 to 1800 K in 100 K steps, holding each T_{NP} for ~30 minutes, during which the mass loss rates were measured in

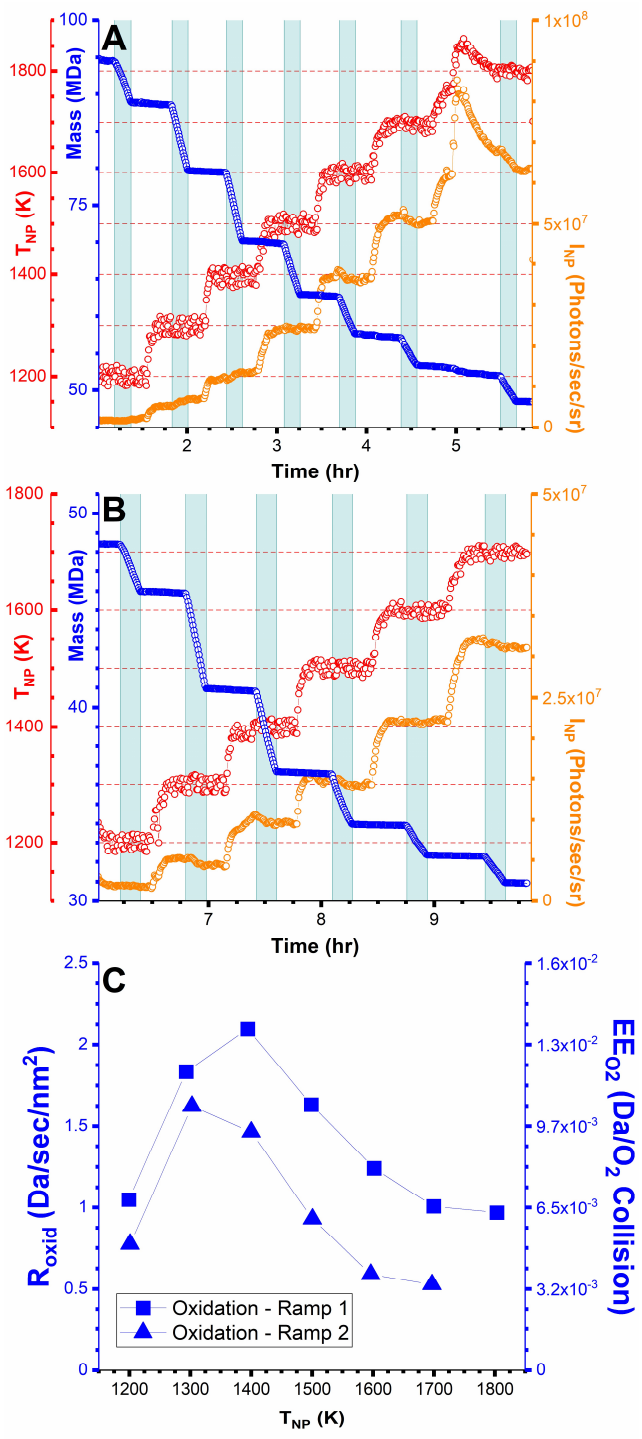

Figure 2: A). A Si NP has both R_{base} and R_{oxid} measured from T_{NP} = 1200 – 1800 K. B). A 2nd T_{NP} ramp is carried out. C). R_{oxid}/EE_{O2} plotted vs. T_{NP} for both ramps.

argon, then with 4.3 x 10^{-5} Torr of O_2 added to the argon (cyan background), then again in argon. R_{oxid} values were calculated from the mass loss rates with O_2 added, minus the average of the R_{base} measurements taken before and after the oxidation periods. Even under the least reactive conditions, $R_{oxid} \gg R_{base}$, as shown by the large increases in slope of M vs. time when O_2 was added. The NP was then cooled back to 1200 K, and a 2nd stepped heating ramp was carried out (**Fig. 2B**).

The R_{oxid} values are plotted vs. T_{NP} in **Fig. 2C**. In the first T_{NP} ramp, R_{oxid} more than doubled between 1200 K and 1400 K, then declined slowly at higher T_{NP}. The R_{oxid} data show no dramatic changes in trend for T_{NP} above and below T_{melt} (1687 K). The mass loss in the first ramp was ~49% of $M_{initial}$. R_{oxid} had similar T_{NP} dependence in the second ramp, but the magnitudes were lower than in the first ramp, even though R_{oxid} is area-normalized to approximately account for decreasing NP size. Roughly two thirds of $M_{initial}$ etched away during the two ramps.

To allow comparisons with experiments at different O_2 pressures, and to give an idea of how efficiently O_2 etches hot Si NPs, R_{oxid} was converted to an etching efficiency, EE_{O2}, given in terms of Daltons of mass lost *per* O_2 collision. EE_{O2} is simply R_{oxid} divided by the O_2 collision rate *per* nm^2 (~154 O_2 collisions/sec/nm^2 for P_{O2} = 4.3 x 10^{-5} Torr). The EE_{O2} scale is shown on the right axis in **Fig. 2C**, showing that at maximum, $EE_{O2} \approx$ 1.36 x 10^{-2} Da/O_2 collision.

A second experiment of this type, on another Si NP with 53.7 MDa initial mass, is shown in **Fig. S8**. In this example, R_{oxid} during the first T_{NP} ramp was nearly constant at ~0.58 Da/sec/nm^2 (EE_{O2} = 3.8 x 10^{-3} Da/O_2 collision) from 1200 – 1400 K, then dropped gradually to ~0.24 Da/sec/nm^2 (1.6 x 10^{-3} Da/O_2 collision) by 1700 K. In the second T_{NP} ramp, the rate at 1200 K was ~40% lower than in the first ramp, however, for the other temperatures the rates during the two ramps were nearly identical.

Oxidative etching also changed the emission intensities of these NPs significantly, but the changes are just what would be expected from decreasing NP size. For the NP in **Fig. 2**, for example, the I_{NP} values during the second T_{NP} ramp were roughly a factor of 2 smaller than in the first ramp, but the mass had also decreased by a factor ~2, and as discussed above, all else being equal, I_{NP} should scale like M. For the NP in **Fig. S8**, I_{NP} decreased by only ~10% between the two ramps, but the mass loss in the first ramp was also smaller – only ~18 %. This behavior contrasts with the substantial *increases* observed under sublimation conditions, however, that probably reflects the fact that the NPs in the oxidation experiments had been preheated, and most of the initial I_{NP} brightening had presumably occurred then.

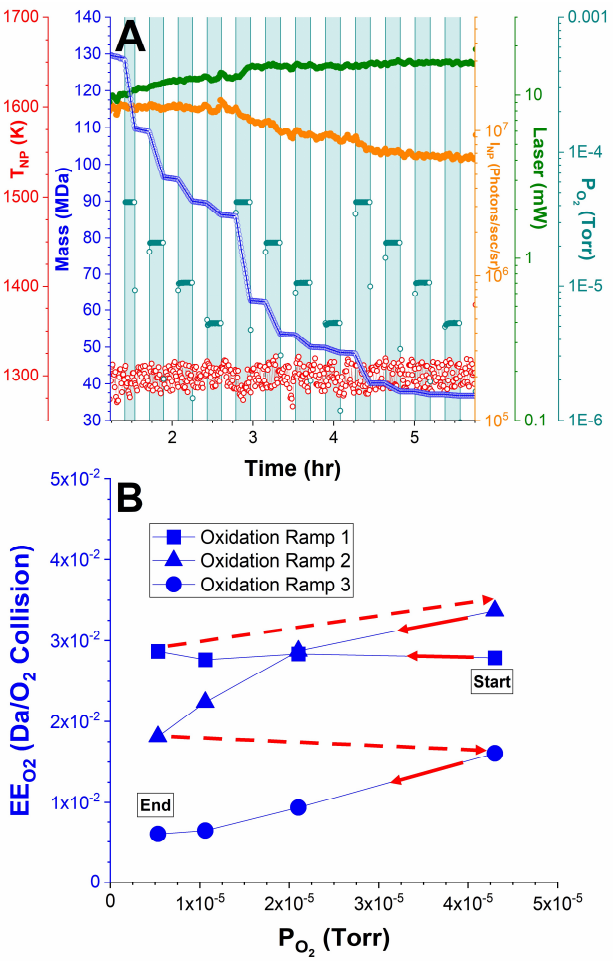

Figure 3: A). A Si NP is held at T_{NP} = 1300 K as P_{O2} is stepped downward three times from 4.3 x 10^{-5} – 5.3 x 10^{-6} Torr. B). EE_{O2} vs. P_{O2} for all ramps.

Fig. 3A shows an experiment where T_{NP} was held constant at 1300 K, near the reactivity peak in **Figs. 2** and **S8**, and P_{O2} was stepped. Before the time record shown, the NP had been Q-stepped at T_{NP} < 1300 K. The NP was an aggregate with $M_{initial}$ = 129.7 MDa, and P_{O2} was stepped ***down*** from 4.3 x 10^{-5} Torr to 5.3 x 10^{-6} Torr, each step corresponding to a ~50% decrease in pressure. Between each step, the O_2 was shut off to allow measurements of R_{base}. At 1300 K,

sublimation is negligible, and $R_{oxid} \gg R_{base}$, even for the lowest O_2 pressures. The P_{O2} ramp was repeated a total of three times to allow evolution of the oxidation behavior to be observed. The total mass loss (~72%) was quite large, with ~34% lost in the first ramp, an additional ~29% during the second ramp, but only ~9% lost in the final ramp. If we assume that the NP was spherical and etched uniformly, the total mass loss would correspond to removing >20 ML's worth of material.

EE_{O2} is plotted versus P_{O2} in **Fig. 3B** for the three ramps. From the raw M vs. time data in **Fig. 3A**, the etching kinetics obviously slowed over time, thus it is important to view **Fig. 3B** with the time sequence in mind, as indicated by red arrows superimposed on the figure. During the first P_{O2} ramp, EE_{O2} was nearly P_{O2}-independent at ~2.85 x 10^{-2} Da/O_2 collision. At the beginning of the second ramp (at high P_{O2}), EE_{O2} (~3.4 x 10^{-2} Da/O_2 collision) was ~20% higher than at the start of the first ramp, but reactivity decreased significantly as the ramp proceeded, and the decrease continued in ramp 3, such that the final EE_{O2} was only ~20% of that in ramp 1. Because EE_{O2} approximately accounts for the effect of decreasing NP surface area, the decrease indicates a substantial reduction in reactivity toward O_2 during the experiment, occurring primarily during ramps 2 and 3.

I_{NP} dropped by ~60% over the course the experiment and M decreased by ~70%, i.e., roughly as expected by volume scaling. Note, however, that if I_{NP} scaled with the NP volume/mass, I_{NP} would have decreased by ~33% during the first ramp (but was actually constant), by another ~43% during the 2nd ramp (actual decrease = 42%), and then decreased by another ~24% during the final ramp, (roughly as observed). Thus, the optical properties of the NP appear to have changed as it oxidized, particularly during the first ramp, where I_{NP} remained large despite the large decrease in NP mass.

C. O_2 Oxidation of Silicon NPs at Constant T_{NP} and P_{O2}

Ramping experiments allow T_{NP} and P_{O2} effects to be surveyed, but quantitative interpretation is complicated because the NPs clearly evolved during the experiments, becoming less reactive over time. To allow NP evolution to be observed more clearly, a set of simpler experiments was done in which NPs were allowed to react over time at constant T_{NP} and P_{O2}. **Fig. 4A** shows an experiment for a 62.5 MDa Si NP. Prior to the start of the data record shown, the NP was trapped, briefly heated to 1200 K to desorb contaminants, and Q-stepped at low T_{NP}. T_{NP} was then set to 1350 K (near the peak reactivity observed in the T_{NP} ramps) for the remainder of the experiment. M vs. time was monitored briefly in 2 mTorr of argon to obtain R_{base}, and then with 4.3 x 10^{-5} Torr of O_2 added for ~4.7 hours, ending with another Ar-only period for a final R_{base} measurement. **Fig. 4B** plots the EE_{O2} values extracted by linear fits to time periods with constant slopes of M vs. time. EE_{O2} was nearly constant at ~5 x 10^{-3} Da/O_2 collision for the first ~2 hours, slowly decreased up to the ~4 hour point, then abruptly decreased to <1% of the initial EE_{O2} for the last ~1.5 hours of the experiment. Based on the bulk Si etching literature, passivation is attributed to formation of a

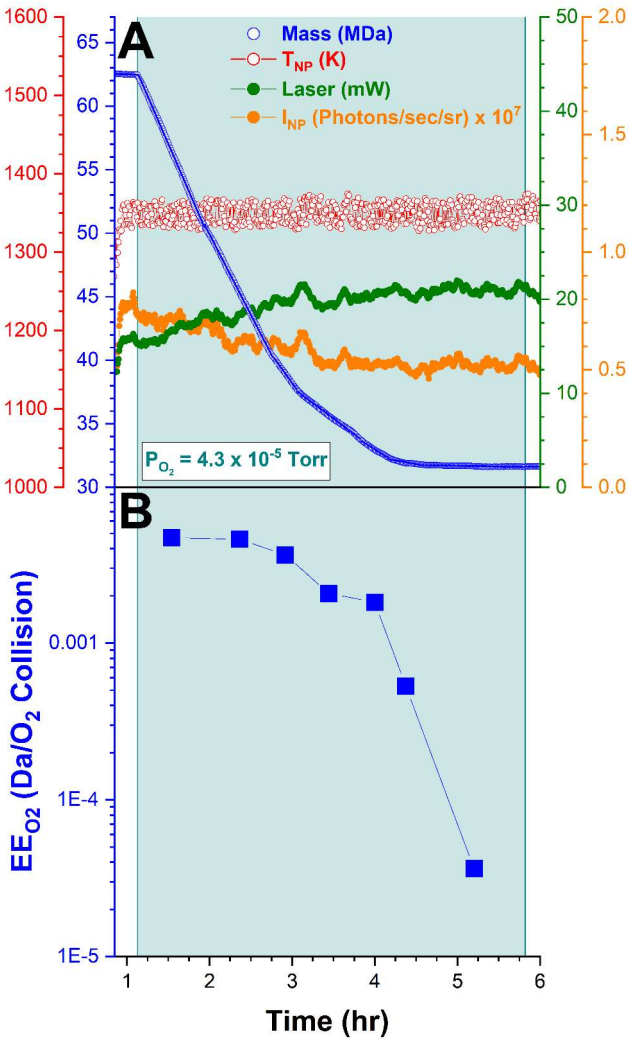

Figure 4: A). A Si NP at T_{NP} = 1350 K and P_{O2} = 4.3 x 10^{-5} (cyan region). B). Evolution of EE_{O2} vs. time.

stable surface oxide layer that prevents additional O_2 sticking/etching. EE_{O2} during this final period was near our sensitivity limit (~10^{-6} Da/O_2 collision), determined by our ability to measure the small change in the slope of M vs. time when the O_2 was turned off at the end of the oxidation period.

Similar experiments were done at T_{NP} values ranging from 1200 K to 1750 K. **Fig. S9** shows an example for oxidation at 1500 K. This 1500 K oxidation experiment was done following the experiment outlined in **Fig. S6**, i.e., the NP had been pre-heated at 2000 K, brief sublimation and oxidation periods were examined at 1800 K and 1500 K. Prior to the start of the experiment shown in **Fig. S9**, the NP was again briefly held at 2000 K to re-melt the NP and desorb any oxide present, then T_{NP} was set to 1500 K and held for a ~4.4 hour oxidation period. EE_{O2} was initially high (~2.5 x 10^{-3} Da/O_2 collision) and was nearly constant for ~2.5 hours as ~30% of the initial mass was lost, then EE_{O2} decreased by two orders of magnitude, eventually dropping to our sensitivity limit. The behavior was quite similar to that observed at 1350 K (**Fig. 4**), but with slightly lower initial EE_{O2} and slightly faster passivation.

Different behavior was observed at both higher and lower T_{NP}. **Fig. 5** shows an experiment in which a Si NP of ~71.4 MDa was first oxidized at 1750 K, then again at 1200 K, in ~4 hour oxidation periods. The experiment began by trapping and Q-stepping the NP at 1200 K in argon (not shown) to determine $M_{initial}$. T_{NP} was then set to 1750 K, R_{base} was measured in argon, and then 4.3 x 10^{-5} Torr of O_2 was added. The initial 1750 K EE_{O2} was ~2.6 x 10^{-3} Da/O_2 collision, i.e., significantly slower than the 1350 K EE_{O2} from **Fig. 4**, as expected from the T_{NP} dependences observed in **Figs. 2** and **S8**. Unlike the behavior at 1350 K, at 1750 K EE_{O2} started to decrease immediately after O_2 exposure but the decrease was slow and EE_{O2} remained well above our sensitivity limit even at the end of the >4 hour 1750 K oxidation period. If passivation results from

formation of a thermally stable oxide layer, the behavior here suggests that surface oxide formation is much slower, presumably because oxide formation is in competition with oxide decomposition/desorption at 1750 K. [50-51] An experiment probing oxide layer desorption at high T_{NP} is described below. The decrease in EE_{O2} at 1750 K was accompanied by modest increases in both I_{NP} and the laser power required to maintain T_{NP}, mostly during the initial ~20 minutes when etching was fastest. At the end of the 1750 K oxidation period, the NP was held in argon for ~15 minutes to re-measure R_{base} and to clean the NP by allowing surface oxides to desorb while the NP was molten.

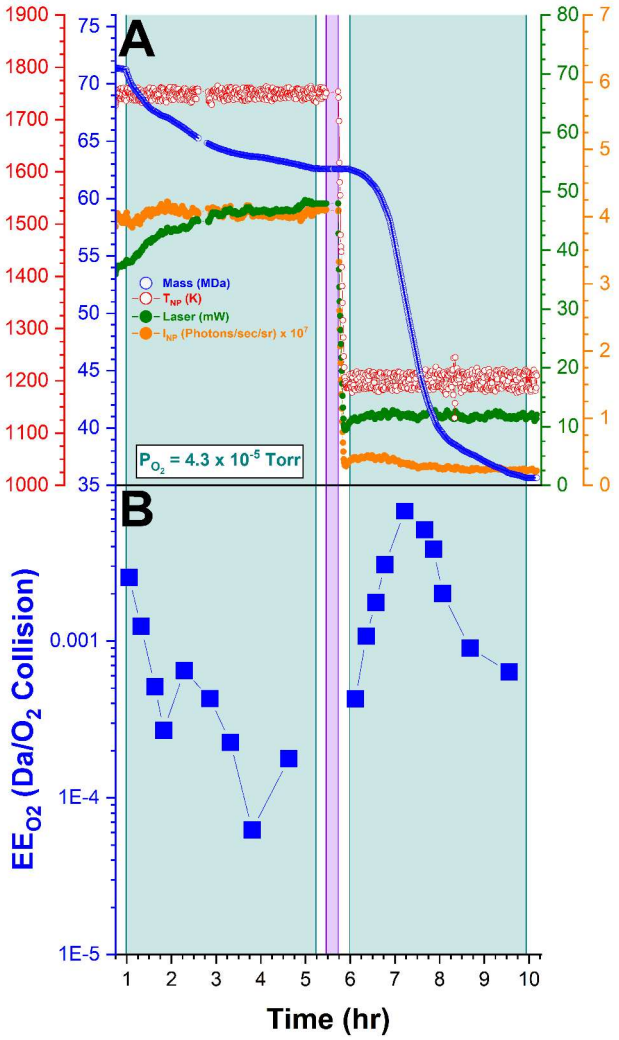

Figure 5: A). A 71.4 MDa Si NP is oxidized at P_{O2} = 4.3 x 10^{-5} Torr under T_{NP} values of 1750 K and 1200 K. I_{NP} and laser power are also tracked to show their evolution as the NP etches. B). EE_{O2} vs. time is shown to decrease at 1750 K, but increase and then decrease at 1200 K.

The short data gap at ~2.5 hours resulted from temporarily losing the secular frequency lock, due to a spontaneous Q step. Therefore, at the end of the ~1750 K period, the NP was Q stepped (purple background) to confirm the correct Q. The NP was then cooled to 1200 K, and R_{base} was measured to be below our detection limit. When O_2 was again introduced, EE_{O2} was initially ~4 x 10^{-4} Da/O_2 collision, i.e.,

substantially smaller than the initial EE_{O2} values observed at 1200, 1300, and 1350 K in **Figs. 2**, **3**, and **4**. EE_{O2} gradually increased by a factor of nearly 20 over the first ~hour of etching, reaching ~6.8 x 10^{-3} Da/O_2 collision, before dropping back to ~6 x 10^{-4} Da/O_2 collision at the point when the experiment was terminated.

The substantial increase in etching rate during the first hour of 1200 K oxidation was unexpected, therefore a similar (shorter) experiment (**Fig. S10**) was carried out for a 133 MDa Si NP. In this case, the NP was pre-heated to 1900 K for cleaning/melting, and then Q-stepped at low T_{NP}. When T_{NP} was set to 1750 K and 4.3 x 10^{-5} Torr of O_2 was added, the initial EE_{O2} was ~2.6 x 10^{-3} Da/O_2 collision – nearly identical to the 1750 K value in **Fig. 5**. As in **Fig. 5**, EE_{O2} immediately began dropping, in this case falling by a factor of ~5 in 1.4 hours (but remaining well above baseline). When T_{NP} was dropped to 1200 K and O_2 was reintroduced, the initial EE_{O2} was again small (~7 x 10^{-4} Da/O_2 collision) but as in **Fig. 5**, it increased as the NP etched, and was still increasing when the experiment was terminated after a ~0.8 hour oxidation period. Thus, this second experiment replicated both the non-passivating behavior at 1750 K, and the initially-low-but-increasing EE_{O2} at 1200 K.

To test whether the unexpected behavior at 1200 K resulted from changes during the preceding 1750 K oxidation periods, experiments were done in which freshly trapped NPs were oxidized at 1200 K without prior oxidation periods. For example, **Fig. 6** shows an experiment in which a Si NP was trapped and heated to T_{NP} = 2000 K in argon for ~10 minutes to melt and clean the NP, then Q-stepped at ~1200 K, giving $M_{initial} \approx$ 60.2 MDa. The NP was briefly re-heated to ~1900 K to desorb any species that might have adsorbed during Q stepping, subliming ~0.3 MLs' worth of material, and then T_{NP} then was set to ~1200 K, R_{base} was measured (~zero), then O_2 was added and the etching reaction was followed for ~6 hours. The initial EE_{O2} was again small (~8.9

x 10^{-4} Da/O_2 collision) but increased by nearly an order of magnitude during the first 1.3 hours, reaching 8 x 10^{-3} Da/O_2 collision. EE_{O2} then began to decline, and in this case the experiment continued long enough to observe EE_{O2} dropping by more than three orders of magnitude after ~5 hours of etching. The similarities to the 1200 K oxidation results in **Figs. 5** and **S10** indicate that the low-but-increasing initial EE_{O2} was not due to prior oxidation at 1750 K, and also suggest that if the experiments in **Figs. 5** and **S10** had been allowed to continue longer, the NPs would eventually have passivated to below our sensitivity limit. I_{NP} in **Fig. 6** decreased substantially during the long oxidation period, but most of the decrease occurred during periods when EE_{O2} was large, as the NP mass/volume decreased by >70 %, i.e., the decrease was mostly attributable to the decreasing emitter size.

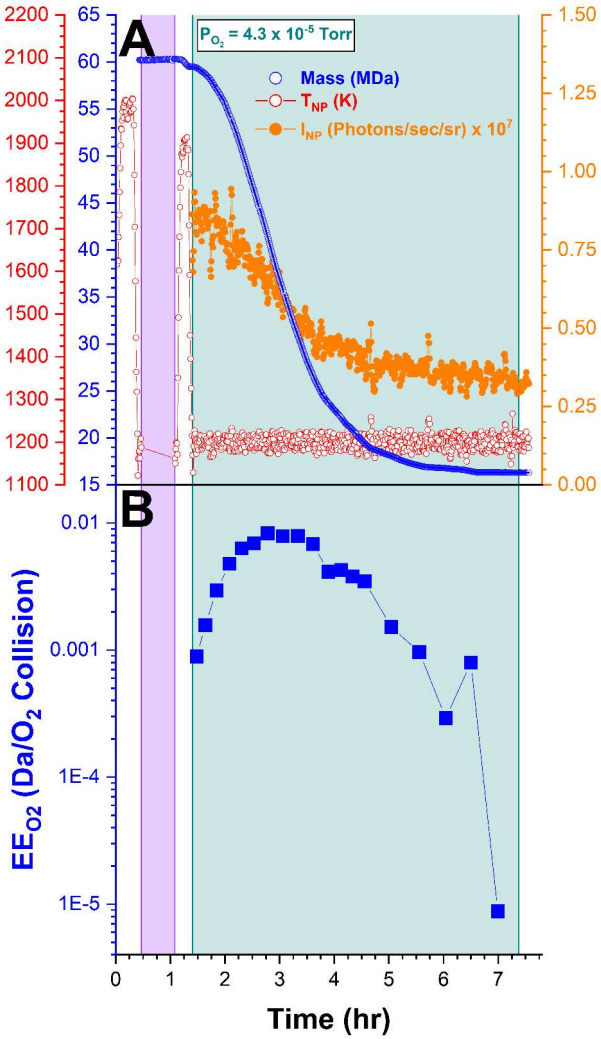

Figure 6: A). A Si NP is pre-heated to 2000 K, Q-stepped, and then re-heated to 1900 K before exposing to O_2 at 1200 K. The NP is then allowed to etch for ~7 hours. B). EE_{O2} vs. time is shown depicting how the oxidation kinetics initially increase followed by a slow decrease indicating passivation of the NP's surface.

Several shorter 1200 K experiments were also done just to examine the initial behavior of EE_{O2}. The experiment in **Fig. S11** was done immediately following the sublimation experiment in **Fig. 1**, i.e., the pre-heating/cleaning for this NP was done in the process of stepping T_{NP} (in argon) to 2050 K, driving sublimation of ~12.7% of the NP initial mass. Similarly, the experiment in **Fig. S12** followed the sublimation experiment in **Fig. S4**, during which T_{NP} had been stepped to 1950 K, subliming ~5% of the initial mass. In both experiments, the EE_{O2} values when O_2 was first introduced at 1200 K were small (~10^{-3} Da/O_2 collision) but increased substantially as the NP began to etch.

Finally, the experiment in **Fig. S13** was done to see if the unexpected 1200 K initial oxidation behavior resulted from the NPs in **Figs. 5**, **6**, and **S10-S12** all having been pre-heated prior to the EE_{O2} measurement. In **Fig. S13**, an NP was trapped and Q-stepped without ever heating above 1200 K, i.e., it was not melted and may have had some surface oxide present. At the beginning of the data record shown, R_{base} was measured at ~1200 K (~zero), then 4.3 x 10^{-5} Torr of O_2 was added for ~1 hour to measure the initial EE_{O2} behavior, with T_{NP} held at 1200 K with a few minor fluctuations. The initial EE_{O2} was ~4.7 x 10^{-3} Da/O_2 collision, i.e., substantially higher than in the 1200 K experiments with pre-heated NPs, but similar to the initial 1200 K EE_{O2} value observed in the T_{NP} ramp experiment from (**Fig. 2**), which also examined an NP that had not been heated above T_{melt} prior to the start of 1200 K oxidation. EE_{O2} was constant for ~20 minutes, then increased to ~1.0 x 10^{-2} after ~1 hour of oxidation, at which point the experiment was ended.

To summarize, NPs that had been held in inert atmosphere at $T_{NP} > T_{melt}$ had unexpectedly small initial EE_{O2} values when etched at 1200 K, however, EE_{O2} increased over time, eventually reaching values comparable to those observed in the 1350 – 1500 K range. For NPs that were not previously heated above T_{melt}, the initial 1200 K EE_{O2} values were substantially higher than for

pre-heated NPs, but EE_{O2} did not increase as much over time. At 1200 K, the NPs all lost >50% of $M_{initial}$ and eventually passivated if the experiments continued long enough, with EE_{O2} dropping by several orders of magnitude. For intermediate temperatures (1350 to 1500 K), the initial EE_{O2} values were large, even for pre-heated/melted NPs, and etching rates were roughly constant for several hours, removing 30 to 50% of $M_{initial}$. All NPs oxidized in the 1350 to 1500 K range also passivated if the oxidation period was long enough. For 1750 K, the initial EE_{O2} values were lower, as might be expected from the T_{NP} ramp experiments in **Figs. 2** and **S8**, and they slowly decreased with time, but they never passivated, i.e., EE_{O2} remained an order of magnitude above our sensitivity limit. Assuming that passivation results from formation of a stable SiO_2 surface layer, it appears that such a layer eventually formed for oxidation temperatures ≤ 1500 K, but for 1750 K the NPs only partially passivated.

D. Low P_{O2} and CO_2 Laser "Flash" Heating to Probe Silicon NP O_2 Reactivity

The experiment in **Fig. 7** was done to examine O_2 etching at temperatures well below 1200 K, and to examine the stability of a passivating oxide layer above 2000 K. An NP was trapped, Q-stepped, then T_{NP} was set to 1200 K, and both R_{base} and EE_{O2} were measured. EE_{O2} was ~8 x 10^{-5} Da/O_2 collision, at the low end of the range for 1200 K initial EE_{O2} values, suggesting that the NP, which was not preheated, might have been partly passivated by some oxide or other surface contaminant. O_2 interactions with the NP at room temperature were tested by blocking the heating laser while adding O_2 to the trap, labeled "a". We could not measure the NP mass while the laser was blocked, but when the O_2 was shut off and the laser was unblocked, returning T_{NP} to 1200 K, the NP mass had not changed significantly. If O_2 had adsorbed and either remained on the NP (as SiO_2) or desorbed as SiO when T_{NP} returned to 1200 K, the mass would have changed. Thus, either O_2 didn't adsorb, or the adsorbed O_2 simply desorbed again as T_{NP} returned to 1200 K.

Next, the heating laser power was decreased by ~70% ("b"), giving T_{NP} too low to be measured spectroscopically, but estimated to be ~875 K, as described previously. [3] Again, O_2 was added to the trap, and this time the mass was found to have decreased by 0.6% after shutting off the O_2 and returning T_{NP} to 1200 K, i.e., O_2 either etched the NP at 875 K, or formed a partially oxidized surface layer that desorbed, removing mass equivalent to ~16% of a Si monolayer as T_{NP} returned to 1200 K. After the 875 K oxidation, etching was re-measured at 1200 K to test how the low T_{NP} O_2 exposures affected subsequent reactivity, and EE_{O2} was found to be 4.5 x 10^{-5} Da/O_2 collision, i.e. about half the initial 1200 K EE_{O2} value, suggesting that partial passivation had occurred.

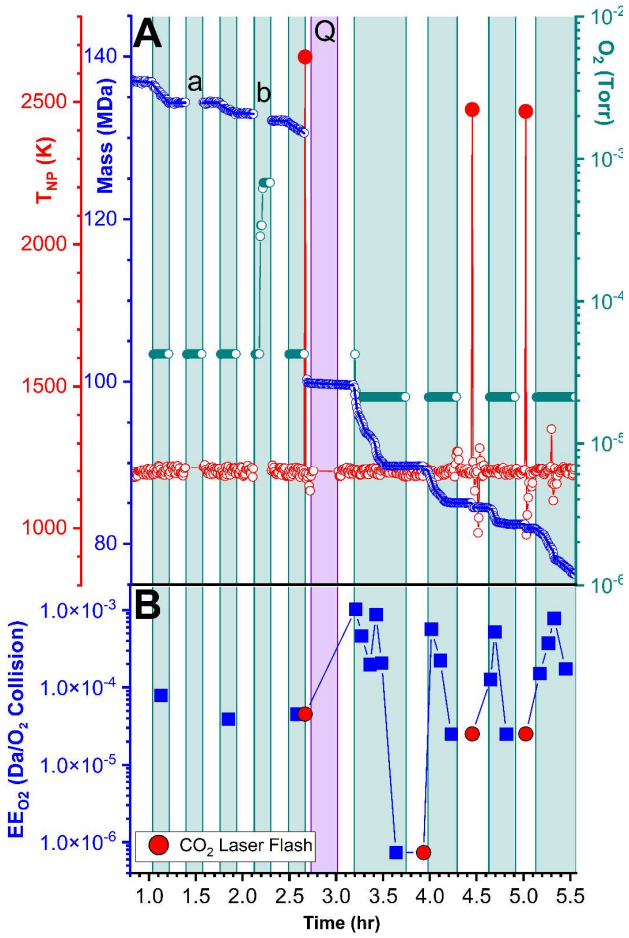

Figure 7: A). M and T_{NP} versus time for a 137 MDa Si NP exploring the effects of etching at low T_{NP}. The label "a" is oxidation of the NP at 300 K, and "b" at 875 K when P_{O2} = 4.3 x 10^{-5} Torr. After the 2.5 hour mark, the CO_2 laser was used to "flash" heat the NP to T_{NP} > 2000 K (red circles). Each flash led to an abrupt increase in EE_{O2}. B). EE_{O2} vs. time with labels of CO_2 flashes.

Next, "flash" heating was used to probe the extent to which passivation could be reversed by brief heating to ≥ 2500 K. The normal 532 nm heating laser was used to maintain T_{NP} at 1200 K, and the heating flashes were done using a 10 W, quasi-cw CO_2 laser to supplement the 532 nm layer. To avoid simply vaporizing the NP, these heating flashes (indicated by red dots in **Fig. 7B**)

were kept brief, and M was measured before and after to observe the effects. The first heating flash was to ~2700 K for 8 seconds in argon atmosphere, resulting in ~30 MDa (~25%) mass loss, and an increase in Q by +68e, the latter attributed to fast thermionic emission at high T_{NP}. From the initial mass, this NP was almost certainly a small aggregate that had not previously been heated above T_{melt}, and the magnitude of the mass loss suggests that the NP probably fragmented during the rapid heating, and presumably also sublimed and melted at 2700 K. After this initial flash, the 1200 K EE_{O2} value was found to be 1 x 10^{-3} Da/collision, i.e., ~20 times the EE_{O2} measured prior to the heating flash. EE_{O2} remained high for only ~15 minutes before abruptly dropping below 10^{-6} Da/collision, i.e., the NP passivated again quite rapidly. The NP was flash heated in argon three more times to ~2500 K (T_{NP} was not measured during the flash at the ~4 hour mark), and in each case, when the 1200 K EE_{O2} was measured, flash heating was found to have restored high reactivity, which, however, passivated on a 10 minute time scale. In these later heating flashes, the mass lost during the flashes was small – less than 1 MDa, indicating that fragmentation did not occur, presumably because the NP had melted during the first flash. In summary, heating to ≥ 2500 K clearly reactivated the passivated NP toward O_2 etching, but the NP re-passivated much more quickly than a fresh NP, suggesting that some oxide must have remained on or near the NP surface, nucleating regrowth of the passivating silica layer.

E. Summary of all Oxidation Results

EE_{O2} vs. T_{NP} and vs. Reaction Time:

All the oxidation results are summarized in **Fig. 8**, with **Fig. 8A** summarizing the T_{NP} dependence, and **Fig. 8B** focusing on the time dependence of EE_{O2} for different NPs at various T_{NP}. **Fig. 8A** includes data from the 1st and 2nd T_{NP} ramps in **Figs. 2** and **S8** (solid red and blue symbols connected by lines), as well individual data points in various color combinations that

represent the *initial* EE_{O2} values from the indicated experiments, for T_{NP} ranging from 1200 to 1800 K. Points with half-open/half-filled symbols are from experiments in which the NP was pre-heated in argon above T_{melt} prior to measuring EE_{O2} at the indicated temperatures. Solid points are from experiments in which the NP was not pre-heated. The three solid green points at 1300 K are the EE_{O2} values at the start of each P_{O2} ramp from in **Fig. 3**, i.e., the ramp 1 point is the initial EE_{O2}.

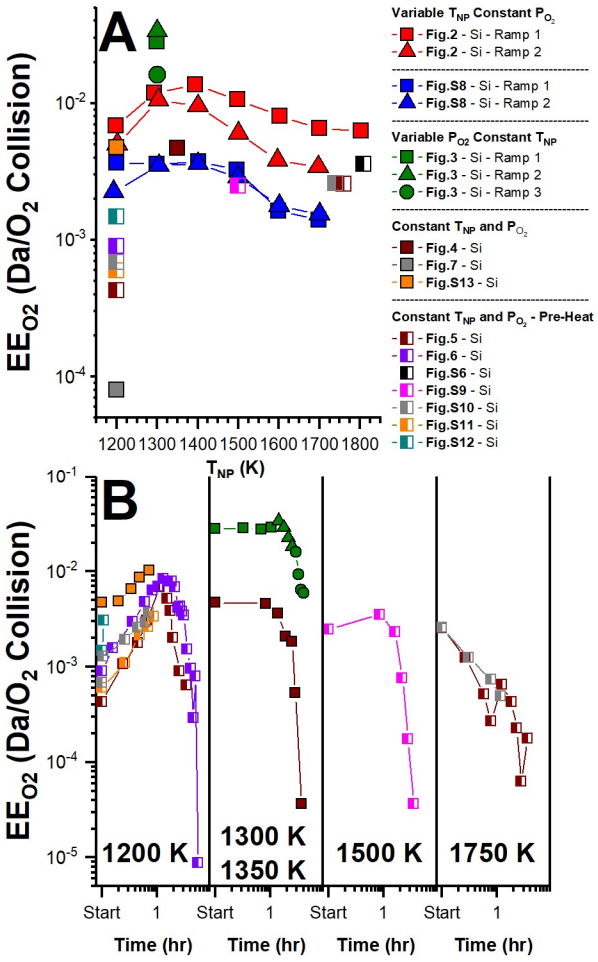

Figure 8: A). Summary of EE_{O2} vs. T_{NP}. Solid symbols indicate non-preheated NPs, with squares implying the first T_{NP} or P_{O2} ramp, triangles the second ramp, and circles the third ramp. Half-filled squares are pre-heated NPs. B). EE_{O2} vs. time at different T_{NP} values.

Fig. 8 shows that there was considerable NP-to-NP variation in both the initial EE_{O2} values and their evolution over time, but there are some systematic trends. **Fig. 8A** shows that reactivity was generally highest in the 1300 to 1400 K range. Reactivity at 1200 K was generally suppressed by preheating the NPs above T_{melt} by an average factor of roughly six, compared to non-preheated NPs. Preheating had no clear effect on EE_{O2} at 1500, 1750, or 1800 K. The NP-to-NP variations are expected, particularly for non-preheated NPs, because there would have been NP-to-NP variations in initial shapes and structure (i.e., primary vs. aggregate NPs). The variations in initial EE_{O2} values for preheated NPs was significantly smaller, and also much smaller than the variations

found for carbon NPs, [2-3] where melting is not possible, and the NP feedstocks have very different structures (diamond, graphitic, etc.).

The other point of interest is how EE_{O2} evolved as the NPs etched, shown in **Fig. 8B** for different oxidation temperatures. For all NPs in all ranges of T_{NP}, EE_{O2} declined at long reaction times, by up to three orders of magnitude, but the time dependence was different for different T_{NP} ranges. At 1200 K, all the preheated NPs started with low EE_{O2} values that increased by more than an order of magnitude during the first hour of etching, during which time, M decreased by between 10 and 30% of $M_{initial}$. EE_{O2} peaked between the first and second hours of etching, then declined at longer etching times, below our sensitivity limit for NPs allowed to react long enough. The total mass losses were in the range of 25-68% of $M_{initial}$. The lone 1200 K time-dependent experiment for a non-preheated NP gave initial reactivity significantly higher than the pre-heated NPs, but EE_{O2} increased more slowly, such that after ~20 minutes, the pre-heated NPs caught up, and after that point reactivity was similar for preheated and non-preheated NPs.

For T_{NP} in the 1300 to 1350 K range, the initial EE_{O2} values varied by a factor of ~6, however, because these NPs were not preheated, large variations were to be expected. At 1300 – 1500 K etching started at relatively fast rates that were roughly constant for about an hour (removing 27 to 35% of $M_{initial}$), then EE_{O2} decreased rapidly, dropping below our sensitivity limit in two of the experiments, and clearly heading in that direction in the third. The total mass loss as the NPs evolved to the point where mass loss became small, was between 43 and 70% of $M_{initial}$. Finally, for the two NPs etched at 1750 K, the behavior was nearly identical, as might be expected for NPs that were molten. EE_{O2} began to decrease immediately when oxidation was started, but slowly, and EE_{O2} remained well above our sensitivity limit after 4 hours. Because EE_{O2} began to

decrease immediately, the total mass losses accompanying the evolution at 1750 K were only 5 to 12%.

Evolution of NP Optical Emission:

The NP optical properties often changed as the NPs were heated and etched, and **Fig. 9A** plots the integrated emission intensity, I_{NP}, for six different Si NPs oxidized at 1200 K and constant P_{O2}, with and without pre-heating above T_{melt}. To allow comparison for NPs with very different masses, the data are plotted against $M/M_{initial}$, but the $M_{initial}$ values are given in the legend and the symbols used are the same as in **Fig. 8**. The two cases where $M/M_{initial}$ starts below 1.0 were NPs that had already lost significant mass during etching at higher T_{NP}, which also served to pre-heat them. In addition to the constant T_{NP} results, the 1200 K points from the first and second T_{NP} ramps in **Figs. 2** and **S8** are included to show how I_{NP} changed due to mass loss and melting during the first ramps. The time sequence of points in the plots runs from highest to lowest $M/M_{initial}$. To account for NP-to-NP variations in $M_{initial}$ and size reductions

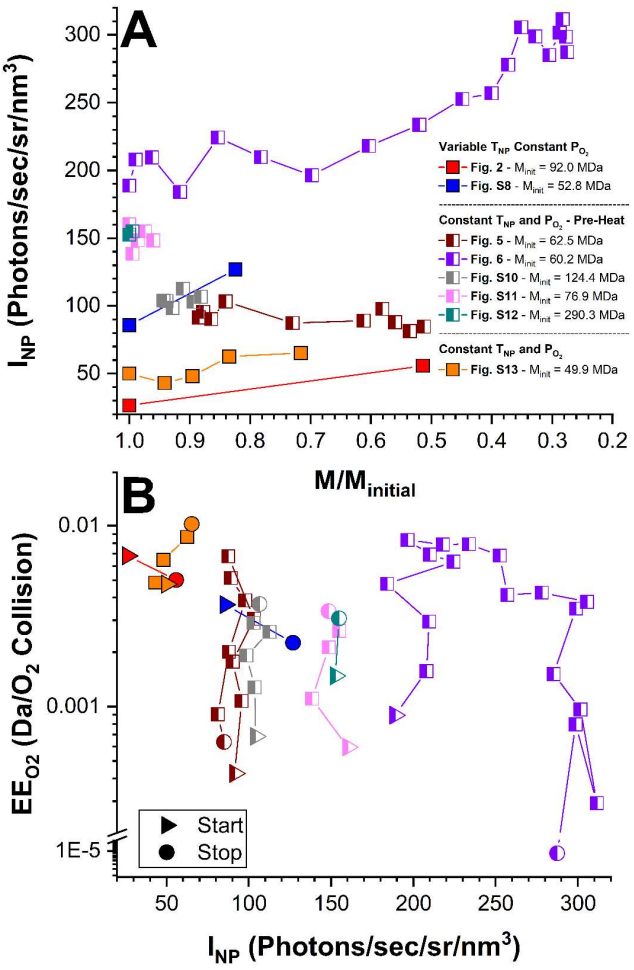

Figure 9: A). Volume corrected I_{NP} for Si NPs at 1200 K vs. M/M_{init}. B). EE_{O2} vs. volume corrected I_{NP} for the same NPs.

from etching, the I_{NP} values are volume-scaled (i.e., M-scaled), which, as discussed above, should compensate for the main size effect.

There were substantial NP-to-NP variations in emissivity, i.e., I_{NP} varied substantially between NPs of similar masses. For all the experiments where there was more than ~20% mass loss, the volume-scaled I_{NP} increased significantly as the NP etched. The one exception was from **Fig. 6**, where the NP had been preheated to 2000 K with significant sublimation mass loss, and in that case the volume-scaled I_{NP} was roughly constant, because the increase had already occurred during preheating. The largest increases were observed in the T_{NP} ramping experiments, where the NPs were not pre-heated, but then were oxidized above T_{melt} between the initial and final 1200 K measurements. The conclusion is that the largest effects come as Si NPs are first heated, with emissivity generally increasing.

For carbon NPs, we found that increasing emission brightness was correlated with decreasing rates for both sublimation[1] and oxidation, [3] and to see if Si NPs also show this correlation, **Fig. 9B** plots EE_{O2} against I_{NP}. Because both EE_{O2} and I_{NP} varied, the starting and ending points of the experiments are indicated with triangular and circular symbols, respectively. For pre-heated NPs (half-filled symbols), EE_{O2} initially increased, then decreased again if the experiment continued long enough, and for most of these experiments, I_{NP} was roughly constant as EE_{O2} increased and decreased. For the experiment in **Fig. 6**, however, I_{NP} was roughly constant during the initial ~order of magnitude increase in EE_{O2}, then increased substantially during the period when EE_{O2} was high and roughly constant (i.e. when the main mass loss occurred), then stabilized at the new higher value as EE_{O2} declined by three orders of magnitude. For the non-preheated NPs, I_{NP} increased significantly during the experiments, with EE_{O2} decreasing in the T_{NP} ramp experiments, and increasing in the 1200 K etching experiment (**Fig. S13**). The conclusion,

again, is that emissivity tended to increase as the NPs were first heated, and during periods of significant mass loss. Conversely, there was little change in I_{NP} associated with the orders-of-magnitude decreases in EE_{O2} observed for NPs that were etched long enough to passivate. It is not clear why emissivity tends to increase during initial heating/fast etching, but it is not surprising that there is little effect of the final transition to passivation on emissivity. Passivation is attributed to formation of a stable silica surface layer, but this layer would be transparent over the spectral range measured, and thin enough not to significantly affect emission from the underlying silicon core.

IV: Discussion

As reviewed in the SI, O_2 etching of Si surfaces has been studied extensively, with a few studies extending into the lower end of the temperature range examined here. From the perspective of understanding the NP mass loss rates, the etching process can be thought of as involving the following main steps: O_2 dissociative adsorption with sticking coefficient S, diffusion and isomerization processes that convert between various O_{ads} geometries and between surface and sub-surface sites, and desorption of Si_xO_y, principally SiO, at least in the temperature range studied in the literature.

O_2 dissociative adsorption on Si(100) was studied by D'Evelyn et al. [8] for 2, 5, and 14 kcal/mol O_2 beam energies at surface temperatures (T_s) up to 1400 K, including measurements of S as a function of oxygen coverage, extrapolated to obtain S_0 (S at zero O coverage). The measured S values correspond to net sticking, i.e., O_2 chemisorption followed by O or O_2 desorption would not have been counted unless desorption occurred at long (>msec) time delays, and that was not observed. Our experiments are also only sensitive to net sticking because O_2 sticking followed by O_2 (or 2 O) desorption has no effect on NP mass.

At 2 kcal/mol collision energy, S_0 was found to be ~1% at room temperature, dropping to a minimum of ~0.3% at 600 K and increasing to ~0.6% by 800 K. Numerical values at higher temperatures were not given, but S_0 was said to continue increasing to 1250 K, and to drop again between 1250 and 1400 K. S_0 was similar for sputter damaged and annealed surfaces but increased by a factor of ~3 on the roughened surface created by steady state etching at temperatures above the SiO desorption onset. O_2 in our experiments was thermal at 300 K, giving an average O_2-surface collision energy of ~0.9 kcal/mol. If we extrapolate their 5 kcal/mol and 2 kcal/mol results to 0.9 kcal/mol, S_0 at 800 K for thermal O_2 would be ~0.09%. Assuming a similar dependence of S_0 on surface temperature, we might estimate that S_0 would be ~0.1% at 1200 K, and probably decrease somewhat at higher T_{NP}.

For room temperature Si(100), D'Evelyn et al. [8] found that the surface saturated (i.e., $S \rightarrow 0$) at 1 ML O_{ads} coverage, but at 800 K, the surface remained unsaturated ($S \approx 0.5 \cdot S_0$) even for 2 ML coverage, indicating that a significant fraction of the chemisorbed oxygen had diffused into sub-surface (selvage) binding sites. In our experiments, where $T_{NP} \geq 1200$ K, we expect that surface-to-selvage O diffusion should be even more facile, particularly for T_{NP} approaching or exceeding T_{melt}.

The same group also studied the kinetics for SiO desorption from Si under both O_2 and O attack, [8, 12-13] for T up to 1400 K. Beam chopping was used to examine the time dependence of SiO desorption and to look for delayed O_2 desorption (none was observed). The kinetics were consistent with a multistep process with two different surface O intermediates: $O_{2(g)} \rightarrow I_1$ (bridge-bonded O) $\leftrightarrow I_2$ (Si-O) $\rightarrow SiO_{(g)}$, and they reported Arrhenius parameters for the $I_1 \leftrightarrow I_2$ and SiO desorption steps, both of which would be fast compared to our O_2 collision rate even at our lowest T_{NP} (1200 K). Because the timescale for interconversion between different adsorbed O geometries

is short, for simplicity, we simply use O_{ads} to refer to any labile adsorbed O species, as distinct from SiO_2, which is more thermally stable and capable of passivating the surface under some conditions. D'Evelyn et al. [8] found that at 1010 K, the total steady state oxygen coverage was below 0.03 ML under their molecular beam flux, and given our P_{O2} and higher temperatures, their kinetic model predicts that O_{ads} should rapidly desorb as SiO under our conditions, maintaining a nearly O_{ads}-free surface.

Passivation is observed to occur during oxidative etching of bulk Si surfaces and has been shown to result from reactions of O_{ads} to nucleate and grow islands of more thermally stable SiO_2, which can expand to cover the surface, blocking further O_2 adsorption. Nucleation and growth of SiO_2 is favored by high O_{ads} coverage, i.e., by a combination of high P_{O2} and low temperatures. SiO_2 surface layers can also decompose and desorb under the right conditions. For example, thin SiO_2 layers on the surface of bulk Si have been shown to react with the underlying Si to form SiO that begins to desorb at temperatures above 1000 K, [32, 42-49] with a 10 nm SiO_2 layer desorbing in an hour at 1400 K. [42] Even bulk silica decomposes at temperatures above ~1800 K, with Si, SiO, Si_2O_2, O, and O_2 reported to be present in the vapor phase. [50-51] Thus, formation and persistence of a passivating SiO_2 layer is favored by low temperatures and high P_{O2}, while for low P_{O2} and high temperatures, SiO_2 formation is suppressed. [8, 10, 12, 14, 16-17, 26-27] Our conditions of T_{NP} and P_{O2} are in the regime where passivation has not been observed for bulk Si.

Our NPs were handled in air prior to introduction to the vacuum system, and presumably had a native oxide layer ~0.5 nm thick. [64] To interpret our results, it is important to know to what extent the NPs retained significant surface oxide at the point when O_2 was introduced to study the etching chemistry. All the NPs spent at least 30 minutes in argon at $T_{NP} \geq 1200$ K prior to O_2 introduction, and preheated NPs were also heated in argon at $T_{NP} \geq 1800$ K for ~20 minutes, i.e.,

well above T_{melt} and in the range where even bulk SiO_2 decomposes and desorbs. Thus, the literature[32, 42-51] suggests that the native oxide surface layer should have desorbed long before O_2 introduction, and several of our observations also support this conclusion. For example, if the pre-heated NPs had retained significant surface oxide, then the non-preheated NPs would have had even more surface oxide, and therefore should have had lower initial reactivity. As shown in **Fig. 8**, however, the non-preheated NPs had higher initial reactivity than the pre-heated NPs. Another point is that because passivation results from growth of SiO_2 islands to cover the surface, [7-8, 12-13, 17, 19-20] NPs that started with significant surface oxide would have passivated more rapidly than initially oxide-free NPs, but as shown in **Fig. 8**, there was not much difference in the passivation time dependence. Similarly, the lowest initial EE_{O2} values were for pre-heated NPs oxidized at 1200 K, and if that low reactivity were due to passivation by a significant oxide layer, then the oxide layer would simply have grown when O_2 was introduced, quickly passivating the NPs. Instead, EE_{O2} was observed to increase substantially during the first hour or two of O_2 etching, before starting the drop toward passivation. Finally, **Fig. 7** shows that when an oxide-passivated NP was heated to 2000 K for even a few seconds, O_2 reactivity was (briefly) restored, confirming that surface oxides are removed at high T_{NP}, and the preheated NPs were held at high T_{NP} for >20 minutes. Thus, both the literature and our observations lead to the conclusion that the pre-heated NPs would not have had significant surface oxide prior to O_2 introduction, and even non-preheated NPs should have lost much of their native oxide layer during 1200 K Q stepping.

The as-trapped NPs would also have had carbonaceous adsorbates (e.g. methanol, ammonium acetate, adventitious carbon), most of which would have desorbed as the NPs were initially heated, but it is possible that pyrolysis might have left elemental carbon on the NP surface, or possibly formed a silicon carbide layer. As discussed in the SI, we have studied O_2 etching of

elemental carbon NPs[2-3] under conditions identical to those used here, and for 1200 K oxidation, the initial EE_{O2} values ranged from 2 x 10^{-2} Da/O_2 collision for graphite to 3 x 10^{-3} Da/collision for diamond, i.e., the carbon NPs etch with initial rates in the same range as those for Si NPs. The SI presents an etching experiment for a SiC NP (**Fig. S14**) under conditions identical to those used in **Fig. 2**, and again, the initial EE_{O2} values are similar to those for Si NPs. Therefore, even if the Si NPs had had significant C or SiC surface contamination, this would not have passivated them against oxidative mass loss, and the C or SiC would have rapidly desorbed (as CO) upon O_2 introduction. The conclusion is that preheated NPs should have been largely free of surface contaminants, and even the non-preheated NPs would have lost most surface contaminants as they were initially heated and charge stepped prior to O_2 introduction.

It is straightforward to estimate how NPs should have etched, assuming their surfaces were initially clean and that S_0 for thermal O_2 can be extrapolated from the Si(100) studies, [8, 13] i.e., with $S_0 \approx 0.1\%$ at 1200 K, probably decreasing at higher T_{NP}. The Si(100) studies also showed that O_{ads} should have mostly desorbed as SiO in our T_{NP} range, maintaining low steady state oxygen coverage. Our typical P_{O2} corresponds to ~154 O_2 collisions/sec/nm^2, thus 0.1% sticking would have resulted in adsorption of ~0.3 O_{ads}/sec/nm^2. If all the O_{ads} desorbed as $SiO_{(g)}$, the initial mass loss rate would have been ~8.6 Da/sec/nm^2, corresponding to $EE_{O2} \approx 5.6$ x 10^{-2} Da/O_2 collision. As shown in **Fig. 8**, the *initial* EE_{O2} values for pre-heated NPs at 1200 K averaged roughly 8 x 10^{-4} Da/collision, i.e., ~70 times smaller. For NPs at higher T_{NP}, preheated or not, the initial EE_{O2} values ranged between ~2 x 10^{-3} and ~5 x 10^{-3} Da/O_2 collision, with one particularly reactive NP with $EE_{O2} \approx 3$ x 10^{-2} Da/collision, i.e., between ~2 and ~20 times lower than would be expected for $S_0 = 0.1\%$. If, as was reported for Si(100) at 2 kcal/mol collision energy, S_0 decreased with

T_{NP} above 1250 K, [8] then our initial etching rates for high T_{NP} may be consistent with the bulk etching rates.

Thus, the literature raises several questions, including: 1. Why are the initial EE_{O2} values at 1200 K for preheated NPs up to 70 times smaller than what might be expected? 2. Why do Si NPs eventually all stop losing mass under oxidizing conditions, at least for $T_{NP} < 1750$ K, even though our conditions were in the range where bulk Si has not been observed to passivate. 3. Why do the 1200 K initial EE_{O2} values for preheated NPs increase by an order of magnitude over the first one to two hours of etching.

There are several factors that could contribute to the lower-than-expected initial EE_{O2} values. The maximum EE_{O2} occurs if all O_2 chemisorption results in SiO desorption, and under these conditions EE_{O2} is proportional to S. Thus, the low 1200 K initial EE_{O2} values could be rationalized by assuming that S for pre-heated NPs is 20 to 70 times smaller than S_0 estimated from the bulk etching literature. EE_{O2} would also be reduced if O_{ads} desorbed as SiO_2, rather than SiO, however, this would only reduce EE_{O2} by a factor of 2, at most. O_{ads} may also desorb as O or O_2, particularly at high temperature, [65] but since the bulk S_0 measurements were of *net* sticking, this effect is already accounted for in the estimate that $S_0 \approx 0.1\%$ at 1200 K.

Our EE_{O2} values are based on measuring *net* mass loss, thus EE_{O2} would also be reduced if a significant fraction of O_{ads} remained on the NP rather than desorbing, and observation of Si NPs passivation implies that there must have been some "non-desorbing O". Non-desorbing O would not only add mass, but would also reduce the amount of mass lost as SiO. To test how this and other assumptions about the etching mechanism would affect the M vs. time and EE_{O2} vs. time behavior, we constructed a simple "bookkeeping" model that tracks the numbers of O and Si atoms in Si NPs as a function of reaction time. The model assumes a spherical NP, which should be

reasonable for pre-heated/melted NPs, and assumes Langmuir O_2 sticking behavior, as was assumed in the bulk Si etching models. [8, 13] The O_2 sticking coefficient, S, is calculated as $S = S_0 \cdot (1 - O{:}Si/(O{:}Si)_{sat})$, where O:Si is the surface layer O:Si ratio and $(O{:}Si)_{sat}$ is an assumed saturation ratio. Both 2:1 and 1:1 (i.e., SiO_2 and SiO) saturation stoichiometries were tested. O adsorbing on the surface was assumed to do one of three things: 1. Desorb as SiO, removing mass, 2. Nucleate/grow surface SiO_2, adding mass and increasing the surface O:Si ratio, or 3. Diffuse to the sub-surface (selvage), reducing the surface O:Si ratio and adding mass. The model tracks the composition of both the surface and selvage layers, fixing the surface layer thickness at 0.25 nm (~one SiO_x layer), but using the selvage thickness as an adjustable parameter that controls the oxygen-sink capacity of the selvage. The propensities toward surface layer SiO_2 nucleation (assumed $\propto [O_{ads}]^2$) and growth (assumed $\propto [SiO_{2,ads}] \cdot [O_{ads}]$) are controlled by separate parameters. O diffusion to the selvage is assumed to be proportional to the surface-selvage concentration difference and is controlled by a final parameter.

We have chosen to illustrate the simulations using the 1500 K oxidation experiment shown in **Fig. S9**. This was a preheated NP with initial mass ~95 MDa, and would have been spherical with diameter just over 50 nm. Four distinct sets of mechanistic assumptions were simulated, and the results are compared to experiment in **Fig. 10**. The simulated results are shown as smooth curves, and the experimental data are shown as points (the M vs. time points are so dense that they appear as a thick continuous curve). Frames A and C compare the M vs. time results, with insets showing the early time behavior, and the text blocks summarizes the model assumptions. Frames B and D compare the EE_{O2} results and show the simulated sticking probability (S) and surface and selvage layer O concentrations (relative to SiO_2). As indicated by color, EE_{O2} and S values are plotted against the axis shown at the left side of frame B, and the surface and selvage O

concentrations are plotted against the axis shown at the right side of frame D. The simulations in **Fig. 10** assumed $(O:Si)_{sat}$ = 2:1 and analogous simulations for $(O:Si)_{sat}$ = 1:1 are shown in **Fig. S15**.

The left column shows the results of models 1 and 2, which both assumed S_0 to be 5×10^{-5}, i.e., 20 times smaller than the estimated 0.1% 1200 K value. The low S_0 resulted in initial mass loss rates and EE_{O2} values that match experiment, and the two models explore different mechanisms to account for the time dependence of EE_{O2}, which was observed to be roughly constant for ~2 hours, and then to drop by ~two orders of magnitude over the following ~2 hours.

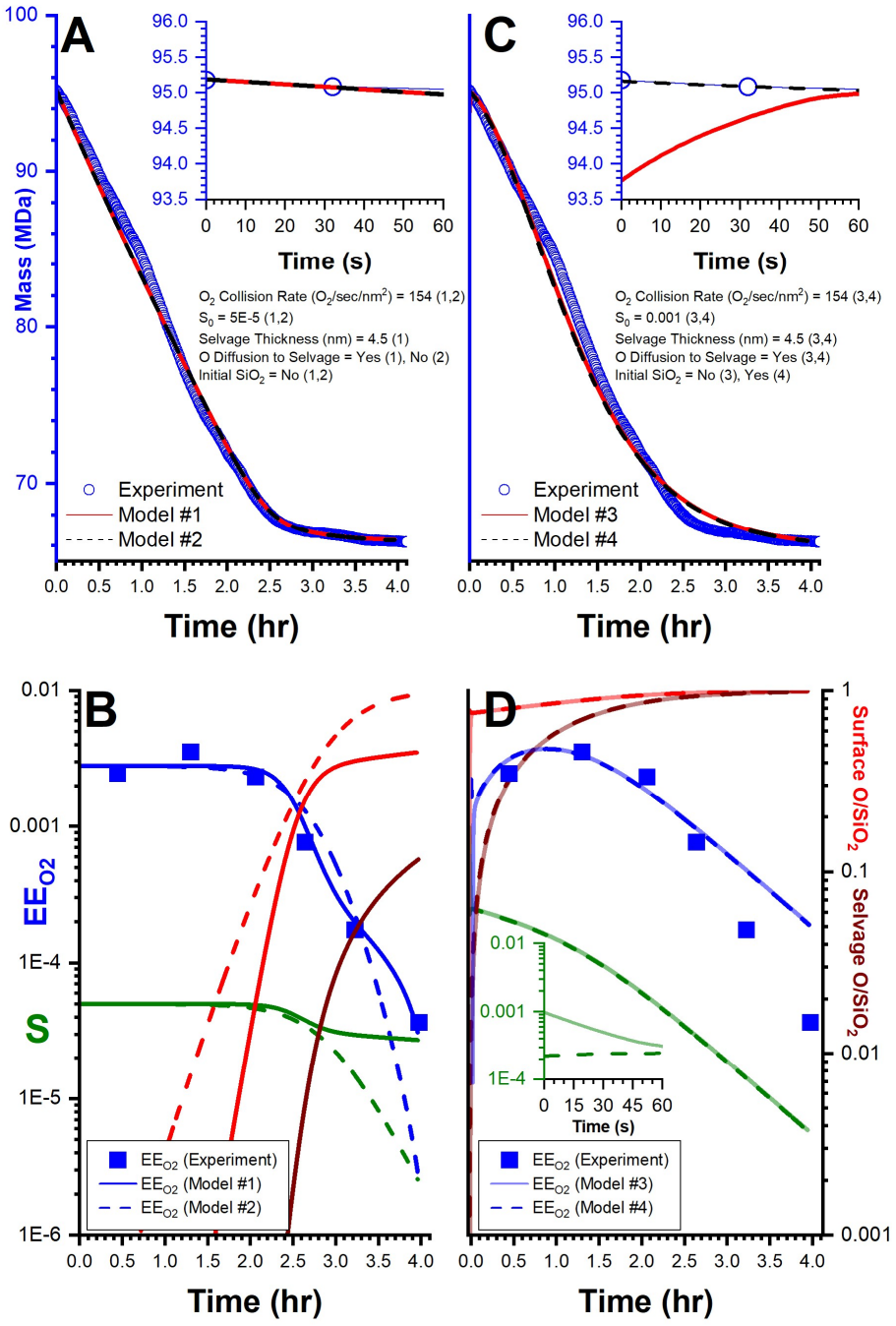

Figure 10: A). M vs. time (blue symbols) for 1500 K oxidation of a Si NP (cf. **Fig. S9**) and fits based on models #1 and #2 shown as superimposed black and red curves. *Inset*: Initial M vs. time. B). Experimental EE_{O2} vs. time (blue squares), and model 1 and 2 EE_{O2} (blue), S (green), Surface O/SiO_2 (red), and Selvage O/SiO_2 (brown). C). and D). Analogous plots for models 3 and 4. *Inset to D)*: Initial S vs. time.

In model 1, SiO_2 nucleation was assumed to be slow, but once SiO_2 nucleated, relatively fast growth was assumed. In addition, O was assumed to diffuse between the surface layer and a 4.5 nm thick selvage layer, removing O_{ads} from the surface, thereby inhibiting formation of surface SiO_2. With these parameters, significant surface SiO_2 (red solid curve) only appeared after ~1.75 hours, but then it grew rapidly, such that at ~2 hours, S (green solid curve) began to decrease noticeably. An important point about this model is that although the simulated mass loss rate and EE_{O2} decreased by a factor of ~100 by the end of the simulation, S decreased by only a factor of ~2, i.e., the NP never actually passivated. The NP remained reactive because surface-to-selvage O diffusion prevented the surface layer O coverage (solid red curve) from reaching saturation ($(O:Si)/(O:Si)_{sat}$ =1.0). Nonetheless, despite O_2 continuing to adsorb and SiO continuing to desorb at a decreasing rate, the mass loss rate slowed dramatically because mass lost as SiO was largely offset by the added mass associated with non-desorbing O accumulating as both surface SiO_2 and selvage oxygen. As the selvage O concentration built up (solid brown curve), surface-to-selvage O diffusion slowed, allowing the surface layer O:Si ratio to increase (solid red curve), which started the decrease in S. If the simulation had continued longer the surface-to-selvage O diffusion would have eventually stopped, allowing the surface to approach SiO_2 stoichiometry, passivating the NP.

In model 2, surface-to-selvage O diffusion was turned off, and SiO_2 nucleation was assumed to be significantly faster than in model 1, both factors favoring earlier nucleation of surface SiO_2. The SiO_2 growth propensity was assumed to be slower than in model 1, however, and as a result it still took ~2 hours for the surface O concentration (dashed red curve) to increase enough to reduce S significantly. Because this model did not allow O diffusion to the selvage, the surface O concentration approached saturation by the end of the simulation, decreasing S by a

factor of ~20 and EE_{O2} by a factor of ~1000. Thus, in model 2, the NP was almost passivated by the end, and would have completely passivated if the simulation had continued longer.

The right column summarizes the results of models 3 and 4, which both assumed S_0 to be 0.1%, i.e., the 1200 K value extrapolated from Si(100) etching behavior. [8] Both models used identical parameters to describe surface SiO_2 nucleation and growth and surface-to-selvage O diffusion, and both assumed a 4.5 nm thick selvage layer, identical to that in model 1. The difference between models 3 and 4 was that model 3 started with the NP free of oxygen, while model 4 assumed that the surface layer already had an almost saturated surface oxide layer, but with no O in the selvage. After the first ~minute, the results for the two models were nearly superimposable, which we indicate using bi-colored, dashed curves. In model 3 (initially clean surface), the initial O_2 chemisorption rate was so high that within ~60 seconds the NP grew a nearly saturated surface SiO_2 layer, essentially matching the layer assumed to be initially present in model 4. The early time behavior of models 3 and 4 is compared in the insets to **Figs. 10C** and **D.** For model 3, the NP quickly gained ~1.25 MDa (~1.3% of $M_{initial}$) corresponding to growth of the surface SiO_2 layer, resulting in a rapid order-of-magnitude decrease in S. In model 4, $M_{initial}$ included the mass of the initial oxide layer, and S increased slightly during the first few minutes as surface-to-selvage O diffusion slightly reduced the initial surface O concentration. In both models, S quickly converged on a value of ~2.7×10^{-4}, after which the models evolved identically. In both models, the initial EE_{O2} values were much smaller than the experimental values (because mass was being added rapidly in model 3, and because the NP started almost passivated in model 4), but after the first few minutes the simulated EE_{O2} values increased to match experiment. In both models, surface-to-selvage O diffusion maintained the surface layer O coverage slightly below saturation for ~2 hours, allowing etching to continue. At that point, the selvage O

concentration had built up enough (brown dashed curve) to slow the surface-to-selvage O diffusion, allowing the surface layer to approach saturation, dropping S by a factor of ~40 and EE_{O2} by a factor of ~20 by the time the simulation ended. Note, however, that neither of the "high S_0" models could match the measured 75-fold decrease in EE_{O2} at long times.

In models 3 and 4 after the first ~minute, and in model 1 during the final ~2 hours, the etching kinetics were controlled by the rate of surface-to-selvage O diffusion, with the eventual transition toward saturation controlled by the amount of O that could be accommodated in the selvage, i.e. by the selvage thickness, which was 4.5 nm in models 1, 3, and 4. The NP in this experiment lost 30% of $M_{initial}$, corresponding to a decrease in NP diameter from ~50 to ~45 nm, thus models 1, 3, and 4 ended with a ~4.75 nm thick layer (including the 0.25 nm surface layer) of near-SiO_2 stoichiometry, on top of a core of unoxidized Si. In reality the O concentration would presumably vary continuously with depth, but with a concentration-weighted average depth of ~5 nm. In model 2, the oxidized surface layer was just 0.25 nm thick, with no subsurface O accumulation.

The results if $(O:Si)_{sat}$ is assumed to be 1:1 are similar (**Fig. S15**), requiring only modest adjustments to the SiO_2 nucleation/growth parameters. The biggest differences, compared to the results for SiO_2 saturation stoichiometry, are that the early-time mass growth for model 3 was only ~0.75 MDa, but on the other hand, the fit to EE_{O2} at long times was much better in models 1, 3, and 4, than for SiO_2 saturation.

The simulations show that models representing four distinct, limiting case etching mechanisms can reproduce the experimental time-dependent mass and EE_{O2} data reasonably well, and the obvious questions are whether the experiments put any limits on the model parameters, and if any of the models can be ruled out entirely. Model 4 assumed that S_0 was 0.1%, as estimated

from Si(100) data,[8, 13] but that the initial S was much lower because the NP was already passivated by SiO_2 or some other contaminant prior to O_2 introduction. As discussed above, however, both our results and the literature indicate that preheated NPs (as this one was) should be at least mostly oxide-free, and that C/SiC contaminants would not passivate the NP, thus ruling out model 4.

Note also that model 4 assumed that the surface layer composition was almost saturated (i.e., SiO_2), but also assumed that the selvage was initially oxygen free. That combination is unphysical, as shown by observations that with increasing temperature, an increasing fraction of the oxygen present on passivated Si surfaces is in the selvage, such that for example, even 2 ML's worth of oxygen did not passivate a Si(100) surface at 800 K.[8] At 1500 K we would, therefore, expect that a near-saturated surface layer would be accompanied by substantial O concentration in the selvage, however, if this more realistic initial condition were used for model 4, the NP would almost immediately passivate because the concentration gradient driving surface-to-selvage O diffusion would be too weak to keep the surface from saturating.

Note that the literature showing substantial selvage O concentrations during oxidation have high temperatures and also rules out model 2, which assumed that the selvage remained oxygen-free throughout the passivation process.

Model 3, like model 4, assumed $S_0 = 0.1\%$ but with the NP surface assumed to start clean ($S = S_0$). For such a large initial S value, the measured initial EE_{O2} value can only be matched if a significant fraction of O_{ads} is assumed to quickly form a nearly saturated SiO_2 layer, slowing the etching reaction into the range observed. This SiO_2 layer formation would add ~1.25 MDa in the first 60 seconds after O_2 introduction, or ~0.75 MDa if the saturation stoichiometry is assumed to be SiO, but as shown in **Fig. S9**, there was no mass gain upon O_2 introduction, and in fact, no measurable O_2-induced mass gains were ever observed for Si NPs, regardless of T_{NP} or other

experimental parameters. Given our mass precision, even a ~0.1% mass increase would easily be detectable as a discontinuity in the trend of M vs. time, and by modeling the behavior for different S_0 values, we can set an upper limit on the initial S to ~2 x 10^{-4}, i.e., one fifth the value estimated by extrapolating the Si(100) results.

We can also set lower limits on the initial S values in each experiment by adjusting S to fit the measured initial EE_{O2} values, setting all other parameters to maximize EE_{O2} (no SiO_2 nucleation or surface-to-selvage O diffusion). For the 1500 K experiment, the lower limit on initial S is ~5 x 10^{-5}, and for other NPs the lower limits vary in proportion to the measured initial EE_{O2} values, summarized in **Fig. 8B**. The lowest lower limits are for the pre-heated NPs oxidized at 1200 K (~1.5 x 10^{-5}), and the highest is for the NP in **Fig. 3** used for the 1300 K P_{O2} ramp experiment (6.5 x 10^{-5}), but all are well below the ~0.1% S_0 value estimated from the bulk Si etching literature. [8, 13]

Only model 1 is not excluded by some combination of our observations and the literature. In model 1, the surface was assumed to be clean, but with initial S_0 = 5 x 10^{-5}. Thus, the assumed S_0 was ~20 times lower than the value estimated by extrapolating the Si(100) data. S_0 was also essentially at the lower limit for S discussed above, because the *initial* amounts of SiO_2 nucleation and surface-to-selvage diffusion were too small to noticeably reduce the mass loss. Only after several hours, as increasing selvage O slowed surface-to-selvage O diffusion, did enough surface SiO_2 begin to accumulate to reduce S significantly, and the simulation suggests that the NP would have continued toward complete passivation after the end of the simulated period. We claim no particular significance for the exact parameter values used in **Fig. 10**, but the initial value of S, (=S_0 for oxide-free NPs) is, as discussed above, constrained to be between ~1.5 x 10^{-5} and ~2 x 10^{-4}.

Another question is why the NPs all eventually passivated for $T_{NP} \leq 1500$ K if the experiments continued long enough, despite our conditions being in a low P_{O2}/high T_{NP} range where passivation of bulk Si has not been observed. Only a few bulk etching experiments at temperatures overlapping our T_{NP} range have been reported, [8, 12] but it is not clear that any of those allowed etching to continue for more than 2 hours, which is the time before any of the NP showed signs for starting to passivate, with full passivation taking several hours longer. Thus, we can't rule out the possibility that bulk Si might begin to passivate under these conditions if the reaction period were long enough. There is reason to think, however, that NPs might passivate more readily than bulk Si. Oxygen clearly diffuses into the selvage during etching of bulk Si at high temperatures, with significant sub-surface O observed even at 800 K, and O diffusion expected to become more facile with increasing temperature. Therefore, at high temperatures the sub-surface region of bulk Si can potentially absorb O for extended periods, reducing the surface O concentration, and thus inhibiting formation of the passivating SiO_2 surface layer. For an NP in our size range, however, the sub-surface volume is limited, which limits how much O can be absorbed before saturation slows the diffusion rate, allowing SiO_2 to start accumulating on the NP surface. Another, related, possibility is that as O accumulates in the limited NP sub-surface volume, SiO_2 begins to nucleate and grow beneath the surface, and the onset of passivation occurs as overlying layers etch away, exposing this SiO_2 which then grows to cover the surface.

A final question is why preheated NPs oxidized at 1200 K had particularly low initial EE_{O2} values, and why EE_{O2} increased by nearly an order of magnitude over the first hour of etching. The initial EE_{O2} values were ~70 times smaller than the value estimated assuming bulk-like behavior (S_0 = 0.1%, most O_{ads} desorbing as SiO), and 5 to 10 times smaller than either non-preheated NPs oxidized at 1200 K or all the NPs oxidized at higher T_{NP}. As noted, the literature

indicates that preheated NPs are unlikely to have significant passivating oxide layers, but even if we assumed the contrary, i.e., that low initial EE_{O2} values resulted from the NPs being nearly oxide-passivated, then EE_{O2} would simply have decreased upon O_2 exposure, rather than increasing by an order of magnitude over time (cf. model 4).

The observation that S increased as the Si(100) surface roughened during steady state etching, [8] suggests a possible explanation for both the low initial EE_{O2} values and the increase in etching rate over time. The preheated NPs were held above T_{melt} for an extended time, and thus should have melted, coalesced if they were originally aggregates, and lost any initial oxide layer. Furthermore, the cooling rate after pre-heating was quite slow, typically 2 to 3 K/second, which should have been slow enough to thoroughly anneal the NPs as they cooled. We suggest that the low initial rates simply reflect the NPs having annealed to have surfaces with few sites capable of dissociatively chemisorbing O_2 at 1200 K. As etching occurred at those sites, however, that would tend to roughen the surface and increase the number reactive sites, which would explain why reactivity increased as material equivalent to a few monolayers of Si etched during the first 1 – 2 hours. The higher initial EE_{O2} and smaller initial increase observed for the non-preheated NP at 1200 K (**Fig. S13**) could be rationalize as resulting from this NP having been heated long enough at 1200 K to desorb the native oxide layer, but without melting, thereby starting with a rough, reactive surface. The higher initial EE_{O2} values at higher oxidation temperatures simply suggest that for high T_{NP} a larger fraction of the initial surface sites are able to actively chemisorb O_2.

For $T_{NP} \geq 1750$ K (above T_{melt}), EE_{O2} gradually decreased over time, but the final sharp decrease signaling the onset of passivation was not observed, at least for the ~4.5 hour oxidation period studied. This behavior could indicate that surface SiO_2 is simply not stable at such high T_{NP}, so that the surface remained largely oxygen free. In that case, it is not obvious why the etching

rates slowed gradually over time, however, it is possible that as fast mixing of O into the molten Si NP increased the O:Si stoichiometry, the surface layer stoichiometry gradually increased to the point of reducing the sticking coefficient. Note, also, that while 1750 K is well above the bulk T_{melt} for Si (1687 K), the stoichiometry-dependent T_{melt} for SiO_x can be significantly higher, [66] suggesting that O diffusion might slow significantly as the stoichiometry is increased, allowing the surface to partially passivate. Given that even bulk SiO_2 begins to decompose and desorb in this temperature range, [50-51] it is likely that the NPs would never completely passivate.

V: Conclusions

We have examined sublimation of Si NPs at temperatures ranging from 1500 to 2050 K, and oxidative etching for temperatures from 1200 K to 1800 K, i.e., from well below to above the bulk Si T_{melt}. The sublimation kinetics slowed substantially as T_{NP} was ramped up and down, particularly during the initial heating, which would have desorbed oxides or other contaminants and melted the NPs.

The oxidative etching kinetics had more interesting dependence on reaction time, and except at the highest temperatures, the NPs all passivated if they were allowed to etch for > 2 hours. A model inspired by the bulk Si etching mechanism[8, 12-13] was developed to simulate the effects of different assumptions about the NP initial conditions and the importance of processes including O_2 sticking, SiO desorption, SiO_2 nucleation and growth, and diffusion of O_{ads} into the selvage volume. We are able to constrain the initial sticking coefficient, S_0, to a narrow range between 2×10^{-4} and a lower limit that varied for each experiment, from ~1.5×10^{-5} to ~6.5×10^{-5}. Our results implicate surface-to-selvage O diffusion and the limited oxygen-sink capacity of the NP cores as being important in controlling passivation of the NPs. Well annealed Si NPs are initially relatively unreactive with O_2 at 1200 K, and the large reactivity increase over time is

attributed to roughening of the NP surface by etching at reactive sites, analogous to roughening observed at lower temperatures for Si(100).

The results are promising for development of the single NP mass spectrometry method as a high and ultra-high temperature kinetics tool. We also plan to report on studies of SiO_x NP reactivity and passivation starting from silica NPs, which can be surface-activated by brief heating to $T_{NP} \gg 2000$ K, generating a reduced surface with initial EE_{O2} quite similar to those for Si NPs, but passivating much more rapidly. With the surface chemistry characterized for Si, silica, and carbon NPs, we then plan to apply the method to a more complex material, SiC, and then to materials like Hf, Zr, or Ta carbides and nitrides, where less is known about the chemistry at the ultra-high temperatures of interest for their applications to thermal protection systems.

VI: Acknowledgements

The Office of Naval Research supported preliminary work under grant number N00014-15-1-2681. The work presented, including development of the etching model and extension to 1200 K etching was supported by the Department of Energy, Office of Science, Basic Energy Sciences, Gas Phase Chemical Physics Program under grant DE-SC-0018049. SLA acknowledges support from the Henry Eyring Endowed Chair. We would like to thank Prof. Timothy Minton (Univ. of Colorado-Boulder) for useful discussions regarding high temperature etching mechanisms.

VII: Associated Content

The following files are available free of charge.

Supporting Information that contains a review of the silicon oxidation literature, additional examples of sublimation and oxidation experiments on silicon NPs, and more information on the

NP etching/passivation model (PDF). Data tables for all of the figures are also included in excel format (.xlsx).

VIII: Corresponding Author

*Corresponding author: anderson@chem.utah.edu, (801)-585-7289

XI: Author Contributions

The manuscript was written through contributions of all authors. All authors have given approval to the final version of the manuscript.

X: Abbreviations

NP, nanoparticle; T_{NP}, nanoparticle temperature; $P_{O2,}$ oxygen partial pressure, EE_{O2}, O_2 etching efficiency; silicon, Si; melting temperature, T_{melt}.

XI: References

1. Long, B. A.; Lau, C. Y.; Rodriguez, D. J.; Tang, S. A.; Anderson, S. L., Sublimation Kinetics for Individual Graphite and Graphene Nano-particles (NPs): NP-to-NP Variations and Evolving Structure-Kinetics and Structure-Emissivity Relationships. *J. Am. Chem. Soc.* **2020,** *142* (33), 14090-14101.

2. Rodriguez, D. J.; Lau, C. Y.; Friese, A. M.; Magasinski, A.; Yushin, G.; Anderson, S. L., High-Temperature Oxidation of Single Carbon Nanoparticles: Dependence on the Surface Structure and Probing Real-Time Structural Evolution via Kinetics. *J Am Chem Soc* **2022,** *144* (11), 4897-4912.

3. Rodriguez, D. J.; Lau, C. Y.; Long, B. A.; Tang, S. A.; Friese, A. M.; Anderson, S. L., O_2-oxidation of individual graphite and graphene nanoparticles in the 1200–2200 K range: Particle-

to-particle variations and the evolution of the reaction rates and optical properties. *Carbon* **2021,** *173*, 286-300.

4. Lander, J. J.; Morrison, J., Low Voltage Electron Diffraction Study of the Oxidation and Reduction of Silicon. *Journal of Applied Physics* **1962,** *33* (6), 2089-2092.

5. Deal, B. E.; Grove, A. S., General Relationship for the Thermal Oxidation of Silicon. *Journal of Applied Physics* **1965,** *36* (12), 3770-3778.

6. Fair, R. B., Oxidation, Impurity Diffusion, and Defect Growth in Silicon—An Overview. *Journal of The Electrochemical Society* **1981,** *128* (6), 1360-1368.

7. Smith, F. W.; Ghidini, G., Reaction of Oxygen with Si(111) and (100): Critical Conditions for the Growth of SiO2. *Journal of The Electrochemical Society* **1982,** *129* (6), 1300-1306.

8. D'Evelyn, M. P.; Nelson, M. M.; Engel, T., Kinetics of the adsorption of O_2 and of the desorption of SiO on Si(100): A molecular beam, XPS, and ISS study. *Surface Science* **1987,** *186* (1), 75-114.

9. Irene, E. A., Models for the oxidation of silicon. *Critical Reviews in Solid State and Materials Sciences* **1988,** *14* (2), 175-223.

10. Walkup, R. E.; Raider, S. I., In situ measurements of SiO(g) production during dry oxidation of crystalline silicon. *Applied Physics Letters* **1988,** *53* (10), 888-890.

11. Gibson, J. M.; Lanzerotti, M. Y., Observation of interfacial atomic steps during silicon oxidation. *Nature* **1989,** *340* (6229), 128-131.

12. Engstrom, J. R.; Bonser, D. J.; Nelson, M. M.; Engel, T., The reaction of atomic oxygen with Si(100) and Si(111): I. Oxide decomposition, active oxidation and the transition to passive oxidation. *Surface Science* **1991,** *256* (3), 317-343.

13. Engstrom, J. R.; Bonser, D. J.; Engel, T., The reaction of atomic oxygen with Si(100) and Si(111): II. Adsorption, passive oxidation and the effect of coincident ion bombardment. *Surface Science* **1992,** *268* (1), 238-264.

14. Feltz, A.; Memmert, U.; Behm, R. J., In situ STM imaging of high temperature oxygen etching of Si(111)(7 × 7) surfaces. *Chemical Physics Letters* **1992,** *192* (2), 271-276.

15. Engel, T., The interaction of molecular and atomic oxygen with Si(100) and Si(111). *Surface Science Reports* **1993,** *18* (4), 93-144.

16. Seiple, J.; Pecquet, J.; Meng, Z.; Pelz, J. P., Elevated temperature oxidation and etching of the Si(111) 7×7 surface observed with scanning tunneling microscopy. *Journal of Vacuum Science & Technology A* **1993,** *11* (4), 1649-1653.

17. Feltz, A.; Memmert, U.; Behm, R. J., High temperature scanning tunneling microscopy studies on the interaction of O_2 with Si(111)-(7 × 7) surfaces. *Surface Science* **1994,** *314* (1), 34-56.

18. Ross, F. M.; Gibson, J. M.; Twesten, R. D., Dynamic observations of interface motion during the oxidation of silicon. *Surface Science* **1994,** *310* (1), 243-266.

19. Udagawa, M.; Niwa, M.; Sumita, I., Local Ordering and Lateral Growth of Initial Thermal Oxide of Si(001). *Japanese Journal of Applied Physics* **1994,** *33* (Part 1, No. 1B), 375-378.

20. Borman, V. D.; Gusev, E. P.; Lebedinski, Y. Y.; Troyan, V. I., Mechanism of submonolayer oxide formation on silicon surfaces upon thermal oxidation. *Physical Review B* **1994,** *49* (8), 5415-5423.

21. Seiple, J. V.; Pelz, J. P., Scanning Tunneling Microscopy study of Oxide Nucleation and Oxidation-Induced Roughening at Elevated Temperatures on the Si(001)-(2 x 1) Surface. *Physical Review Letters* **1994,** *73* (7), 999-1002.

22. Sofield, C. J.; Stoneham, A. M., Oxidation of silicon: the VLSI gate dielectric. *Semiconductor Science and Technology* **1995,** *10* (3), 215-244.

23. Seiple, J. V.; Pelz, J. P., Evolution of atomic-scale roughening on Si(001)-(2×1) surfaces resulting from high temperature oxidation. *Journal of Vacuum Science & Technology A* **1995,** *13* (3), 772-776.

24. Mott, N. F.; Rigo, S.; Rochet, F.; Stoneham, A. M., Oxidation of Silicon. In *Sir Nevill Mott ? 65 Years in Physics*, World Scientific: 1995; Vol. Volume 12, pp 685-708.

25. Lu, H. C.; Gusev, E. P.; Garfunkel, E.; Gustafsson, T., An ion scattering study of the interaction of oxygen with Si(111): surface roughening and oxide growth. *Surface Science* **1996,** *351* (1), 111-128.

26. Williams, E. D.; Fu, E. S.; Li, B., Evolution of Morphology During Etching of Si. *MRS Proceedings* **1996,** *466*, 157.

27. Komeda, T.; Nishioka, Y., Layer-by-Layer Etching of Si(111) Surface by Oxygen at Elevated Temperature. *Japanese Journal of Applied Physics* **1997,** *36* (Part 1, No. 3B), 1582-1585.

28. Raschke, M. B.; Bratu, P.; Höfer, U., Optical second-harmonic investigations of the isothermal desorption of SiO from the Si(100) and Si(111) surfaces. *Surface Science* **1998,** *410* (2), 351-361.

29. Hannon, J. B.; Bartelt, M. C.; Bartelt, N. C.; Kellogg, G. L., Etching of the Si(001) Surface with Molecular Oxygen. *Physical Review Letters* **1998,** *81* (21), 4676-4679.

30. Åkermark, T.; Ganem, J. J.; Trimaille, I.; Vickridge, I.; Rigo, S., Temperature and Pressure Dependence of the Oxygen Exchange at the SiO_2−Si Interface, $O_2 \leftrightarrow SiO_2$, during Dry Thermal Oxidation of Silicon. *The Journal of Physical Chemistry B* **1999,** *103* (45), 9910-9914.

31. Brichzin, V.; Pelz, J. P., Effect of surface steps on oxide-cluster nucleation and sticking of oxygen on Si(001) surfaces. *Physical Review B* **1999,** *59* (15), 10138-10144.

32. Starodub, D.; Gusev, E. P.; Garfunkel, E.; Gustafsson, T., Silicon Oxide Decomposition and Desorption during the Thermal Oxidation of Silicon. *Surface Review and Letters* **1999,** *06* (01), 45-52.

33. Daineka, D. V.; Pradère, F.; Châtelet, M.; Fort, E., High temperature oxidation of Si(100) by neutral oxygen cluster beam: Coexistence of active and passive oxidation areas. *Journal of Applied Physics* **2002,** *92* (2), 1132-1136.

34. Ogawa, S.; Yoshigoe, A.; Ishidzuka, S.; Teraoka, Y.; Takakuwa, Y., Consumption kinetics of Si atoms during growth and decomposition of very thin oxide on Si(001) surfaces. *Thin Solid Films* **2006,** *508* (1), 169-174.

35. Teraoka, Y.; Yoshigoe, A.; Moritani, K., Mechanisms of concurrent SiO desorption with oxide layer formation at Si(001) surface. *Electrical Engineering in Japan* **2008,** *164* (3), 60-68.

36. Enta, Y.; Nakazawa, H.; Sato, S.; Kato, H.; Sakisaka, Y., Silicon thermal oxidation and its thermal desorption investigated by Si 2p core-level photoemission. *Journal of Physics: Conference Series* **2010,** *235*, 012008.

37. Nakamura, Y.; Isogawa, M.; Ueda, T.; Yamasaka, S.; Matsui, H.; Kikkawa, J.; Ikeuchi, S.; Oyake, T.; Hori, T.; Shiomi, J.; et al., Anomalous reduction of thermal conductivity in coherent nanocrystal architecture for silicon thermoelectric material. *Nano Energy* **2015,** *12*, 845-851.

38. Lee, J.; Lee, S. Y.; Jeong, H. Y.; Cho, S. O., Oxygen Content-Controllable Synthesis of Non-Stoichiometric Silicon Suboxide Nanoparticles by Electrochemical Anodization. *Nanomaterials* **2020,** *10* (11), 2137.

39. Choi, C. H.; Liu, D.-J.; Evans, J. W.; Gordon, M. S., Passive and Active Oxidation of Si(100) by Atomic Oxygen: A Theoretical Study of Possible Reaction Mechanisms. *Journal of the American Chemical Society* **2002,** *124* (29), 8730-8740.

40. Hemeryck, A.; Richard, N.; Estève, A.; Djafari Rouhani, M., Diffusion of oxygen atom in the topmost layer of the Si(100) surface: Structures and oxidation kinetics. *Surface Science* **2007,** *601* (11), 2339-2343.

41. Arora, P.; Li, W.; Piecuch, P.; Evans, J. W.; Albao, M.; Gordon, M. S., Diffusion of Atomic Oxygen on the Si(100) Surface. *The Journal of Physical Chemistry C* **2010,** *114* (29), 12649-12658.

42. Tromp, R.; Rubloff, G. W.; Balk, P.; LeGoues, F. K.; van Loenen, E. J., High-Temperature SiO_2 Decomposition at the SiO_2/Si Interface. *Physical Review Letters* **1985,** *55* (21), 2332-2335.

43. Liehr, M.; Lewis, J. E.; Rubloff, G. W., Kinetics of high-temperature thermal decomposition of SiO2 on Si(100). *Journal of Vacuum Science & Technology A* **1987,** *5* (4), 1559-1562.

44. Watanabe, H.; Fujita, K.; Ichikawa, M., Thermal decomposition of ultrathin oxide layers on Si(111) surfaces mediated by surface Si transport. *Applied Physics Letters* **1997,** *70* (9), 1095-1097.

45. Watanabe, H.; Fujita, S.; Maruno, S.; Fujita, K.; Ichikawa, M., Selective thermal decomposition of ultrathin silicon oxide layers induced by electron-stimulated oxygen desorption. *Applied Physics Letters* **1997,** *71* (8), 1038-1040.

46. Johansson, U.; Zhang, H.; Nyholm, R., Thermal desorption of oxides on Si(100): a case study for the scanning photoelectron microscope at MAX-LAB. *Journal of Electron Spectroscopy and Related Phenomena* **1997,** *84* (1), 45-52.

47. Miyata, N.; Watanabe, H.; Ichikawa, M., Thermal Decomposition of an Ultrathin Si Oxide Layer around a Si(001)- (2×1) Window. *Physical Review Letters* **2000,** *84* (5), 1043-1046.

48. Xue, K.; Xu, J. B.; Ho, H. P., Nanoscalein situinvestigation of ultrathin silicon oxide thermal decomposition by high temperature scanning tunneling microscopy. *Nanotechnology* **2007,** *18* (48), 485709.

49. Enta, Y.; Osanai, S.; Ogasawara, T., Activation energy of thermal desorption of silicon oxide layers on silicon substrates. *Surface Science* **2017,** *656*, 96-100.

50. Porter, R. F.; Chupka, W. A.; Ingiiram, M. G., Mass Spectrometric Study of Gaseous Species in the Si-SiO2 System. *The Journal of Chemical Physics* **1955,** *23* (1), 216-217.

51. Schick, H. L., A Thermodynamic Analysis of the High-temperature Vaporization Properties of Silica. *Chemical Reviews* **1960,** *60* (4), 331-362.

52. Shornikov, S.; Archakov, I. Y.; Shul'ts, M., Mass spectrometric study of vaporization and thermodynamic properties of silicon dioxide. I. Composition of the gas phase and partial vapor pressures of the molecular forms over silicon dioxide. *Russian journal of general chemistry* **1998,** *68* (8), 1171-1177.

53. Shornikov, S.; Archakov, I. Y.; Shul'ts, M., Mass spectrometric study of vaporization and thermodynamic properties of silicon dioxide: II. Determination of partial vaporization coefficients of silicon dioxide. *Russian journal of general chemistry* **1999,** *69* (2), 187-196.

54. Howder, C. R.; Bell, D. M.; Anderson, S. L., Optically Detected, Single Nanoparticle Mass Spectrometer With Pre-Filtered Electrospray Nanoparticle Source. *Rev. Sci. Instrum.* **2014,** *85*, 014104 -014110.

55. Long, B. A.; Rodriguez, D. J.; Lau, C. Y.; Anderson, S. L., Thermal emission spectroscopy for single nanoparticle temperature measurement: optical system design and calibration. *Appl. Opt.* **2019,** *58* (3), 642-649.

56. Long, B. A.; Rodriguez, D. J.; Lau, C. Y.; Schultz, M.; Anderson, S. L., Thermal Emission Spectroscopy of Single, Isolated Carbon Nanoparticles: Effects of Particle Size, Material, Charge, Excitation Wavelength, and Thermal History. *J. Phys. Chem. C* **2020,** *124*, 1704-1716.

57. Schlemmer, S.; Illemann, J.; Wellert, S.; Gerlich, D., Nondestructive High-Resolution And Absolute Mass Determination Of Single Charged Particles In A Three-Dimensional Quadrupole Trap. *J. Appl. Phys.* **2001,** *90* (10), 5410-5418.

58. Gerlich, D.; Decker, S., Trapping Ions at High Temperatures: Thermal Decay of C_{60}^{+}. *Appl. Phys. B: Lasers Opt.* **2014,** *114*, 257-266.

59. Bell, D. M.; Howder, C. R.; Johnson, R. C.; Anderson, S. L., Single CdSe/ZnS Nanocrystals in an Ion Trap: Charge and Mass Determination and Photophysics Evolution with Changing Mass, Charge, and Temperature. *ACS Nano* **2014,** *8*, 2387–2398.

60. Bohren, C. F.; Huffman, D. R., *Absorption and Scattering of Light by Small Particles*. Wiley: New York, 1983.

61. Kawamura, H.; Fukuyama, H.; Watanabe, M.; Hibiya, T., Normal spectral emissivity of undercooled liquid silicon. *Measurement Science and Technology* **2005,** *16* (2), 386.

62. Bowman, H.; Schoonover, R. M.; Carroll, C. L., Density Scale Based on Solid Objects. *J. Res. Natl. Bur. Stand., A* **1974,** *78* (1), 13-40.

63. Hultgren, R.; Metals, A. S. f.; Commission, U. S. A. E., *Selected Values of the Thermodynamic Properties of the Elements*. American Society for Metals: 1973.

64. Morita, M.; Ohmi, T.; Hasegawa, E.; Kawakami, M.; Ohwada, M., Growth of native oxide on a silicon surface. *Journal of Applied Physics* **1990,** *68* (3), 1272-1281.

65. Murray, V. J.; Smoll, E. J.; Minton, T. K., Dynamics of Graphite Oxidation at High Temperature. *J. Phys. Chem. C* **2018,** *122* (12), 6602-6617.

66. In *CRC Handboook of Chemistry and Physics*, Rumble, J. R., Ed. CRC Press/Taylor and Francis Group: Boca Raton, FL.

TOC graphic

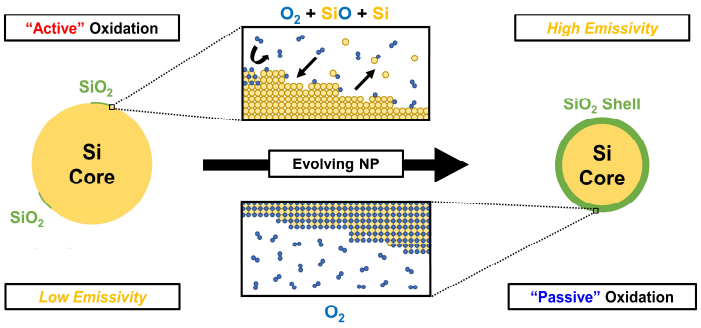
"Active" Oxidation
O_2 + SiO + Si
High Emissivity
SiO_2
Si Core
SiO_2
Evolving NP
SiO_2 Shell
Si Core
Low Emissivity
O_2
"Passive" Oxidation

O_2 Oxidation and Sublimation Kinetics of Single Silicon Nanoparticles at 1200 to 2050 K: Variation of Reaction Rates, Evolution of Structural and Optical Properties, and the Active-to-Passive Transition

*Daniel J. Rodriguez, Chris Y. Lau, Abigail M. Friese, Bryan A. Long, and Scott L. Anderson**

Department of Chemistry, University of Utah, 315 S. 1400 E., Salt Lake City, UT 84112

*Corresponding author: anderson@chem.utah.edu, (801)-585-7289

Supporting Information

A) Literature Overview of Si/O_2 Chemistry

The chemistry of Si with O_2 is relevant to the semiconductor industry where the performance of MOSFET devices depends strongly on the Si/SiO_2 interface,[1-3] and for high temperature materials such as silicon carbide (SiC), where oxidation of the surface leads to formation of SiO_2. Because of its importance, there is considerable literature on this process, albeit mostly at lower temperatures than in the experiments presented here. In essence, the O_2-oxidation of Si can be broken into several key steps.

First, there is the initial dissociative chemisorption of O_2 at some surface temperature (T_s) with sticking coefficient, S. For a partially oxidized surface, S is reduced in comparison to S_0 (the sticking coefficient for a clean oxide-free surface). D'Evelyn et al.[4] measured S_0 for Si(100) at various T_s values: ~1% at 300 K, ~0.3% at 600 K, and ~0.6% at 800 K for Si (100). At T_s > 800 K, S_0 was observed to slowly increase, then to fall again for T_s > 1250 K. They also found that S_0 was a factor of three higher for lightly etched surfaces, compared to freshly annealed Si(100). Engstrom et al.[5] measured adsorption kinetics of both O_2 and O for Si(100). For O_2, S_0 = 3% at 300 K, and S_0 for atomic O was unity, but it was confirmed that after 1-5 monolayers (MLs) of oxygen coverage (depending on T_s), the surface saturated and the sticking coefficient (S) decreased to near zero for both O_2 and O. At low T_s, saturation occurred at 1 ML coverage, but by 800 K, even 2 ML coverage only reduced S by ~50%. Seiple et al.[6] also analyzed Si (100) determining S_0 = 4% at 900 K for collisions of O_2.

At the high temperatures of interest in our experiments, most of the O atoms resulting from O_2 chemisorption quickly desorb as SiO and etch the surface or diffuse/isomerize between different sites on the surface and the sub-surface (selvage). The observation that Si surfaces can eventually passivate against further O_2 attack has been shown to result from nucleation and growth of SiO_2 islands, which are more thermally stable than O_{ads} and can grow to cover the surface under the right conditions. Models for Si(100) oxidation[5, 7-9] have identified several geometries for O_{ads} that are intermediates to both SiO desorption and SiO_2 formation, including on-dimer O (ODO), dimer bridging O (DBO), and back-bonded O (BBO). D'Evelyn et al.[4] recognized that several forms of O_{ads} had to exist, and proposed that both etching and

passivation involve O attached at steps or other low-coordination sites. Engstrom et al.[10] proposed a kinetic model where the DBO species was responsible for all nucleation and growth of SiO_2, however, Choi et al.[7] showed that, in addition to the DBO configuration, the ODO and BBO were also stable, implying multiple O_{ads} species can be involved in passive oxidation. The same conclusions were also made in calculations by Hemeryk et al.[8] and Arora et al.[9], illustrating BBO's role in sub-surface diffusion. Interestingly, this BBO structure is also significant to active oxidation, i.e., etching of the surface via SiO desorption. While Engstrom et al.[10] considered a silanone species or SiO-like intermediate to be critical for active oxidation, Choi et al.[7] only found evidence of BBO formation prior to etching. Again, this illustrates how passivation (i.e., SiO_2 formation) and active etching (SiO desorption) occur via coupled and competing pathways. As noted in the manuscript, because we are insensitive to the O_{ads} geometry, we simply use O_{ads} to refer to any adsorbed O atoms, as distinct from oxygen incorporated into SiO_2.

In essence, the oxidation mechanism is controlled by competition between SiO desorption and SiO_2 nucleation and growth. "Passive" oxidation, i.e., passivation by a SiO_2 surface layer is favored by conditions that favor the nucleation/growth and thermal stability of SiO_2,[4-6, 10-39] corresponding to high P_{O2} and low T_s. "Active" oxidation, i.e. continuous etching, is favored by conditions that result in low O_{ads} coverage, preventing SiO_2 nucleation/growth, or that make surface SiO_2 unstable with respect to decomposition and desorption, i.e., high T_s and low P_{O2}. In the transitional range between these limits, both active and passive oxidation occur, and while most O_{ads} might desorb as SiO, some O_{ads} (or selvage O) might react to nucleate SiO_2 islands that eventually grow to passivate the surface. The parameters leading to active vs. passive oxidation have been summarized in P_{O2}-T phase diagrams.[11, 14, 21]

The growth mode of SiO_2 on Si has also been studied. In the transition regime, Engstrom et al.[10] observed that the SiO_2 growth is layer-by-layer at $T_s < 900$ K, but at $T_s > 1050$ K, i.e., under our conditions, SiO_2 growth is in the form of 3D islands. In STM experiments by Feltz et al.[18, 21], the same observation is noted at $P_{O2} = 10^{-9} – 10^{-6}$ Torr and T = 850 – 1130 K, and Smith et al.[14] also noted conical 3D SiO_2 under conditions of 4.5×10^{-3} Torr and 1300 K. Island formation during simultaneous active and passive oxidation has been interpreted as indicating that oxide clusters tend to nucleate at step sites. Then, as the clusters

grow, they pin underlying step sites and impede any further etching from O_2. However, in regions where Si is exposed, etching may continue unimpeded, causing the surface to "roughen" over time, which aids in the formation of the 3D SiO_2 structures. Provided enough time, the surface becomes completely passivated, and the etching reaction will cease all together. For $T_s > 1400$ K, there is far less information available on Si oxidation, but there is indication that semi-stable oxides can appear on a molten Si surface at 1650 K.[40] If T_s is increased to >1800 K (above bulk Si's melting point, 1687 K) then sublimation of both Si and SiO_2 compete with the oxidation kinetics.

The SiO_2 passivating layer can be unstable at high temperatures. If silicon with an surface oxide layer is held in vacuum above ~1000 K, both oxides and sub-oxides have been observed to be decompose by reaction with the underlying silicon: $Si_{(s)} + SiO_{2(s)} \rightarrow 2SiO_{(g)}$, eventually exposing unoxidized Si.[35, 41-48] At $T_s = 1400$ K, for example, a 10 nm thick SiO_2 layer on bulk silicon was found to desorb in an ~hour.[41] Walkup et al.[16] showed that when Si was oxidized to the point of forming a passivating SiO_2 layer, SiO molecules were detected in the gas phase several minutes after terminating the O_2 flow, attributed to the SiO_2 + Si decomposition reaction. These results suggest that the much thinner (~0.5 nm[49]) native oxide present on our as-trapped NPs should be mostly or entirely lost during the long 1200 K Q-stepping period preceding the oxidation studies, and should be entirely absent for "preheated" NPs that were held in argon at $T_{NP} \geq 1800$ K for ~20 minutes. Finally, our highest T_{NP} experiments were in the temperature range where both bulk Si and bulk SiO_2 are observed to sublime in vacuum, with Si atoms dominating the vapor phase for Si,[50] and a distribution of Si, SiO, O_2, O, and Si_2O_2 species observed for bulk SiO_2.[51-54]

Finally, a number of oxidation experiments have been reported for Si NPs,[55-58] although not for single NPs. For example, Liao et al.[57] studied reactions of ensembles of Si NPs (diameter = 10 nm) by tandem differential mobility analysis. Over a temperature range from 900 – 1400 K, particle mobility diameters were found to *increase* by ~1 nm, dependent upon reaction temperature and oxygen volume fraction, i.e., there was net NP growth due to formation of the oxide layer. In contrast, we never observed mass gain under our conditions, presumably because for our low P_{O2}, the rate of mass lost to SiO desorption always exceeded the rate of mass addition in the form of oxygen. P_{O2} was orders of magnitude higher in

their experiments, evidently in the range of parameter space where oxide growth exceeded etching. Thus, our results are more similar to bulk surface science experiments, where P_{O2} was also low.

B) Determining Charge (Q) and Calculation of NP Mass (M)

Consider **Fig. S1** where a Si NP (~88.5 MDa) was exposed to a VUV lamp, leading to a series of single electron Q steps (ΔQ), evident in the figure as quantized steps (ΔF_z) in the secular frequency (F_z), where ($\Delta F_z/F_z = \Delta Q/Q$). The series of steps were fit to determine that the initial Q in this case was +52 e. For NPs with Q ≤ 60 e, we are generally able to determine Q exactly, i.e., with uncertainty < 1 e. For higher Q, the uncertainty in Q is ~1%, which adds to the mass uncertainty. The uncertainty in the M values extracted from **Eqn. 1** (main text) is primarily due to the uncertainties in V_0, measured with ~0.1% accuracy, and in the geometric parameter, z_0, which includes both the precision with which the actual trap was

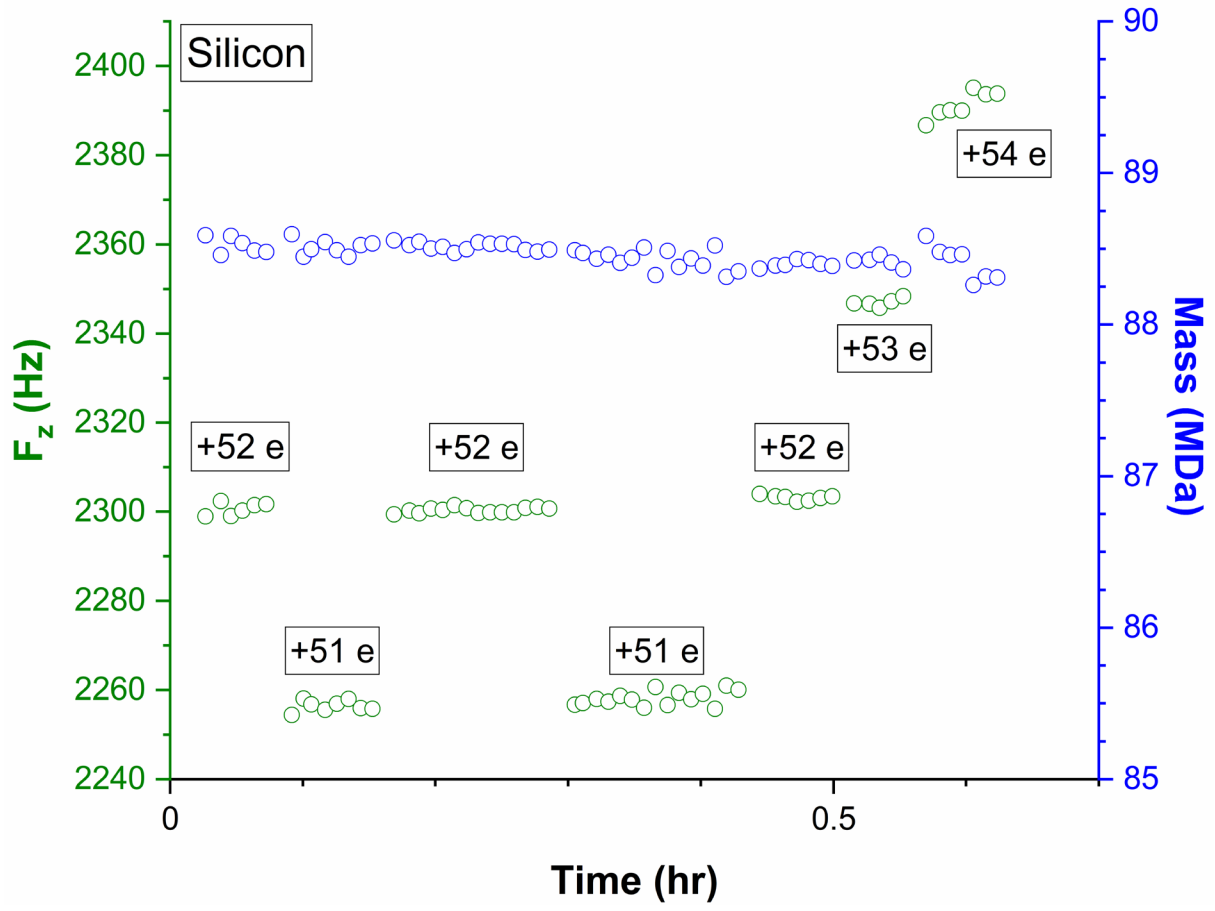

Figure S1: Charge stepping sequence using the VUV lamp for a Si NP. The initial charge state, Q, was determined to be +52 e, and the initial mass of the NP was ~88.5 MDa.

constructed, and any effects of anharmonicity on the secular frequency measurements. The corresponding uncertainty in the absolute value of extracted masses is roughly ±1.3%, or ±2.3% in cases where Q could not be determined exactly. The relative uncertainties in comparing different mass measurements are lower, typically on the order of 0.2%, and the uncertainty in fitting sets of points to determine the slope of M vs. time, or to look for abrupt mass changes upon O_2 introduction are better yet, typically <0.1%.

C) Silicon NP Emission Spectroscopy – Spectral Measurements

Fig. S2 shows the evolution of emission spectra collected in the course of doing the experiment in **Fig. 1**, where T_{NP} was ramped up and down over the 1550 – 2050 K range several times while measuring sublimation mass loss. The total mass loss in **Fig. 1** was ~12.9%, thus any effects on emission intensity from the shrinking size would be much smaller than the observed intensity changes, and should be adequately corrected using the volume scaling approach described previously.[59-62] The spectra are labeled "Heating 1", "Cooling 1" to indicate the ramp when they were collected, and the times in seconds when each spectrum was collected are indicated. The main difference between spectra is that the "Heating 1" spectra, i.e., those collected as the NP was heated for the first time, were considerably weaker than spectra taken at the T_{NP} later in the experiment. Once the NP had been heated to high T_{NP}, the emission intensities were relatively stable thereafter. Note that the change in intensity was much smaller for the higher T_{NP} values, indicating that whatever changes occurred during the first heating ramp had mostly occurred at lower T_{NP}.

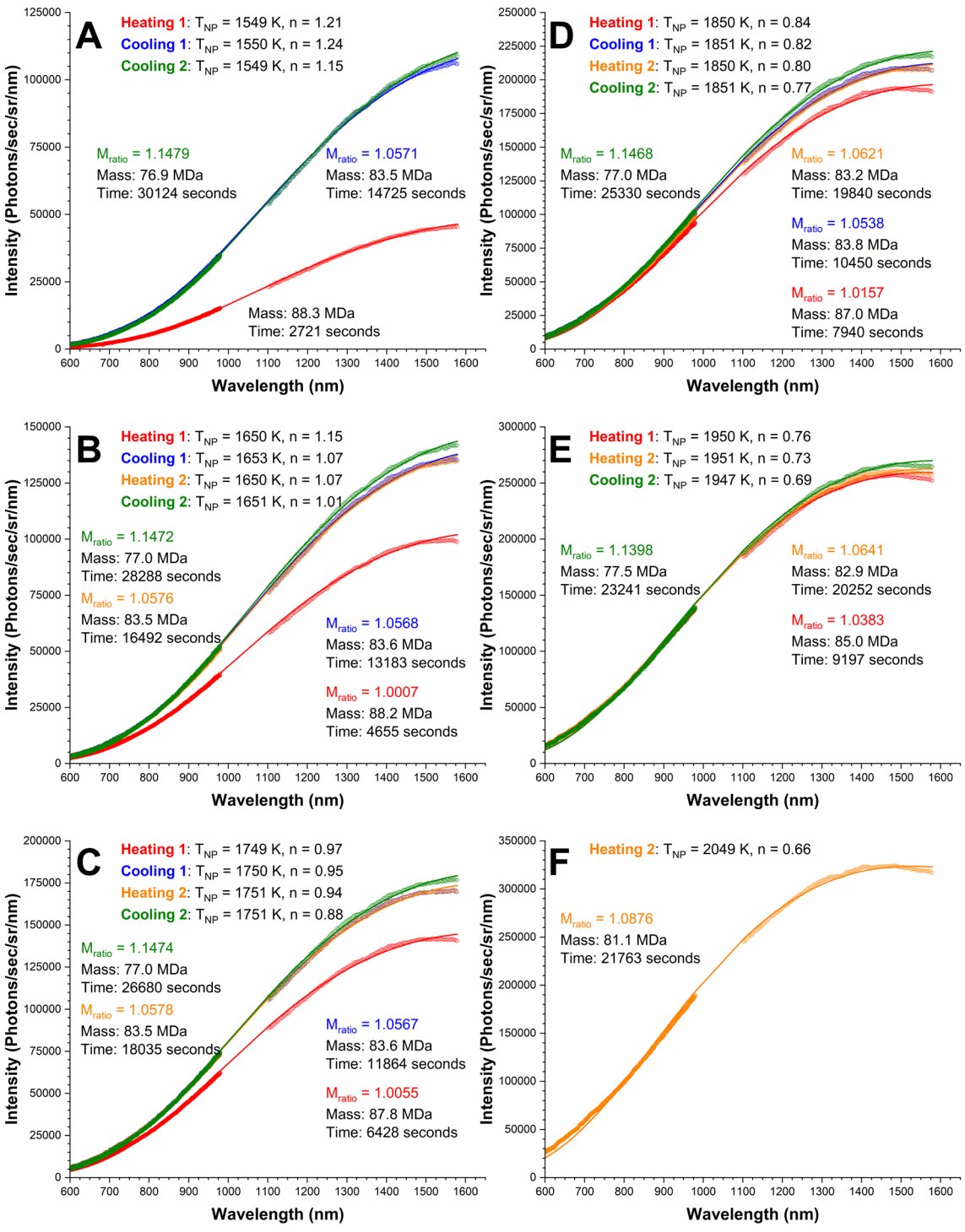

Figure S2: Emission spectra from **Fig. 1** for a Si NP at different times. A). ~1550 K. B). ~1650 K. C). ~1750 K. D). ~1850 K. E). ~1950 K. F). ~2050 K.

D) Silicon NP Emission Spectroscopy – Summary

Fig. S3 shows how the integrated emission intensities (I_{NP}), the "n" spectral fitting parameter, and the heating laser power required to hold the NP at each T_{NP} step varied during the experiment in **Fig. 1**. The I_{NP} values in **Fig. S3A** increased rapidly with T_{NP}, as expected (note log scale). The "Heating 1" data are fit moderately well by $I_{NP} \propto T_{NP}^{9.0}$, and the data during the subsequent cooling and heating ramps are well fit by $I_{NP} \propto T_{NP}^{5.9}$. The large exponent for the initial heating ramp reflects the irreversible emission brightening shown in **Fig. S2**, and it is clear that much of the brightening occurred between 1550 and 1650 K. The ~T^6 dependence after the Heating 1 ramp is typical for the visible and nIR portion of NP thermal emission spectra.

Fig. S3B shows how the "n" parameter changed as the NP is heated and cooled. Roughly speaking, increasing the n parameter results in more curvature and sharper peaking of the fitting function. For all heating and cooling cycles, the n values, and their variation with T_{NP} were quite similar.

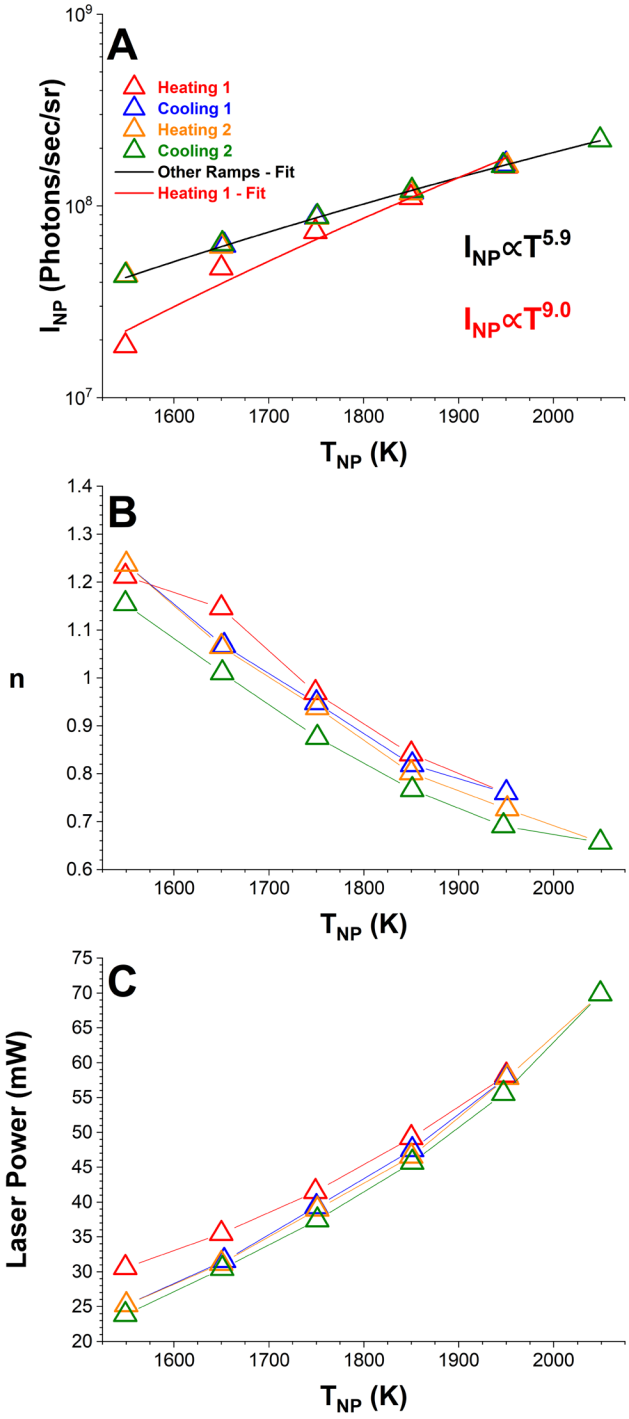

Figure S3: Summary of a Si NP's (**Fig. 1**) optical properties vs. T_{NP}. A). I_{NP}. B). "n" parameter. C). 532 nm laser power.

The graph of laser power vs. T_{NP} in **Fig. S3C** also provides some insight. Here the laser powers have not been scaled to account for the NP size, and it is interesting to compare the laser powers required to reach various T_{NP} values over the course of the experiment, to the resulting I_{NP} values. For example, in the 1st heating ramp the laser power at ~1550 K was ~31 mW and I_{NP} was ~2.0 x 10^7, increasing to ~58 mW with $I_{NP} \approx$ 1.5 x 10^8 at ~1950 K, i.e., increasing T_{NP} by a factor of ~1.3 required ~1.9 times higher laser power and produced ~7.5 times more visible and nIR emission. This implies that laser power was proportional to $T_{NP}^{\sim 3.2}$, while as noted above, I_{NP} was proportional ~$T_{NP}^{\sim 9.0}$ during the initial heat up.

As has been discussed previously,[61] T_{NP} is determined by the balance between laser heating and the sum of cooling by buffer gas collisions, sublimation, and thermal radiation. Assuming unit energy accommodation, the collisional cooling power for an NP of this size would range from ~1.7 to ~2.4 x 10^{-12} W, for T_{NP} ranging from ~1550 K to ~2050 K. Given that $\Delta H_{sublimation}$ of Si is ~4.7 eV/atom, even at the maximum mass loss rate (~108 Si atoms/sec at 2050 K, **Fig. 1**), the sublimation cooling would be <1 keV/sec or <10^{-16} W, i.e., negligible. The radiative cooling power can be estimated from the Stefan-Boltzmann law, with some assumption about the wavelength-dependent emissivity. Kawamura et al.[63] reported the emissivity of molten Si to be ~0.2, and together with **Eqn. 3** (main text), we might roughly estimate the average NP emissivity to be ~0.1 for NPs. In that case, the radiated power would range from ~2.5 to ~7.7 x 10^{-10} W over the same T_{NP} range, i.e., for any reasonable assumption about emissivity, radiative cooling is responsible for ~99% of the total cooling in our experiments. Thus, the fact that the T_{NP} dependence of the heating laser power was different than that for I_{NP} implies that both the NP emissivity and its absorptivity for the 532 nm heating laser increased significantly as the NP was initially heated, but differently. Note that after the initial heating, the laser power required, particularly at the lower T_{NP} values, did not undergo further changes.

E) Another Silicon NP Sublimation Experiment

A second Si NP was studied following the same experimental protocol as **Fig. 1**. This NP was larger, with initial mass of 306 MDa (**Fig. S4A**), and was certainly an aggregate. At ~0.5 hours, the NP

was charge stepped at T_{NP} = 1200 K (not shown). Then the NP's mass was monitored every ~30 seconds as T_{NP} was stepped between 1550 to 1950 K in several heating/cooling ramps. For ~30 minutes at each set point T_{NP}, mass loss rates were determined by fitting regressions through the M vs. time points. The log of the mass loss rates measured in this experiment are shown in **Fig. S4B** in Da/sec/nm^2. At lower T_{NP}, the mass loss rate is T_{NP} independent and affected from a combination of sublimation + reactions with background gases. At T_{NP} >1700 K, the rate is mostly sublimation.

I_{NP} is also plotted and follows the same path as the laser power. In the 1st heating ramp at 1550 K, I_{NP} was ~6.5 x 10^7, and when increased to 1950 K, I_{NP} increased to ~4.3 x 10^8.

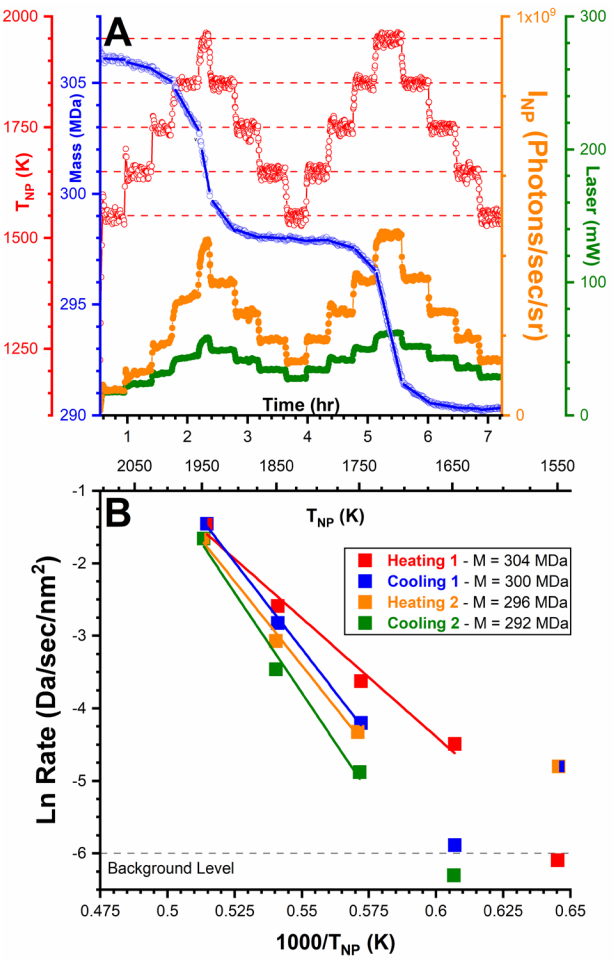

Figure S4: Another T_{NP} ramping experiment for a Si NP in an argon background of 2 mTorr.

This ~1.3 increase in T_{NP} required an ~6.6 increase in I_{NP}, i.e., I_{NP} is roughly proportional to $T_{NP}^{\sim 7.9}$. The initial gain in I_{NP} is comparable to that of the Si NP in **Fig. 1** and signifies that the emissivity of both NPs scaled faster than an ideal blackbody when initially heated to high T_{NP}.

F) Sublimation of a Silicon NP at Constant T_{NP}

In **Fig. S5**, a Si NP was twice pre-heated to 2000 K separated by a brief period at ~1350 K. This was done because Si NPs often undergo rapid thermionic emission when first heated to high T_{NP}, and it was necessary to re-adjust the trapping conditions after a few minutes to avoid loss of the NP. Note that the NP optical properties also changed significantly during the 2000 K heating, as shown by the very different laser

powers required to hold 2000 K during the first and second preheating periods, and by the near doubling of the 2000 K emissivity from the first to second preheating periods.

After pre-heating, the NP was Q-stepped at 1300 K (purple background) to determine $M_{initial}$ which was 48.0 MDa, consistent to it being a small aggregate of ~20 MDa primary particles that should have melted and coalesced during the 2000 K preheating. Finally, T_{NP} was set to ~1900 K and held for ~7.5 hours to observe how $R_{sublimation}$ evolved with time. $R_{sublimation}$ over the 7.5 hour period was ~0.2 Da/sec/nm^2, with only minor fluctuations, visible as small slope changes.

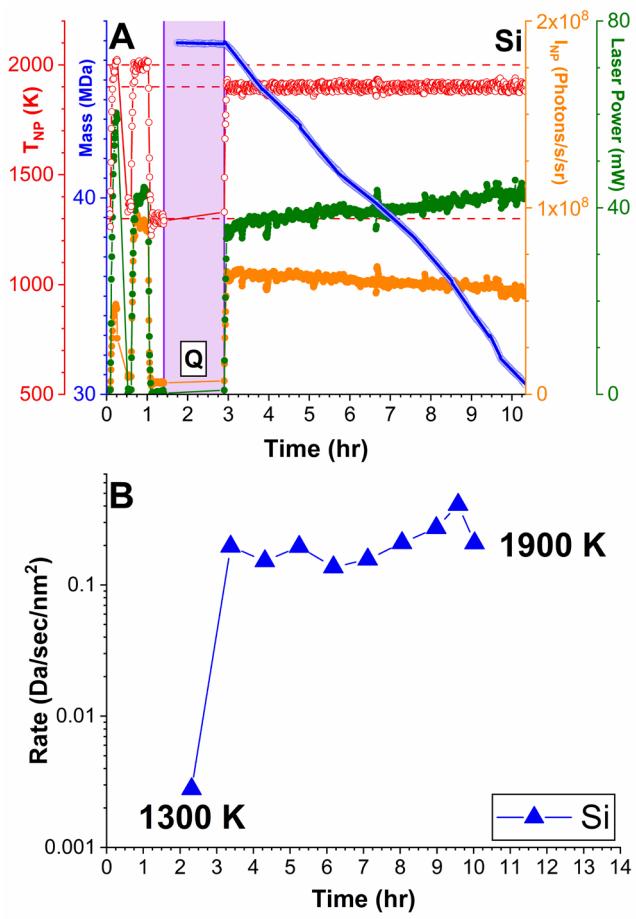

Figure S5: A). A Si NP at T_{NP} = 1900 K for ~7.5 hours. B). R vs. time. Note the faster R values at 1900 K indicating sublimation.

G) Determination of an Oxidation Rate for a Silicon NP

Fig. S6 shows a simple kinetics experiment on a Si NP to illustrate how we measure oxidation rates. The "Thermal History" inset shows the cleaning/Q-stepping process prior to the start of the record shown in the main figure. The Si NP was trapped, and T_{NP} was gradually increased to ~2000 K, desorbing contaminants as well as Si, but also causing thermionic emission generating a Q state that is stable at high T_{NP}. The NP was then cooled to ~1200 K for a period of Q-stepping, followed by increasing T_{NP} to the initial temperature for the kinetics experiment, 1800 K. Note that 1800 K is well above the bulk Si T_{melt} and in the range where $R_{base} \approx R_{sublimation}$. The experiment started by holding the NP in argon at 1800 K and measuring R_{base} = 2.8 x 10^{-2} Da/sec/nm^2 (I). Then O_2 was added at P_{O2} = 4.3 x 10^{-5} Torr (II), resulting in a

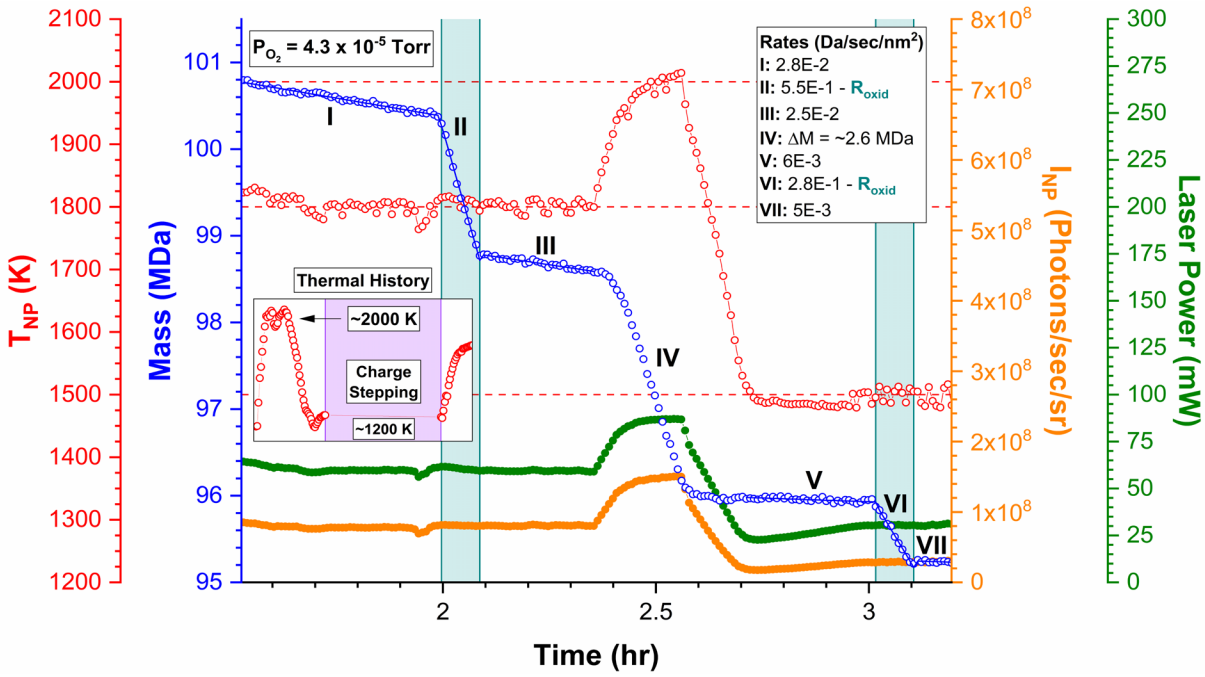

Figure S6: A Si NP held at 1800 K and 1500 K for measuring R_{oxid} and R_{base}. *Inset*: Prior to the start, the NP was first heated to 2000 K, then Q-stepped at ~1200 K.

~20-fold increase in the mass loss rate, which continued at nearly constant rate as the NP lost ~1.6% of its mass, stopping only when the O_2 flow was stopped to allow R_{base} to be re-measured. R_{oxid} was determined by subtracting R_{base} (here the average of R_{base} in periods I and III) from the total mass loss rate under oxidizing conditions, giving R_{oxid} = 5.5 x 10^{-1} Da/sec/nm^2.

Next, T_{NP} was ramped to just above 2000 K to remove any easily desorbed material, including oxides, by driving sublimation of ~2.6 MDa of mass, corresponding to roughly one ML's worth of material. T_{NP} was then dropped to 1500 K for a second oxidation experiment, this time at T_{NP} well below the bulk T_{melt}. At 1500 K, $R_{sublimation}$ should be negligible, thus the small R_{base} in period V (6 x 10^{-3} Da/sec/nm^2) is attributed to background reactions. In period VI, P_{O2} was 4.3 x 10^{-5} Torr, and again, the rate of mass loss increased, this time by a factor of almost 50, and R_{oxid}, after subtracting R_{base} was found to be 2.8 x 10^{-1} Da/sec/nm^2, i.e., about half the area-normalized rate observed at 1800 K. There were some minor fluctuations in T_{NP} during the constant T_{NP} periods attributed to variations in the heating laser power (due to instabilities in the control program), and in general both I_{NP} and the laser power tracked T_{NP}, as expected.

H) Effects of O_2 on Silicon NP Emission Spectra at T_{NP} = 1800 K and 1500 K

Fig. S7 compares four sets of three emission spectra taken during the kinetics experiment in **Fig. S6**, designed to test whether there were significant changes in spectral intensity or shape under sublimation conditions (2 mTorr Ar) vs. oxidizing conditions (Ar + 4.3 x 10^{-5} Torr O_2). The sets of spectra were taken just before, during, and just after O_2 flow was turned on or off. For example, **Fig. S7A** shows the spectra taken in conjunction with the first transition (from Ar only to Ar + O_2) at 1800 K, and spectra are labeled "Sublimation", "O_2 On", and "Oxidation". B shows the spectra associated with the transition from Ar + O_2 back to Ar-only conditions at 1800 K, and C and D show the analogous spectra for 1500 K. As shown, the three spectra were very similar within each set, with intensities changing by less than 1% and with no obvious systematic effect of oxidizing vs. inert conditions. The insets provide a closer look at the raw data

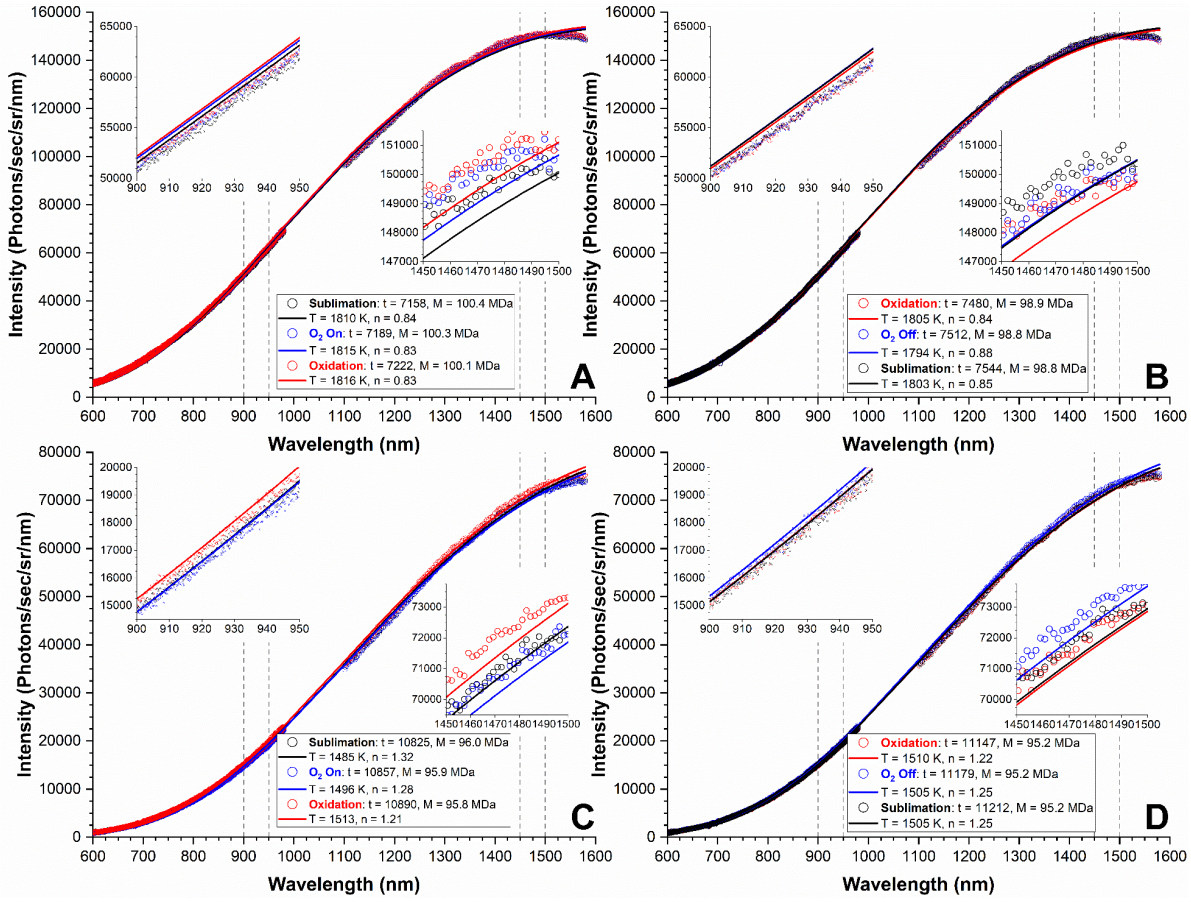

Figure S7: A-B). The transitions of Ar to Ar + O_2 at T_{NP} = 1800 K for a Si NP as well as Ar + O_2 to Ar. C-D). The same NP and atmospheric transitions, but at T_{NP} = 1500 K.

(symbols) and fits (lines). The left inset shows a portion of the "visible" (900 – 950 nm), and the right inset shows part of the "nIR" (1450 – 1500 nm).

The first spectrum taken was under "sublimation" conditions (black) which had parameters of T_{NP} = 1810 K and n = 0.84 (**Fig. S7A**). In addition, it had the lowest intensity, probably because it had the lowest T_{NP} of the set. When O_2 was switched on (blue), T_{NP} increased by 5 K (due to instability of the laser control – reaction exothermicity is negligible), the emissivity parameter, n, decreased by 0.01, and I_{NP} also increased slightly. The "oxidation" spectrum (red) was taken next, after P_{O2} had stabilized, and had the highest I_{NP} of the set, probably because it also had the highest T_{NP}, but n remained fixed at 0.83. The insets also show the limitations of the fitting process used to extract T_{NP}. The fits are good, but not perfect, probably due mostly to the assumption of a simplified power law to model emissivity. The transitions when O_2 was stopped at 1800 K, and the O_2 on and off transitions at 1500 K are shown in frames B-D. Again, there was little difference in spectra taken under oxidizing and inert conditions. The T_{NP} and n parameters are summarized in the figure legends.

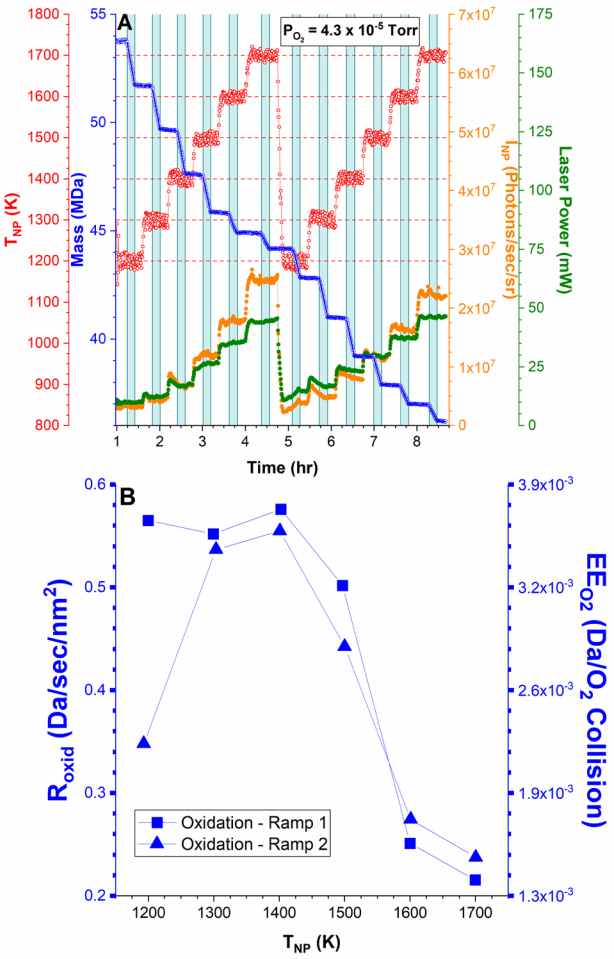

Figure S8: A). A Si NP from T_{NP} = 1200 – 1700 K measuring R_{oxid} at P_{O2} = 4.3 x 10^{-5} Torr. I_{NP} and laser power vs. time are also plotted. B). R_{oxid} vs. T_{NP} for both ramps.

I) Another example of Silicon NP Oxidation at Variable T_{NP}

Fig. S8A depicts M vs. time similar to that in **Fig. 2**. A 53.7 MDa Si NP was alternatively held in Ar and Ar with 4.3 x 10^{-5} Torr of O_2 with T_{NP} stepped between 1200 K and 1700 K. I_{NP} and laser power

are also plotted and rise with increasing T_{NP}, as expected. **Fig. S8B** shows the R_{oxid} values extracted by fitting the slopes of M vs. time and correcting for the much smaller $R_{baseline}$ values measured between each oxidation period. The same symbol scheme in **Fig. 2** was used. R_{oxid} broadly peaked at 1200 – 1400 K and declined as T_{NP} increased. The initial R_{oxid} in this T_{NP} range during the 1st heat ramp was ~5.8 x 10^{-1} Da/sec/nm^2, or about ~72% slower than for the NP in **Fig. 2**. In the 2nd heat ramp, R_{oxid} also peaked at T_{NP} ≈ 1400 K, but this time the 1200 K rate was substantially smaller, and the other rates were also slightly smaller than in the first ramp.

J) Another Example of Oxidation of a Silicon NP at Constant T_{NP} and P_{O2}

Fig. S9 illustrates the effects of long-term oxidation on a 95.2 MDa Si NP at ~1500 K. This experiment was done using the same Si NP in **Fig. S6**, i.e., the NP had been preheated and briefly oxidized

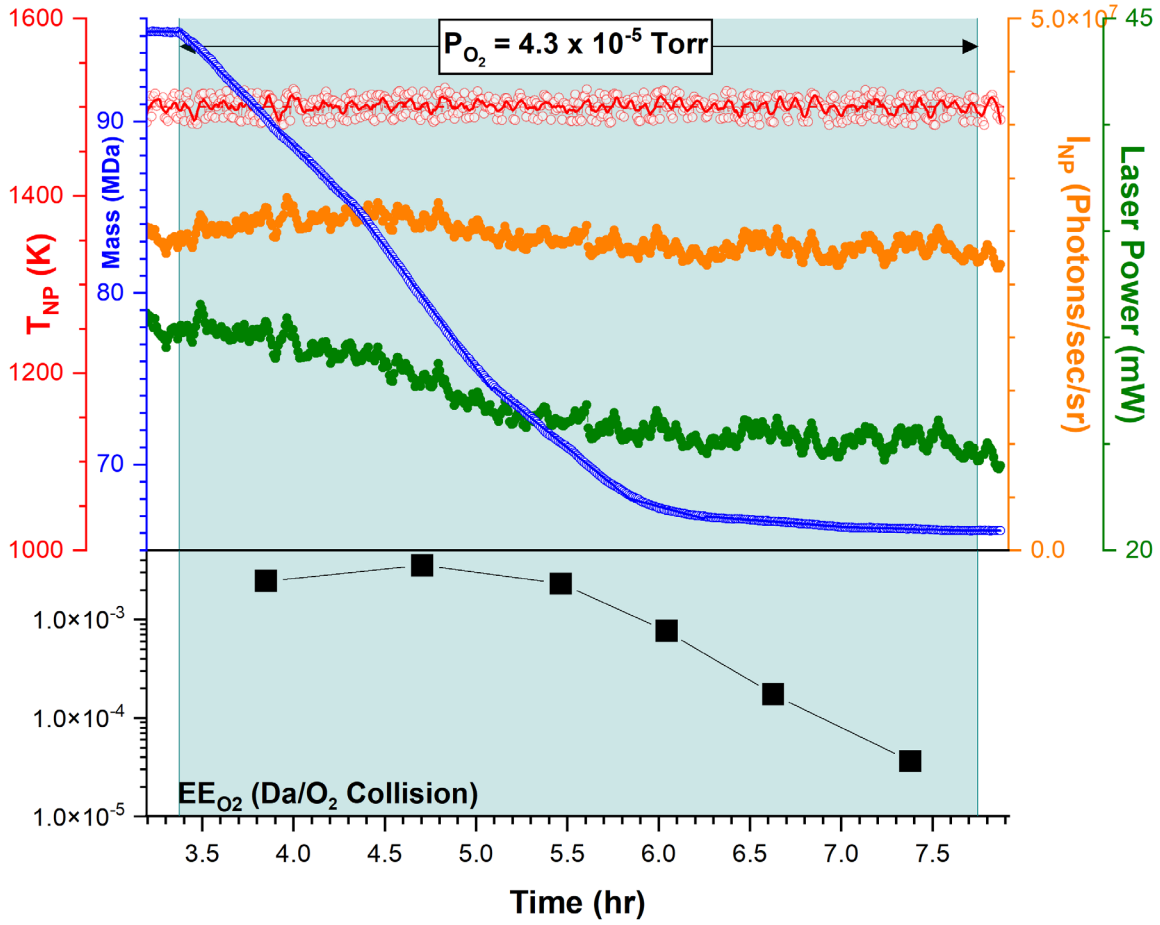

Figure S9: A Si NP is oxidized at constant conditions of T_{NP} = 1500 K and P_{O2} = 4.3 x 10^{-5} Torr until its EE_{O2} value dropped to our sensitivity limit signaling its passivation.

at 1800 K and 1500 K before the long 1500 K oxidation period shown. After briefly re-measuring $R_{baseline}$, the NP was held for ~4.4 hours at P_{O2} = 4.3 x 10^{-5} Torr. The initial EE_{O2} was similar to that measured briefly at 1500 K in **Fig. S6**, was roughly constant for several hours, then abruptly dropped by an order of magnitude around the 6 hour mark and continued to drop until the experiment was ended. The final EE_{O2} was nearly 2 orders of magnitude lower than the initial value. This data set is modeled in **Fig. 10**.

K) Another Constant T_{NP}, P_{O2} Oxidation Experiment for $T_{NP} > T_{melt}$

In an experiment similar to **Fig. 5**, **Fig. S10** shows a constant T_{NP} and P_{O2} experiment on a 133 MDa Si NP. Beforehand, the NP was heated to 1900 K, lowered to 1200 K for Q-stepping, and then re-heated back to ~1750 K (not shown). At T_{NP} = 1750 K, the NP then was then oxidized for the next ~1.4

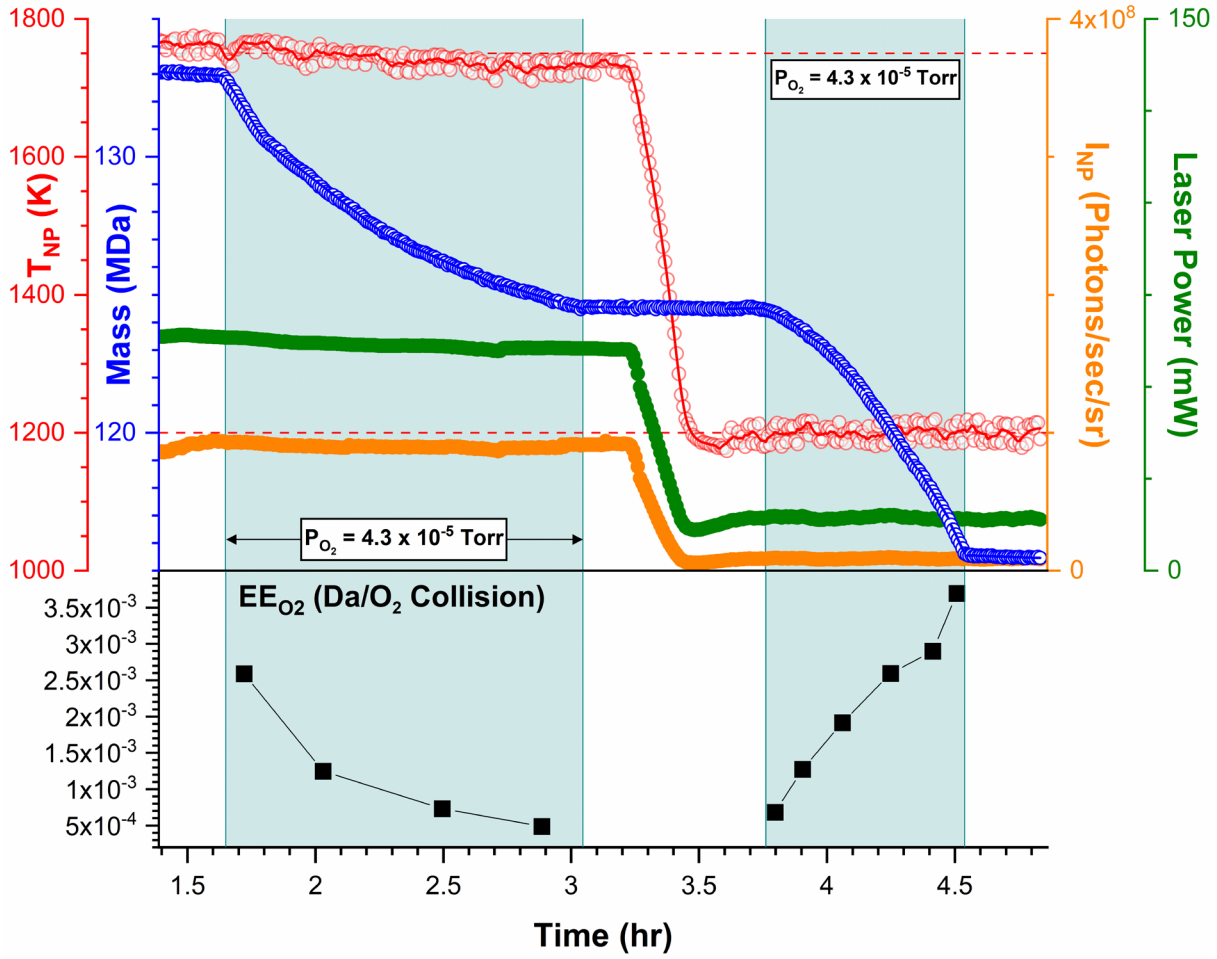

Figure S10: A 133 MDa Si NP was heated to 1750 K and 1200 K where it was oxidized at P_{O2} = 4.3 x 10^{-5} Torr. EE_{O2} vs. time decreased in the 1st half (high T_{NP}) and increased in the 2nd half (low T_{NP}).

hours, resulting in EE_{O2} steadily decreasing with time. At the time the O_2 was shut off, EE_{O2} had dropped to ~5 x 10^{-4} Da/O_2 collision, and the result suggests that it would have continued to decline slowly if the oxidation period had been continued. Instead, the NP was held at 1750 K, to desorb any surface oxide present, then T_{NP} was cooled to 1200 K. Interestingly, when O_2 was re-introduced, EE_{O2} started at a low value, then gradually increased by a factor of ~5.4 during the ~0.8 hour oxidation period, and was still increasing when the oxidation period was ended. The longer-time behavior would presumably have been similar to that shown in **Fig. 5**, i.e., the NP would have eventually passivated.

L) Additional O_2 Oxidation at T_{NP} = 1200 K and Constant P_{O2}

The first example, **Fig. S11**, shows a 77.0 MDa Si NP oxidizing at T_{NP} = 1200 K. This experiment was done immediately after the sublimation experiment in **Fig. 1**, i.e., the NP had been preheated to 2050 K, and therefore should have been oxide free and melted before T_{NP} was reduced to 1200 K. When O_2 was added the NP began to etch, but then M stabilized due to the O_2 flow having accidently been reduced substantially. When the error was corrected at ~8.75 hours, the etching mass loss resumed, gradually increasing over the course of the ~70 minute oxidation period. I_{NP} and laser power are also shown and track with T_{NP}, i.e., remaining stable throughout the experiment.

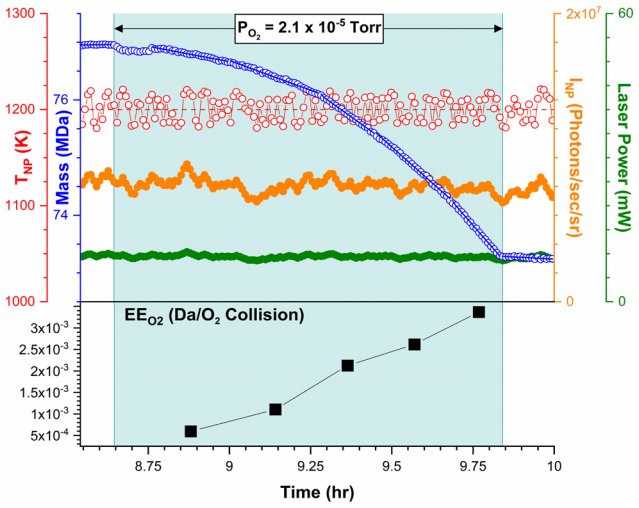

Figure S11: A Si NP was oxidized at T_{NP} = 1200 K and P_{O2} = 2.1 x 10^{-5} Torr.

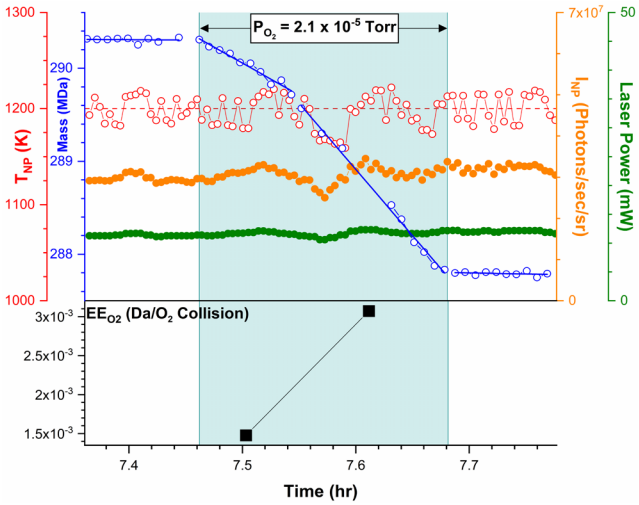

Figure S12: A Si NP is oxidized briefly at T_{NP} = 1200 K and P_{O2} = 2.1 x 10^{-5} Torr.

Another example for a Si NP at T_{NP} = 1200 K and P_{O2} = 2.1 x 10^{-5} Torr is shown in **Fig. S12**, which was done immediately following the sublimation experiment shown in **Fig. S4**, i.e., this NP had also been preheated/melted prior to the 1200 K oxidation experiment, which was run only long enough to verify that EE_{O2} initially increased (by a factor of 2.1) as the NP oxidized. Again, T_{NP}, I_{NP}, and laser power tracked together, i.e., were constant, apart from a control glitch at ~7.57 hours, where they all fluctuated together.

Finally, an experiment on a 49.9 MDa Si NP that was not preheated above 1200 K is shown in **Fig. S13.** In this example EE_{O2} increased by a factor of ~2.2 times over ~1 hour starting at ~4.7 x 10^{-3} Da/O_2 collision.

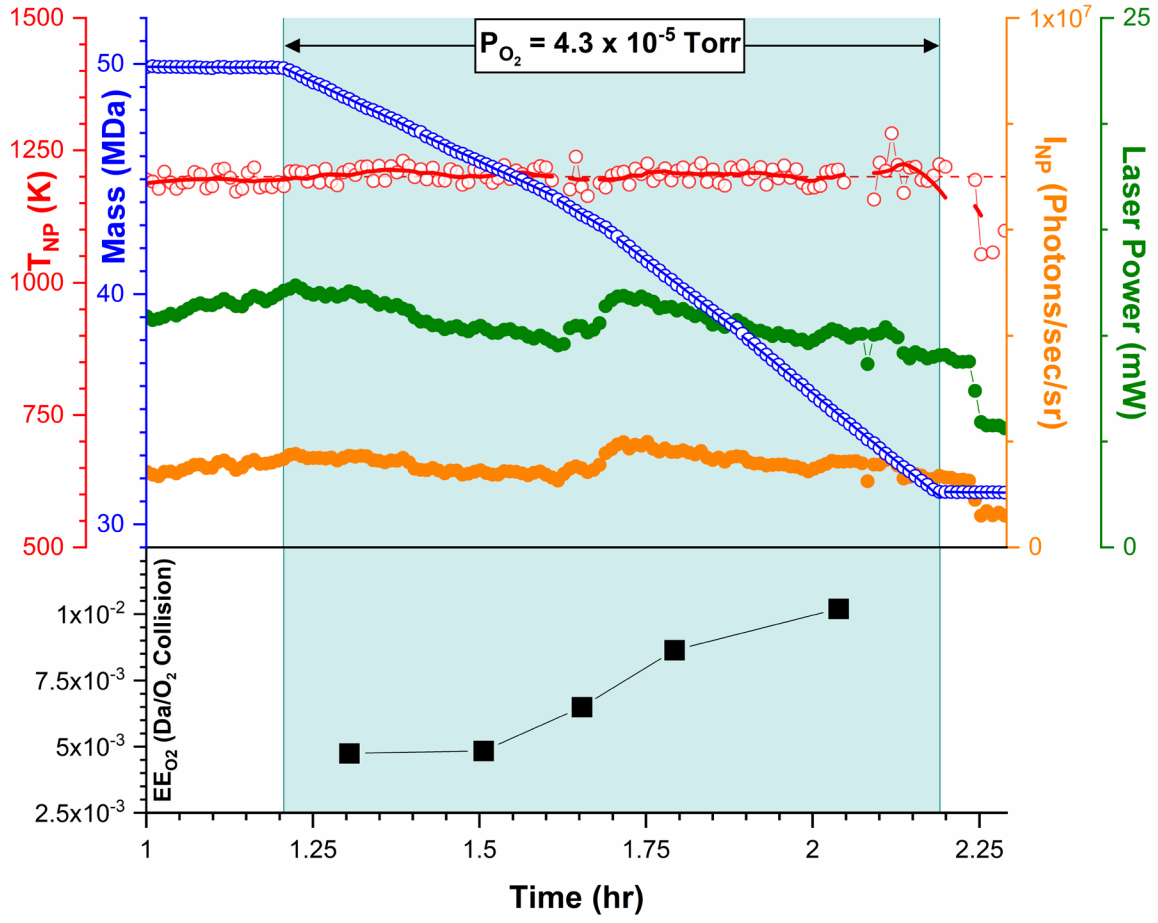

Figure S13: A Si NP at T_{NP} = 1200 K that was not pre-heated. The NP is oxidized at P_{O2} = 4.3 x 10^{-5} Torr, and EE_{O2} is observed to increase with time.

M) O_2 Oxidation of a Silicon Carbide NP

The possibility that C or SiC might passivate the NPs' surfaces due to pyrolysis of adventitious carbonaceous contaminants can be evaluated by considering the oxidation of elemental carbon and SiC NPs under conditions similar to those used in the present study. We previously reported detailed studies of oxidation of NPs of graphite, graphene, graphene oxide, carbon black, diamond, and nano-onion NPs.[61-62] For oxidation at 1500 K, all except the nano-onions oxidized with initial EE_{O2} values between ~10^{-3} and ~10^{-2} Da/O_2 collision, and in the few experiments done at 1200 K,[61] the initial EE_{O2} values were similar. If we assume that the main carbon-containing desorption product is CO,[64-65] then this corresponds to loss of between ~10^{-4} and ~10^{-3} C atoms/O_2 collision. The initial EE_{O2} values for Si NPs (**Fig. 8**) range from ~10^{-3} to 3 x 10^{-2} Da/O_2 collision, corresponding to loss of between 3.6 x 10^{-5} and 1 x 10^{-3} Si atoms/O_2 collision, i.e., elemental carbon etches with efficiency similar to that for Si NPs. Nano-onion carbon (i.e., multiwall fullerene) NPs are nearly inert to O_2, however, this is only true for

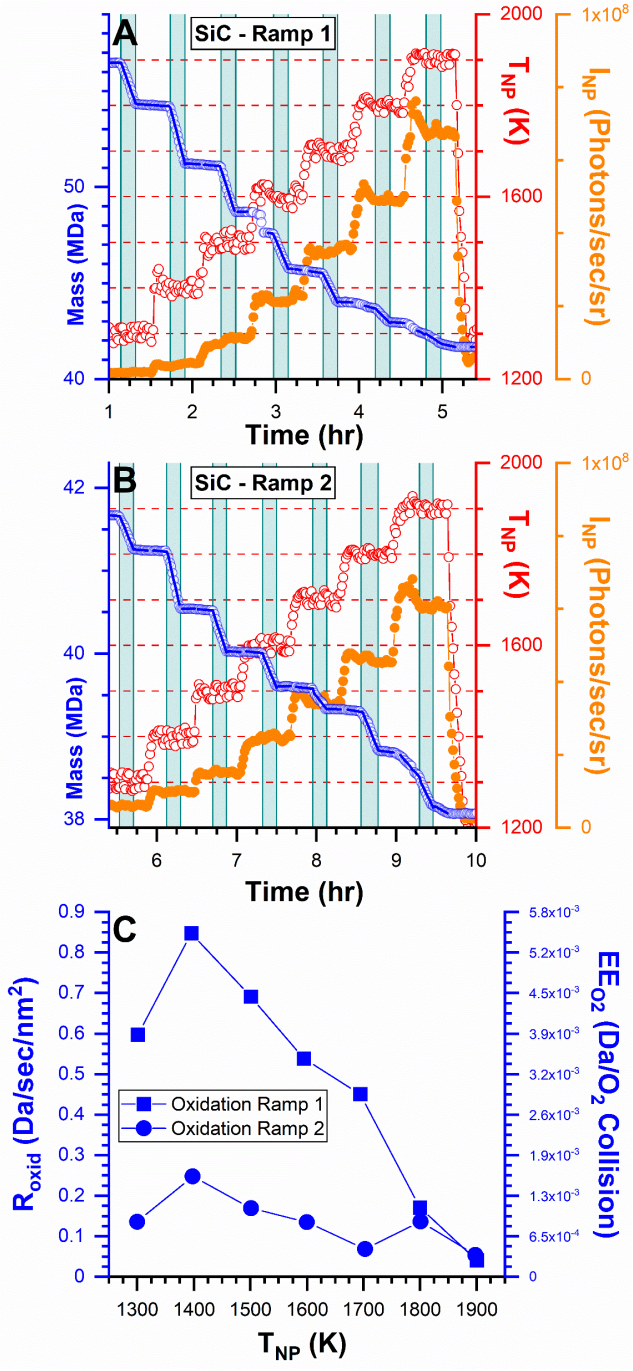

Figure S14: A). M and T_{NP} vs. time for the first heating ramp for a SiC NP from 1300 – 1900 K. Cyan shaded backgrounds indicate periods of oxidation by O_2. B). The 2nd heating ramp for the SiC NP. C). R_{oxid} vs. time for both heating ramps. EE_{O2} scale is shown on the right.

NPs with complete, nearly-defect free fullerene-like surface layers, and it is unlikely that enough carbonaceous adsorbates would have remained on the NP surfaces after the initial heating to form complete shells, even if Si could template that structure (also unlikely).

The experiment in **Fig. S14** shows an example of the O_2 etching kinetics observed for a SiC NP (#6820HK, *Skyspring Nanomaterials*). During the initial T_{NP} ramp, EE_{O2} ranged from ~5 x 10^{-3} Da/O_2 collision at low T_{NP} to ~10^{-4} Da/O_2 collision at high T_{NP}, however, this low value was at least partly due to the NP having largely passivated during the 5 hour T_{NP} ramp, as shown by the very low EE_{O2} values in the second ramp. Passivation presumably resulted from formation of a SiO_2 surface layer, as in Si NPs. Assuming that the initial etching resulted is desorption of SiO and CO in equal numbers, these EE_{O2} values correspond to removing ~2.5 x 10^{-4} atoms/O_2 collision, again comparable to the initial etching efficiencies of Si NPs. Thus, even if the Si NPs were partially covered with elemental carbon or SiC, these materials would not passivate the NP against mass loss, and would etch away quickly upon O_2 exposure.

N) Simulations of 1500 K Oxidation Assuming the Surface Layer Saturates at SiO

The simulations are described in the main text. The only different here is that the NP surface layer was assumed to saturate at SiO composition, rather than SiO_2, as in **Fig. 10.** As in that figure, the left column summarizes simulations for models 1 and 2, where S_0 = 5 x 10^{-5}, and the right column summarizes the results for models 3 and 4, where S_0 = 0.1%. The main differences are that for model 3, the predicted initial mass gain was smaller than when SiO_2 saturation was assumed, but still large enough to be easily detected (it wasn't). Some aspects of the fits are better with SiO_2 saturation, and some are slightly better assuming SiO saturation, but in general, the fitting parameters and conclusions are quite similar, and can be seen in the main text. **Figs. 10** and **S15** show that models representing distinct etching mechanisms can fit the data for both SiO and SiO_2 saturation, but as discussed in the main text, all but model 1 can be ruled out by a combination of our results and the literature. The conclusions about the upper and lower limits on S_0 are not affected by the assumed surface layer saturation stoichiometry.

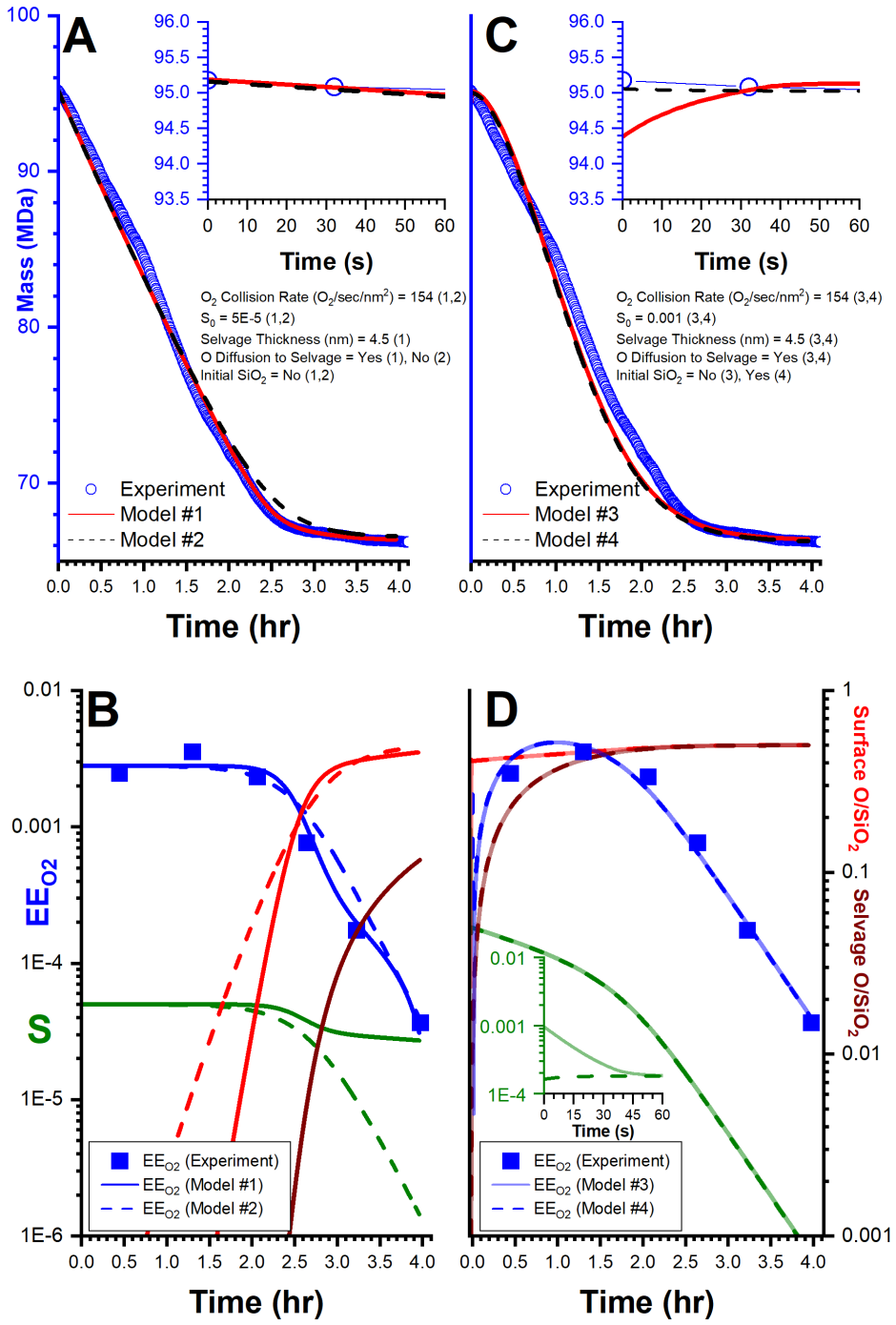

Figure S15: Simulations for passivation of a Si NP at 1500 K (**Fig. S9**) when assuming saturation occurs at SiO stoichiometry. A). M vs. time for models #1 and #2 where $S_0 = 5 \times 10^{-5}$. Model #1 assumes diffusion to selvage layer, while #2 limits O_{ads} to the surface layer. *Inset*: Initial M vs. time. B). EE_{O2} vs. time for experiment and models #1 and #2, where #1 does not lead to a fully passivated NP, but #2 does. C). M vs. time for models #3 and #4 with $S_0 = 0.001$. Diffusion to selvage layer is allowed in both, but #4 assumes the NP starts with some oxide present on the surface. *Inset*: Initial M vs time, and #3 leads to initial growth of the NP. D). EE_{O2} vs. time for frame C. Passivation occurs in both models #3 and #4. *Inset*: Initial S vs. time.

References:

1. Weber, W.; Brox, M., Physical Properties of SiO_2 and Its Interface to Silicon in Microelectronic Applications. *MRS Bulletin* **1993,** *18* (12), 36-42.

2. Buchanan, D. A., Scaling the gate dielectric: Materials, integration, and reliability. *IBM Journal of Research and Development* **1999,** *43* (3), 245-264.

3. Gusev, E. P., Ultrathin Oxide Films for Advanced Gate Dielectrics Applications Current Progress and Future Challenges. In *Defects in SiO_2 and Related Dielectrics: Science and Technology*, Pacchioni, G.; Skuja, L.; Griscom, D. L., Eds. Springer Netherlands: Dordrecht, 2000; pp 557-579.

4. D'Evelyn, M. P.; Nelson, M. M.; Engel, T., Kinetics of the adsorption of O_2 and of the desorption of SiO on Si(100): A molecular beam, XPS, and ISS study. *Surface Science* **1987,** *186* (1), 75-114.

5. Engstrom, J. R.; Bonser, D. J.; Engel, T., The reaction of atomic oxygen with Si(100) and Si(111): II. Adsorption, passive oxidation and the effect of coincident ion bombardment. *Surface Science* **1992,** *268* (1), 238-264.

6. Seiple, J. V.; Pelz, J. P., Evolution of atomic-scale roughening on Si(001)-(2×1) surfaces resulting from high temperature oxidation. *Journal of Vacuum Science & Technology A* **1995,** *13* (3), 772-776.

7. Choi, C. H.; Liu, D.-J.; Evans, J. W.; Gordon, M. S., Passive and Active Oxidation of Si(100) by Atomic Oxygen: A Theoretical Study of Possible Reaction Mechanisms. *Journal of the American Chemical Society* **2002,** *124* (29), 8730-8740.

8. Hemeryck, A.; Richard, N.; Estève, A.; Djafari Rouhani, M., Diffusion of oxygen atom in the topmost layer of the Si(100) surface: Structures and oxidation kinetics. *Surface Science* **2007,** *601* (11), 2339-2343.

9. Arora, P.; Li, W.; Piecuch, P.; Evans, J. W.; Albao, M.; Gordon, M. S., Diffusion of Atomic Oxygen on the Si(100) Surface. *The Journal of Physical Chemistry C* **2010,** *114* (29), 12649-12658.

10. Engstrom, J. R.; Bonser, D. J.; Nelson, M. M.; Engel, T., The reaction of atomic oxygen with Si(100) and Si(111): I. Oxide decomposition, active oxidation and the transition to passive oxidation. *Surface Science* **1991,** *256* (3), 317-343.

11. Lander, J. J.; Morrison, J., Low Voltage Electron Diffraction Study of the Oxidation and Reduction of Silicon. *Journal of Applied Physics* **1962,** *33* (6), 2089-2092.

12. Deal, B. E.; Grove, A. S., General Relationship for the Thermal Oxidation of Silicon. *Journal of Applied Physics* **1965,** *36* (12), 3770-3778.

13. Fair, R. B., Oxidation, Impurity Diffusion, and Defect Growth in Silicon—An Overview. *Journal of The Electrochemical Society* **1981,** *128* (6), 1360-1368.

14. Smith, F. W.; Ghidini, G., Reaction of Oxygen with Si(111) and (100): Critical Conditions for the Growth of SiO2. *Journal of The Electrochemical Society* **1982,** *129* (6), 1300-1306.

15. Irene, E. A., Models for the oxidation of silicon. *Critical Reviews in Solid State and Materials Sciences* **1988,** *14* (2), 175-223.

16. Walkup, R. E.; Raider, S. I., In situ measurements of SiO(g) production during dry oxidation of crystalline silicon. *Applied Physics Letters* **1988,** *53* (10), 888-890.

17. Gibson, J. M.; Lanzerotti, M. Y., Observation of interfacial atomic steps during silicon oxidation. *Nature* **1989,** *340* (6229), 128-131.

18. Feltz, A.; Memmert, U.; Behm, R. J., In situ STM imaging of high temperature oxygen etching of Si(111)(7 × 7) surfaces. *Chemical Physics Letters* **1992,** *192* (2), 271-276.

19. Engel, T., The interaction of molecular and atomic oxygen with Si(100) and Si(111). *Surface Science Reports* **1993,** *18* (4), 93-144.

20. Seiple, J.; Pecquet, J.; Meng, Z.; Pelz, J. P., Elevated temperature oxidation and etching of the Si(111) 7×7 surface observed with scanning tunneling microscopy. *Journal of Vacuum Science & Technology A* **1993,** *11* (4), 1649-1653.

21. Feltz, A.; Memmert, U.; Behm, R. J., High temperature scanning tunneling microscopy studies on the interaction of O_2 with Si(111)-(7 × 7) surfaces. *Surface Science* **1994,** *314* (1), 34-56.

22. Ross, F. M.; Gibson, J. M.; Twesten, R. D., Dynamic observations of interface motion during the oxidation of silicon. *Surface Science* **1994,** *310* (1), 243-266.

23. Udagawa, M.; Niwa, M.; Sumita, I., Local Ordering and Lateral Growth of Initial Thermal Oxide of Si(001). *Japanese Journal of Applied Physics* **1994,** *33* (Part 1, No. 1B), 375-378.

24. Borman, V. D.; Gusev, E. P.; Lebedinski, Y. Y.; Troyan, V. I., Mechanism of submonolayer oxide formation on silicon surfaces upon thermal oxidation. *Physical Review B* **1994,** *49* (8), 5415-5423.

25. Seiple, J. V.; Pelz, J. P., Scanning Tunneling Microscopy study of Oxide Nucleation and Oxidation-Induced Roughening at Elevated Temperatures on the Si(001)-(2 x 1) Surface. *Physical Review Letters* **1994,** *73* (7), 999-1002.

26. Mott, N. F.; Rigo, S.; Rochet, F.; Stoneham, A. M., Oxidation of Silicon. In *Sir Nevill Mott ? 65 Years in Physics*, World Scientific: 1995; Vol. Volume 12, pp 685-708.

27. Sofield, C. J.; Stoneham, A. M., Oxidation of silicon: the VLSI gate dielectric. *Semiconductor Science and Technology* **1995,** *10* (3), 215-244.

28. Lu, H. C.; Gusev, E. P.; Garfunkel, E.; Gustafsson, T., An ion scattering study of the interaction of oxygen with Si(111): surface roughening and oxide growth. *Surface Science* **1996,** *351* (1), 111-128.

29. Williams, E. D.; Fu, E. S.; Li, B., Evolution of Morphology During Etching of Si. *MRS Proceedings* **1996,** *466*, 157.

30. Komeda, T.; Nishioka, Y., Layer-by-Layer Etching of Si(111) Surface by Oxygen at Elevated Temperature. *Japanese Journal of Applied Physics* **1997,** *36* (Part 1, No. 3B), 1582-1585.

31. Raschke, M. B.; Bratu, P.; Höfer, U., Optical second-harmonic investigations of the isothermal desorption of SiO from the Si(100) and Si(111) surfaces. *Surface Science* **1998,** *410* (2), 351-361.

32. Hannon, J. B.; Bartelt, M. C.; Bartelt, N. C.; Kellogg, G. L., Etching of the Si(001) Surface with Molecular Oxygen. *Physical Review Letters* **1998,** *81* (21), 4676-4679.

33. Åkermark, T.; Ganem, J. J.; Trimaille, I.; Vickridge, I.; Rigo, S., Temperature and Pressure Dependence of the Oxygen Exchange at the SiO_2−Si Interface, $O_2 \leftrightarrow SiO_2$, during Dry Thermal Oxidation of Silicon. *The Journal of Physical Chemistry B* **1999,** *103* (45), 9910-9914.

34. Brichzin, V.; Pelz, J. P., Effect of surface steps on oxide-cluster nucleation and sticking of oxygen on Si(001) surfaces. *Physical Review B* **1999,** *59* (15), 10138-10144.

35. Starodub, D.; Gusev, E. P.; Garfunkel, E.; Gustafsson, T., Silicon Oxide Decomposition and Desorption during the Thermal Oxidation of Silicon. *Surface Review and Letters* **1999,** *06* (01), 45-52.

36. Daineka, D. V.; Pradère, F.; Châtelet, M.; Fort, E., High temperature oxidation of Si(100) by neutral oxygen cluster beam: Coexistence of active and passive oxidation areas. *Journal of Applied Physics* **2002,** *92* (2), 1132-1136.

37. Ogawa, S.; Yoshigoe, A.; Ishidzuka, S.; Teraoka, Y.; Takakuwa, Y., Consumption kinetics of Si atoms during growth and decomposition of very thin oxide on Si(001) surfaces. *Thin Solid Films* **2006,** *508* (1), 169-174.

38. Teraoka, Y.; Yoshigoe, A.; Moritani, K., Mechanisms of concurrent SiO desorption with oxide layer formation at Si(001) surface. *Electrical Engineering in Japan* **2008,** *164* (3), 60-68.

39. Enta, Y.; Nakazawa, H.; Sato, S.; Kato, H.; Sakisaka, Y., Silicon thermal oxidation and its thermal desorption investigated by Si 2p core-level photoemission. *Journal of Physics: Conference Series* **2010,** *235*, 012008.

40. Hibiya, T.; Hokama, S.; Koike, Y.; Rinno, M.; Kawamura, H.; Fukuyama, H.; Higuchi, K.; Watanabe, M., Surface oxidation of electromagnetically levitated molten silicon under a condition of oxygen-supersaturation. *Scripta Materialia* **2006,** *54* (4), 695-699.

41. Tromp, R.; Rubloff, G. W.; Balk, P.; LeGoues, F. K.; van Loenen, E. J., High-Temperature SiO_2 Decomposition at the SiO_2/Si Interface. *Physical Review Letters* **1985,** *55* (21), 2332-2335.

42. Liehr, M.; Lewis, J. E.; Rubloff, G. W., Kinetics of high-temperature thermal decomposition of SiO2 on Si(100). *Journal of Vacuum Science & Technology A* **1987,** *5* (4), 1559-1562.

43. Watanabe, H.; Fujita, K.; Ichikawa, M., Thermal decomposition of ultrathin oxide layers on Si(111) surfaces mediated by surface Si transport. *Applied Physics Letters* **1997,** *70* (9), 1095-1097.

44. Watanabe, H.; Fujita, S.; Maruno, S.; Fujita, K.; Ichikawa, M., Selective thermal decomposition of ultrathin silicon oxide layers induced by electron-stimulated oxygen desorption. *Applied Physics Letters* **1997,** *71* (8), 1038-1040.

45. Johansson, U.; Zhang, H.; Nyholm, R., Thermal desorption of oxides on Si(100): a case study for the scanning photoelectron microscope at MAX-LAB. *Journal of Electron Spectroscopy and Related Phenomena* **1997,** *84* (1), 45-52.

46. Miyata, N.; Watanabe, H.; Ichikawa, M., Thermal Decomposition of an Ultrathin Si Oxide Layer around a Si(001)- (2×1) Window. *Physical Review Letters* **2000,** *84* (5), 1043-1046.

47. Xue, K.; Xu, J. B.; Ho, H. P., Nanoscalein situinvestigation of ultrathin silicon oxide thermal decomposition by high temperature scanning tunneling microscopy. *Nanotechnology* **2007,** *18* (48), 485709.

48. Enta, Y.; Osanai, S.; Ogasawara, T., Activation energy of thermal desorption of silicon oxide layers on silicon substrates. *Surface Science* **2017,** *656*, 96-100.

49. Morita, M.; Ohmi, T.; Hasegawa, E.; Kawakami, M.; Ohwada, M., Growth of native oxide on a silicon surface. *Journal of Applied Physics* **1990,** *68* (3), 1272-1281.

50. Tanaka, H.; Kanayama, T., Thermal desorption of Si clusters from Si and Si-deposited Ta surfaces. *Journal of Vacuum Science & Technology B: Microelectronics and Nanometer Structures Processing, Measurement, and Phenomena* **1997,** *15* (5), 1613-1617.

51. Porter, R. F.; Chupka, W. A.; Ingiiram, M. G., Mass Spectrometric Study of Gaseous Species in the Si-SiO2 System. *The Journal of Chemical Physics* **1955,** *23* (1), 216-217.

52. Schick, H. L., A Thermodynamic Analysis of the High-temperature Vaporization Properties of Silica. *Chemical Reviews* **1960,** *60* (4), 331-362.

53. Shornikov, S.; Archakov, I. Y.; Shul'ts, M., Mass spectrometric study of vaporization and thermodynamic properties of silicon dioxide. I. Composition of the gas phase and partial vapor pressures of the molecular forms over silicon dioxide. *Russian journal of general chemistry* **1998,** *68* (8), 1171-1177.

54. Shornikov, S.; Archakov, I. Y.; Shul'ts, M., Mass spectrometric study of vaporization and thermodynamic properties of silicon dioxide: II. Determination of partial vaporization coefficients of silicon dioxide. *Russian journal of general chemistry* **1999,** *69* (2), 187-196.

55. Okada, R.; Iijima, S., Oxidation property of silicon small particles. *Applied Physics Letters* **1991,** *58* (15), 1662-1663.

56. Yang, D. Q.; Gillet, J.-N.; Meunier, M.; Sacher, E., Room temperature oxidation kinetics of Si nanoparticles in air, determined by x-ray photoelectron spectroscopy. *Journal of Applied Physics* **2004,** *97* (2), 024303.

57. Liao, Y.-C.; Nienow, A. M.; Roberts, J. T., Surface Chemistry of Aerosolized Nanoparticles:Thermal Oxidation of Silicon. *The Journal of Physical Chemistry B* **2006,** *110* (12), 6190-6197.

58. Vazquez-Pufleau, M., A Simple Model for the High Temperature Oxidation Kinetics of Silicon Nanoparticle Aggregates. *Silicon* **2021,** *13* (1), 189-200.

59. Long, B. A.; Lau, C. Y.; Rodriguez, D. J.; Tang, S. A.; Anderson, S. L., Sublimation Kinetics for Individual Graphite and Graphene Nano-particles (NPs): NP-to-NP Variations and Evolving Structure-Kinetics and Structure-Emissivity Relationships. *J. Am. Chem. Soc.* **2020,** *142* (33), 14090-14101.

60. Long, B. A.; Rodriguez, D. J.; Lau, C. Y.; Schultz, M.; Anderson, S. L., Thermal Emission Spectroscopy of Single, Isolated Carbon Nanoparticles: Effects of Particle Size, Material, Charge, Excitation Wavelength, and Thermal History. *J. Phys. Chem. C* **2020,** *124*, 1704-1716.

61. Rodriguez, D. J.; Lau, C. Y.; Long, B. A.; Tang, S. A.; Friese, A. M.; Anderson, S. L., O_2-oxidation of individual graphite and graphene nanoparticles in the 1200–2200 K range: Particle-to-particle variations and the evolution of the reaction rates and optical properties. *Carbon* **2021,** *173*, 286-300.

62. Rodriguez, D. J.; Lau, C. Y.; Friese, A. M.; Magasinski, A.; Yushin, G.; Anderson, S. L., High-Temperature Oxidation of Single Carbon Nanoparticles: Dependence on the Surface Structure and Probing Real-Time Structural Evolution via Kinetics. *J Am Chem Soc* **2022,** *144* (11), 4897-4912.

63. Kawamura, H.; Fukuyama, H.; Watanabe, M.; Hibiya, T., Normal spectral emissivity of undercooled liquid silicon. *Measurement Science and Technology* **2005,** *16* (2), 386.

64. Murray, V. J.; Marshall, B. C.; Woodburn, P. J.; Minton, T. K., Inelastic and Reactive Scattering Dynamics of Hyperthermal O and O_2 on Hot Vitreous Carbon Surfaces. *J. Phys. Chem. C* **2015,** *119*, 14780-14796.

65. Murray, V. J.; Smoll, E. J.; Minton, T. K., Dynamics of Graphite Oxidation at High Temperature. *J. Phys. Chem. C* **2018,** *122* (12), 6602-6617.